UNIVERSITY OF CALIFORNIA SAN DIEGO

Aerosols, Air Quality Equity, and Climate Impacts: Idealized Modeling to Inform Climate Policy

A dissertation submitted in partial satisfaction of the
requirements for the degree Doctor of Philosophy

in

Earth Sciences

by

Pascal Polonik

Committee in charge:

Professor Katharine Ricke, Chair
Professor Jennifer Burney, Co-Chair
Professor Adrian Borsa
Professor Joshua Graff Zivin
Professor Shang-Ping Xie

2023

The Dissertation of Pascal Polonik is approved, and it is acceptable in quality and form for publication on microfilm and electronically.

University of California San Diego

2023

TABLE OF CONTENTS

LIST OF FIGURES

LIST OF TABLES

ACKNOWLEDGEMENTS

I would like to acknowledge Professors Kate Ricke and Jen Burney as co-chairs of my committee for their immeasurable support throughout my entire PhD. They are incredible scientists, strong advocates for students, and kind and empathetic people. They have far exceed normal advisor expectations and I feel incredibly lucky to have learned from them both. I would also like to acknowledge the Burney, Ricke, Levy Group (BLRG) and the many members of my PhD cohort that have provided a entertainment and emotional support - including but not limited to (alphabetically) Alexander Andriatis, Ben Gruber, Athina Lange, Tricia Light, Max Rintoul, Marissa Saenger, Jessica Wan, Duncan Wheeler, and Bethan Wynne-Cattanach. Last but not least, I would like to acknowledge my partner, Linnea Ransom, for her boundless personal and professional support, providing much needed stability through globally challenging times.

Chapter 2, in full, is a reprint of the material as it appears in AGU Earth's Future 2021. Polonik, Pascal; Ricke, Katharine; Burney, Jennifer. AGU, 2023. The dissertation author was the primary investigator and author of this paper. Chapter 3, in full, is a reprint of the material as has been accepted for publication with The Proceedings of the National Academies of Sciences, 2023, Polonik, Pascal; Reese, Sean; Ricke, Katharine; Burney, Jennifer. PNAS, 2023. The dissertation author was the primary investigator and author of this paper. Chapter 4, in full is currently being prepared for submission for publication of the material. Polonik, Pascal; Ricke, Katharine; Burney, Jennifer. The dissertation author was the primary investigator and author of this paper.

VITA

2015	Bachelor of Science, University of California Berkeley
2015	Bachelor of Arts, University of California Berkeley
2018	Master of Science, Ludwig Maximillian University, Munich
2023	Doctor of Philosophy, University of California San Diego

PUBLICATIONS

Polonik, P., et al. 2019. Comparison of gas analyzers for eddy covariance: Effects of analyzer type and spectral corrections on fluxes. Agricultural and Forest Meteorology, 272, pp.128-142. doi: https://doi.org/10.1016/j.agrformet.2019.02.010

Polonik, P., et al. 2020. The challenge of simulating the sensitivity of the Amazonian cloud microstructure to cloud condensation nuclei number concentrations, Atmos. Chem. Phys., 20, 1591–1605, https://doi.org/10.5194/acp-20-1591-2020

Polonik, P., et al. 2021. Paris Agreement's ambiguity about aerosols drives uncertain health and climate outcomes. AGU Earth's Future. https://doi.org/10.1029/2020EF001787

Bluhm, R*, Polonik, P.*, et al. 2022. Disparate air pollution reductions during California's COVID-19 economic shutdown. Nature Sustainability. https://doi.org/10.1038/s41893-022-00856-1

Polonik, P. et al., 2023. Air Quality Equity in U.S. Climate Policy. Proceedings of the National Academies of Sciences. *In Press.*

ABSTRACT OF THE DISSERTATION

Aerosols, Air Quality Equity, and Climate Impacts: Idealized Modeling to Inform Climate Policy

by

Pascal Polonik

Doctor of Philosophy in Earth Sciences

University of California San Diego, 2023

Professor Katharine Ricke, Chair
Professor Jennifer Burney, Co-Chair

Improved understanding of the physical impacts to the climate caused by anthropogenic emissions has led to an increased focus on the role of policy on limiting mitigating the cause and the impacts of climate change. The emissions trajectory that society takes will play a major role in determining a wide variety of climate impacts from health to economic growth. This dissertation explores how idealized modeling can be used to inform the potential outcomes of the policies meant to mitigate the negative impacts of climate change and optimize the benefits of emission reduction. Chapter 1 explores the potential trade-offs between increased temperatures and reduced health impacts of considering aerosol emissions in international climate policy.

Using an idealized model, it is possible to demonstrate that both health and temperature benefits can result from considering either health or temperature separately. Chapter 2 interrogates whether climate policy in the United States can be used to reduce existing racial inequities in air pollution exposure. The modeling shows that prioritizing by exclusively income or cost in national policy would result in worsening inequities, but that prioritizing by race explicitly has the opposite effect. Using a set of more realistic air quality simulations with randomized emission reduction, it appears that the transportation has a unique potential for air quality equity improvements. Lastly, Chapter 3 focuses on statistical models that use natural variation in annual weather to predict how climate will influence human outcomes. Using an idealized outcome variable and real data of global gross domestic product, it is possible to demonstrate that imperfect measurement networks and the mean shift in climate both work to underestimate future climate impacts.

Chapter 1

Introduction

Emissions of greenhouse gases and conventional pollutants from human activity have warmed Earth's climate [1] and degraded air quality [2, 3]; these changes in turn negatively impact human welfare, equity, and societal function. The decisions we make collectively about how to ameliorate and respond to these harms will have far-reaching consequences, but there is significant uncertainty in our understanding of both physical impacts and the impact of available policy levers.

Although there are many remaining avenues for improving scientific understanding of how emissions influence the climate and human health, the biggest uncertainty in future outcomes is human decision-making about the rate, location, and type of emission reduction, and the human response to a changed environment. The atmosphere is chaotic and the climate system is complex, but we now collectively understand a large portion of the underlying physics that govern radiative transfer and the general circulation. Human decisions and reactions, on the other hand, cannot be reduced to a set of governing equations. However, despite their complexity, we can draw on the current understanding of the Earth system in simplified models to better understand how decisions influence outcomes and how people respond to change. In this dissertation I use idealized modeling to constrain how various policy decisions could influence human outcomes.

In Chapter 2, I explore how idealized Paris Agreement implementation decisions at the

country level can change air pollution and global temperatures. Since aerosols mask a portion of global warming from greenhouse gases, their reduced emissions can unintentionally cause global temperature rise. This is relevant to climate policy because aerosols are co-emitted with greenhouse gases, so the effectiveness of greenhouse gas mitigation may be hampered by reductions in cooling aerosols. However, some aerosol species also cause warming and they are all damaging to human health, meaning there can be tradeoffs or co-benefits from aerosols when reducing greenhouse gas emissions.

In Chapter 3, I focus on potential air pollution and equity co-benefits of greenhouse gas emission reduction in the United States. Again using an idealized decision framework, but a more sophisticated air quality model and county-level emissions, I quantify how implementing the country's reduction targets might impact racial air quality equity. By testing how different criteria (e.g. income) for choosing emission reduction location impact air quality equity, it is possible to test whether these approaches will in fact reduce existing inequities as is the stated priority of the U.S. government. Furthermore, by testing slightly more realistic randomized emission reductions I test whether reductions in certain sectors are disproportionately effective at improving equity.

In Chapter 4, I turn towards the global empirical impact models often used to project future effects of climate change. I use an idealized outcome to quantify how statistical models that estimate the impact of temperature (T) and precipitation (P) are impacted by imperfect measurement of T and P, the correlation between T and P, and the aggregation to large spatial scales at which societal data are often available (e.g. countries). The goal of this chapter is to bridge the physical science and the causal analysis often used by economists to improve the understanding of society's response to global change.

Together, these chapters help explain interactions between the physical environment and human outcomes, specifically around climate policy implementation.

Chapter 2

Paris Agreement's ambiguity about aerosols drives uncertain health and climate outcomes

2.1 Abstract

Anthropogenic aerosols are hazardous to human health but have helped offset warming from greenhouse gases (GHGs), creating a potential regulatory tradeoff. As countries implement their GHG reduction targets under the Paris climate agreement, the co-emissions of aerosols and their precursors will also change. Since these co-emissions vary by country and by economic sector, each country will face different tradeoffs between aerosol-driven health or temperature co-benefits. We combine simple parameterizations of physical processes and health outcomes to examine three idealized climate policy approaches that are consistent with the Paris Agreement targets, which i) optimize for local air quality, ii) reduce global temperature change, or iii) reduce emissions equally from all domestic economic sectors. We evaluate aerosol impacts on premature mortality and global mean temperature change under these three policy approaches and find that by 2030 the three policies yield differences of over one million annual premature deaths and global temperature differences of the same magnitude as those from GHG reductions. We also show that implementing equal reductions between all economic sectors can actually result in less beneficial health and temperature outcomes than either of the other options, especially in

less industrialized regions. We therefore conclude that aerosol-related co-benefits and aerosol accounting guidelines should be explicitly considered in setting international climate policy.

2.2 Introduction

The Paris Agreement, a major international effort to limit global warming to 1.5-2 °C, requires every participating country to submit a Nationally Determined Contribution (NDC), in which each country outlines the steps they believe are required to achieve the joint goal. The NDCs are non-binding, flexible, and vary substantially between different countries. NDCs differ in several important dimensions, including which greenhouse gases (GHGs) are considered, which economic sectors are expected to reduce emissions, which year's emissions serve as the baseline, whether absolute emissions or emission intensity (i.e. emissions per gross domestic product (GDP) or population) will be reduced, or whether reductions are considered in absolutes or relative to a business as usual scenario. Many NDCs emphasize the importance of addressing climate change but do not state any concrete or quantifiable emissions reductions. The NDCs are largely unstructured text documents, and their phrasing is often ambiguous. This can leave substantial flexibility in their implementation [4]. For example, several different emissions pathways (e.g., reductions in different sectors) could lead to the same stated outcome, or conversely, the same stated goal might correspond to very different changes in emissions, depending on the accounting details and assumptions [5].

One confounding factor not addressed by the NDCs is the influence of atmospheric particulate matter (aerosols). Both anthropogenic emissions of (GHGs) and aerosols alter Earth's climate, but most countries only consider GHGs in their NDCs. However, GHG emissions are closely tied to aerosol emissions since many human activities simultaneously produce both [6, 7]. As countries implement their GHG reduction commitments, aerosol emissions will also change [8].

Joint consideration of GHGs and aerosols is critical because, while GHG emissions might

be thought of as unambiguously harmful, from a climate change perspective, the influence of aerosols is complex and uncertain [9]. Aerosols typically only have a lifetime of 5-10 days, but their impacts are pervasive due to their continuous emission. They can directly absorb and scatter radiation (direct effect), influence the formation and evolution of clouds as cloud condensation nuclei (indirect effects), alter vertical temperature profiles and thereby cloud dynamics (semi-direct effects), and modify surface albedo (e.g. darken snow). These effects can all change radiative transfer and thereby change radiative forcing, which is the net change in the energy balance of the Earth system due to some imposed perturbation [10]. The impact on the energy budget depends on the aerosol chemical composition and size distribution, which vary in space and time [11]. In contrast to aerosols, the radiative forcing of greenhouse gases is substantially more spatially and temporally uniform due to longer lifetimes and simpler chemical properties. Radiative forcing leads to temperature changes, and in aggregate, anthropogenic aerosols have offset a third of warming from anthropogenic GHG emissions [12], though the aerosol impacts are much more uncertain than the GHG impacts [13]. Despite net global cooling, some aerosols like black carbon have a net warming effect globally while others, like sulfates, cause cooling [14, 15]. The climate impacts of aerosols can have profound global implications [16]. However, in the context of policy, aerosols have historically been regulated in response to their impact on local air quality, rather than climate impacts, because air pollution has a host of negative health consequences that can lead to premature mortality [3, 17, 18].

Air quality improvements have short-term, local benefits, which can incentivize regulation [19]. Climate change mitigation on the other hand, is normally considered a short-term cost with long-term, global benefits, which lowers the incentive for domestic regulations. Including aerosols in economic analyses of climate regulation has been shown to make emissions reduction financially favorable in the short-term as well as the long-term [20]. Aerosol regulation has historically come in the form of air quality regulations, but the cooling role of aerosols has led to concern that such regulation could amplify planetary warming [21]. Meanwhile, others have argued that targeted reduction of warming aerosols could be leveraged for an additional cooling

effect that would aid efforts to limit warming [22, 23], though simultaneous changes to the emission of other species counter the intended cooling [24]. Regardless of the sign of the effect, the use of climate-impact metrics that incorporate near-term climate forcers (NTCFs, which include gases and particles with short lifetimes that cause radiative forcing) can better predict climate outcomes, especially for ambitious emissions reduction pathways like those proposed in the Paris Agreement [25].

Here, we quantify aerosol-induced premature mortality and temperature effects in 2030 under different implementation strategies for meeting the targets associated with the Paris Agreement. We consider black carbon (BC), organic carbon (OC), sulfur dioxide (SO_2), and nitrogen oxides (NO_x) using global gridded anthropogenic emissions data that specifies emissions by economic sector. OC, SO_2, and NO_x are associated with negative radiative forcing (surface cooling) impacts, while BC is associated with positive radiative forcing, though all four lead to negative health outcomes. We simulate multiple operationalizations of the NDCs for each country using idealized physical assumptions and decision priorities that demonstrate the consequences of countries' ambiguous aerosol co-emissions in implementing their NDC target GHG reductions.

2.3 Methods

We examine outcomes under three country-level decision-making priorities: (1) minimization of global temperature change (climate priority), (2) minimizing local air pollution (air quality (AQ) priority), and (3) political expediency in the form of proportional cross-sectoral reductions, i.e., no aerosol-specific policy (equal-by-sector). The underlying emissions rely on the no-climate-policy baseline shared socioeconomic pathway (no-policy SSP, [26, 27]). SSP3 is a nationalist, low-growth scenario with costly mitigation whose baseline corresponds to the Representative Concentration Pathway 7.0 (RCP7.0) [28]; SSP5 is a scenario with high fossil fuel development whose baseline corresponds to RCP8.5 [29].

Some NDCs specify which greenhouse gases are covered by the agreement, while others

do not. Unless otherwise specified, we assume that all targets refer to carbon dioxide equivalent (CO_2e), where CO_2e is emission rate of carbon dioxide (CO_2), methane (CH_4), and nitrous oxide (N_2O) scaled by the global warming potential (GWP; CO_2: 1, CH_4: 28, N_2O: 265) [30]. We limit the analysis to only CO_2 for countries that specify that targets are only for CO_2 (e.g. China). We define the notation, $CO_2[e]$, to refer to CO_2e or CO_2 emissions as specified by each country's NDC. We do not consider additional gases (e.g. chlorofluorocarbons (CFCs), sulfur hexafluoride (SF_6)), even if they are specified, due to data availability; errors from omission are likely small since CO_2, CH_4, and N_2O constitute the vast majority of CO_2e emissions. We also consider four NTCFs: BC, OC, SO_2 (as the main precursor for sulfate aerosols), and NO_x (as the main precursor for nitrate aerosols). All emissions are divided into eight economic sectors: agriculture, energy, industry, transportation, residential/commercial, solvents, waste, and shipping.

2.3.1 Idealized decision-making

To minimize temperature change or air pollution, we identify each sector's impact per $CO_2[e]$ emission and sequentially reduce the most sectorally impactful emissions of $CO_2[e]$ and NTCF co-emissions. These represent the extreme, unconstrained cases and therefore represent bounding cases under the assumption that countries meet their Paris Agreement goals.

In the case of no aerosol-specific policy (equal-by-sector), we alter each sector's anthropogenic emissions equally to meet the GHG target. For example, a 20% reduction in GHGs between 2020 and 2030 would yield linearly decreasing emissions of all GHGs and NTCFs for each sector, and therefore also of the total. We include the equal-by-sector implementation because it could be seen as the simplest implementation, wherein every economic sector within a country is expected to contribute equally towards the common goal. We view this as a politically expedient implementation because all greenhouse gas emitting sectors would bear proportional burdens in meeting domestic emissions commitments. All the priorities assume that the country-level relationship between GHGs and each NTCF remains constant (at 2020 values) between 2020 and 2030, though this relationship changes in the unmodified SSP scenarios - particularly

on longer time scales - because of technological developments.

For the climate priority and AQ priority, we calculate the aerosol impact per CO_2[e] emissions for each sector in each country (see sections 2.4, 2.5). These metrics allow us to identify the most impactful sectors to change. For the climate priority, we calculate global aerosol forcing per CO_2[e] and for the AQ priority we calculate population-weighted aerosol concentration per CO_2[e]. All emissions reductions are then made from the most impactful sector. If that sector has fewer CO_2[e] emissions than are required to meet the NDC target, that sector's emissions are reduced to zero and the remainder is taken from the next most impactful sector, and so on. The operationalization of the three decision making priorities is illustrated in Figure 2.1. A few countries specify sectors in their NDC; in those cases, we limit the analysis to those sectors (see section 2.2 for further discussion).

We assume that the country-level relationship between NTCFs and CO_2[e] emissions remains constant at the 2020 ratio for each sector. In some countries, emissions are anticipated to increase between 2020 and 2030 despite emissions reductions targets, because targets are relative to a business as usual (BAU) scenario (i.e. a country says they will emit a certain percent less than they would have in 2030 without climate policies). In those cases, emissions are added to the least damaging sector, but are not allowed to exceed the 2030 no-policy SSP sectoral emissions. For countries with no stated reduction targets, we use unaltered 2030 SSP emissions. This methodology results in bounding, idealized cases, not a realistic representation of future changes. The temporal evolution of global emissions for each priority and each species are shown in Figure A2.1.

2.3.2 NDC quantification

We implement existing NDC tabulations with a few notable exceptions. Our estimates were based on the CD-LINKS protocol (CD-LINKS), which is very similar to the table provided by [31]. The NDC tabulation used for this study is publicly available (see data availability); all deviations from CD-LINKS are noted. For countries that specify emission reduction targets, these

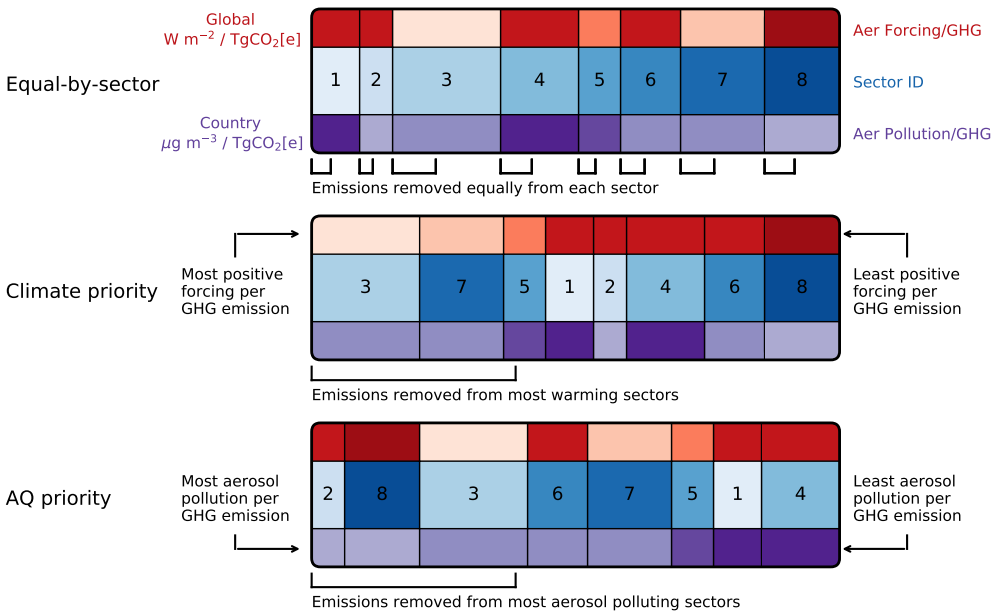

Figure 2.1. Schematic of three idealized priorities for greenhouse gas reduction for one (fictional) country. Blue color and numbers indicate the economic sector. The width of each sector indicates the magnitude of the sector's $CO_2$2[e] emissions. Red indicates the global aerosol forcing per CO_2[e] of the sector and purple indicates the local air quality impact per CO_2[e] of the sector. Brackets indicate removed emissions. In each case the same total CO_2[e] emissions are removed, but from a different combination of economic sectors. Each sector's aerosol emissions are altered between 2020 and 2030 in proportion with greenhouse gas emissions

tables provide a baseline year and a percent reduction of emissions from that baseline by a target year. The target year is normally 2030. When target years are after 2030, we linearly interpolate to 2030 between the base year and target year. When target years are before 2030, we assume the country will take until 2030 to actually achieve their goal. Despite the current uncertain status of the United States (US) in the Paris Agreement, we implemented US targets from CD-LINKS as we did for other countries. Many countries provide conditional and unconditional targets, where the condition refers to foreign aid. When multiple options exist, we implement the most ambitious targets.

For NDC targets that are stated in CO_2[e] intensities (i.e. emissions per GDP or per capita), we use the country-level population and GDP projections provided on the SSP database (https://bit.ly/33nNwL7). When the use of GDP is required, the country's SSP GDP time series is harmonized with historical World Bank (WB) GDP data [32] by scaling SSP GDP projections by the ratio of 2018 WB GDP to linearly interpolated 2018 SSP GDP. WB GDP is converted to 2005 international dollars for consistency with the SSP GDP using the WB GDP deflator [33].

India and China both have intensity targets based on GDP. Based on our calculations, India is expected to meet its 2030 targets, even without climate policy implementation (Figure A2.2), which is consistent with previous NDC quantification [31]. We therefore use the unmodified, no-policy SSP emissions projections for India. For SSP5, China also exceeds its targets without additional policy. However, China also states that it will peak emissions by 2030, which is a more ambitious target. Therefore, we implement a smooth transition (linear derivative) from 2020 to 2030 so that the change of annual emissions is zero by 2030. For SSP3, China does not automatically meet the intensity target, so we implement the target as we would for other countries (Figure A2.2). Several countries specify economic sectors for their planned emissions reduction. We only reduce emissions from those economic sectors. Though it initially seems like an added level of specificity to include sectors specified in an NDC, it can actually introduce ambiguity. In our interpretation, some countries plan to reduce their total emissions from a subset of economic sectors, whereas some plan to reduce a percentage of the emissions from

those sectors. The global impact of this difference is small, but this distinction does not appear to be included in CD-LINKS. Upon review we also identified a few sectors specified in NDCs that were not included in the CD-LINKS tabulation, which we have added and noted in the supplement.

For all countries that do not have explicit climate reduction goals, GHG and NTCF emissions are assumed to follow a no-policy scenario (SSP3 or SSP5); this applies to all three priorities and the unmodified case. For countries who state that their CO_2[e] reductions will be relative to BAU rather than relative to a baseline year, we assume that the no-policy SSP represents BAU and we apply GHG reductions from 2030 SSP emissions (i.e. 2030 is both the baseline year and the target year).

After we calculate the intended 2030 CO_2[e] emissions for each country (which are based entirely on the NDCs and are therefore the same for all three priorities), we assume that each country has followed the SSP until 2020 and will implement their Paris Agreement commitments between 2020 and 2030. For countries with BAU-based targets, this can result in an increase in CO_2[e] emissions between 2020 and 2030, rather than a reduction, but emissions will still be lower in 2030 than they would have been in the unmodified no-policy SSP. In all cases, once the total CO_2[e] emission changes have been calculated, those changes are implemented through modifications to specific sectors as described in 2.1.

2.3.3 Input data

Historical (pre-2015) mean annual global gridded anthropogenic emissions of GHGs and NTCFs were primarily taken from the Community Emissions Data System (CEDS, [34]), available on the input4mips database. The only exception is N_2O, which was taken from the EDGAR emissions database [35] since gridded CEDS N_2O emissions are not available. The EDGAR data set has more detailed sectors than the CEDS data set; the mapping used to aggregate EDGAR sectors to CEDS sectors is given in Table A2.1. These data do not include biomass burning, aircraft, or land use change emissions. The 0.5 x 0.5 degree gridded products were

aggregated by country using population weighting at border grid cells. This aggregation excludes shipping emissions except those that occur within country borders, which are attributed to the country in which they occur. Population data were from NASA's Socioeconomic Data and Applications Center (SEDAC) database and have 0.125 degree spatial resolution (CIESIN, 2005). All calculations are conducted on aggregated data, though we do produce an altered gridded product for the three priorities. Converting aggregated modifications to a grid can result in errors at the border grid cells. These errors are small for large countries and insignificant globally but can be substantial for small countries.

Future projections of emissions under the SSPs were also taken from the input4mips database [36, 37]. Again, gridded N_2O emissions are not available. Therefore, we use global (non-gridded) N_2O projections from the SSP database and assume that each grid cell's fraction of global N_2O emissions remains constant from the most recent EDGAR historical emissions [35]. and scale the most recent emissions accordingly into the future.

We included all economic sectors in the dataset: agriculture, energy, industry, transportation, residential/commercial, solvents, waste, and shipping. The solvent sector has zero BC, OC, SO_2, and NO_x emissions, so it has neither aerosol forcing nor health impacts. However, it does have associated GHG emissions. When maximizing health benefits, the solvent sector is therefore somewhat trivial and will only be targeted after all other options are depleted, since there is no air quality benefit from reducing zero aerosol emissions. However, when minimizing temperature change, zero aerosol forcing is nontrivial since forcing can be positive or negative.

2.3.4 Calculating temperature change from emissions

We convert country-level anthropogenic NCTF emissions to radiative forcing (W m^{-2}) using the same aerosol forcing coefficients as [20], who provide a table for converting emission to global radiative forcing for SO_2, BC, and OC. These coefficients incorporate both the direct and indirect aerosol effects. Strong dependence of aerosol on emission location has recently been demonstrated in coupled earth system models [38]. This variation is partially accounted for

in the table via separate conversions for 12 global regions, though the variation in the table used here is significantly smaller than is shown in [38]. For NO_x emissions, we use the conversion rate used in the Finite Amplitude Impulse Response (FaIR) model [39, 40]. This coefficient does not account for any spatial heterogeneity and only parameterizes the direct effect [30]. After converting emissions to radiative forcing, we convert radiative forcing to global mean surface temperature change using FaIR. As described in the FaIR documentation, we generate an ensemble of 100 combinations of climate parameters and proceed with only those that are constrained by the historical temperature observations provided in FaIR. Using those parameters, we simulate temperature with the RCP8.5 scenario for SSP5 and RCP6.0 for SSP3, but we modified CO_2, CH_4, and N_2O to match our calculated 2000-2030 emissions and add our NTCF forcing calculations as an external aerosol forcing (in lieu of NTCF emissions). We do this for the unmodified case and the three policy priorities. We align simulations with most recent observations (2016). We also conduct the same set simulations again with the NTCF forcing from the unmodified SSP and the GHG emissions from the different priorities; this demonstrates the influence of the GHGs alone (which by definition is nearly identical for the three priorities). This means that there are a total of seven FaIR simulations for each SSP: one with GHG emissions and NTCF forcing from the unmodified SSP, three with GHG emissions from the three priorities and NTCF forcing from the unmodified SSP, and three with GHG emissions and NTCF forcing from the three priorities.

2.3.5 Calculating mortality from emissions

We estimate a country-level conversion of emissions to aerosol concentrations using annual mean, historical (2000-2014) CMIP6 GISS-E2.1 output with one-moment aerosols as available on the MIP database [41, 42]. This model was selected because it has all the desired variables. We use a linear regression between grid-level total emissions and surface-level (i.e. lowest vertical grid cell) concentrations for each country and the resulting slope defines the change in concentration to a change in emission. Our regressions for SO_2, OC, BC, and NO_x

emissions are with surface-level sulfate (SO4), organic aerosol (OA), BC, and nitrate (NO3) respectively. Applying the slope to annual average emissions therefore yields annual average surface concentrations. The coefficients for countries with poor fits (r2¡0.3) or negative slopes are replaced by the coefficients that result from using all land grid cells; this occurs for several small countries and countries with low emissions, causing the relationship to be poorly defined (regression coefficients available - see data availability in Acknowledgements). We also assume that these aerosol species are not coarse mode and therefore that their mass directly corresponds to the concentration of particulate matter with diameter under 2.5μm (PM2.5), a metric which is often used to calculate aerosol-induced health impacts.

Concentrations are converted to premature mortality using a relationship between exposure and the hazard ratio to obtain the attribution function (AF) as explained by [3]. We calculate the slope of the AF at the country's background PM2.5 concentration as determined by model output surface PM2.5. This slope describes the change in the AF with a change in the PM2.5 concentration. Uncertainties are calculated using the slope of the upper and lower bounds of the 95% confidence interval. The premature mortality is then calculated as the product of this slope with the crude death rate of that country, the total population of that country, and the population-weighted mean PM2.5 concentration from the four considered constituents. This methodology includes only the anthropogenic contribution to mortality from the four considered constituents, though it accounts for increased background from other sources. Under these simplifications, we consider the nonlinearity of the health impacts of PM2.5 but do not account for some factors that an epidemiological study would incorporate, such as population age distribution and seasonal PM2.5 variation.

2.4 Results

2.4.1 Sectoral heterogeneity of aerosol impacts

As a reference case and as a backbone for the modified cases, we use unmodified no-policy SSPs. We first look at the sectoral and spatial breakdown of aerosol impacts under these unmodified SSPs. Aerosol radiative forcing can be positive or negative. Therefore, from a global temperature perspective, aerosols can enhance or mask the warming caused by GHGs. Conversely, non-zero aerosol concentrations in populated areas will always produce undesirable health outcomes.

There is substantial variation between sectors and countries of these aerosol climate and health impacts, which illustrates that different countries may require different approaches even if pursuing identical policy objectives for climate or health optimization (SSP3: Figure A2.3; SSP5: Figure A2.4). We find that residential/commercial emissions are often associated with positive radiative forcing, especially in less wealthy countries. Industry and energy sectors are consistently associated with negative radiative forcing. These two sectors also often comprise a disproportionately large fraction of GHG emissions, especially in wealthy countries. Per GHG emission, industry, residential/commercial, and sometimes waste emissions have the largest impact on aerosol exposure since their emissions tend to coincide with high population density. The solvent sector has no aerosol impact because there are no BC, OC, SO_2, or NO_x emissions associated with that sector in the dataset.

2.4.2 Spatial variability of aerosol impacts

Each country's contribution to global radiative forcing from anthropogenic NTCFs and each country's population-weighted surface aerosol concentrations from anthropogenic NTCFs are shown in Figure 2.2, averaged over 2030 under SSP3. They are shown once without normalization with a linear colorbar (a, b) and once normalized by greenhouse gas emissions with a quadratic colorbar (c,d).

We find negative aerosol forcing associated with most countries' 2030 emissions, with the exception of many in Africa (Figure 2.2a). (Figure A2.4 shows the analogous figure for SSP5.) India has the greatest forcing impact (-177 mWm^{-2}), followed by China (-146 mW^{-2}), Russia (-53 mW^{-2}) and the USA (-33 mW^{-2}). In China, the negative forcing from SO_2 emissions slightly outweighs positive forcing from BC, with relatively small additional negative contributions from NO_x and OC. Over half of the SO_2 emissions in China are from the industry sector and almost a quarter are from the energy sector. China's BC emissions are approximately one third from energy and one third from residential and commercial sources. In India, the contribution from SO_2 dominates the forcing since two thirds of the positive BC forcing is already canceled out by the smaller negative forcing from NO_x and OC. Two thirds of India's SO_2 emissions are from the energy sector and a quarter are from the industry sector. The global PM2.5 burden is also dominated by India and China (Figure 2.2b). The largest contributor is NO_x; in China the largest NO_x sources are the industry and energy sectors, and in India the largest NO_x sources are the transportation and energy sectors.

The normalized maps (Figure 2.2 c,d) demonstrate the geographic distribution of aerosol impacts relative to each country's GHG emissions. Highly industrialized countries with large GHG emissions, such as China and the USA therefore have a smaller aerosol impact than many less industrialized countries. Figure 2.2c demonstrates the difference in forcing for Africa compared to much of the rest of the world. For many African countries, BC emissions outweigh the other NTCFs, causing a net positive forcing, which is large relative to those countries' CO_2[e] emissions. A large majority of the BC emissions in those African countries are from the residential and commercial sector. Although the pattern is less pronounced, we draw a similar conclusion from the normalized concentration; less industrialized economies tend to have more aerosol pollution per GHG emission. This representation is less relevant to global decision-making but gives insight into the potential air pollution impacts of changing country-level GHG emissions. The patterns from SSP5 are consistent with those from SSP3 (Figure A2.5).

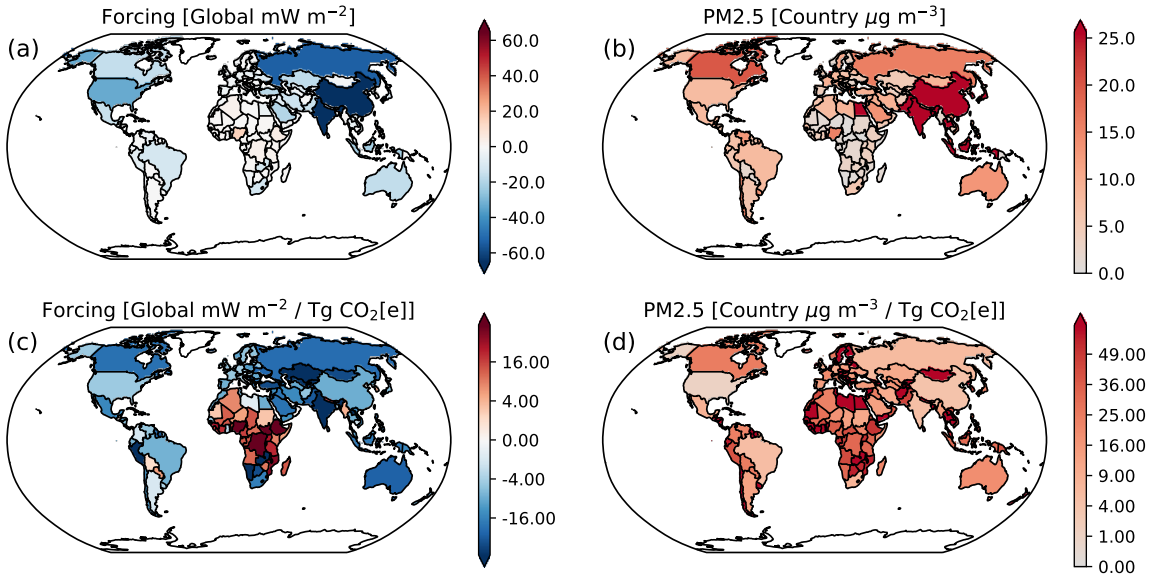

Figure 2.2. Map of annual mean anthropogenic NTCF radiative forcing (a, c) and annual mean surface PM2.5 concentration from NTCFs (b, d) for unmodified SSP3 emissions in 2030. (a, b) show non-normalized data with a linear colorbar; (c, d) show normalized data with a quadratic colorbar.

2.4.3 Global consequences of ambiguity about aerosols

When we implement our three decision priorities for emissions reductions under the Paris Agreement, we demonstrate the range of possible outcomes associated with aerosol ambiguity in the NDCs. These priorities each entail the same CO_2[e] reductions from the Paris Agreement, but prioritize reductions from different sectors, resulting in three different combinations of aerosol emissions for each country.

The net global impact of the three decision priorities is summarized in Figure 2.3. In 2030, we estimate global mean surface temperature increase from preindustrial to be about 1.19 C for SSP3 (Figure 2.3a, gray) and 1.25 C for SSP5 (Figure 2.3b, gray). The temperature change from GHGs alone are nearly identical under the three priorities (Figure 2.3 a,b, dashed lines) because they are all implementations of the Paris Agreement CO_2[e] targets with no modifications to the aerosol emissions. Minor differences are due to some countries (notably China) specifying only CO reductions, not other GHGs, resulting in minor ambiguity even

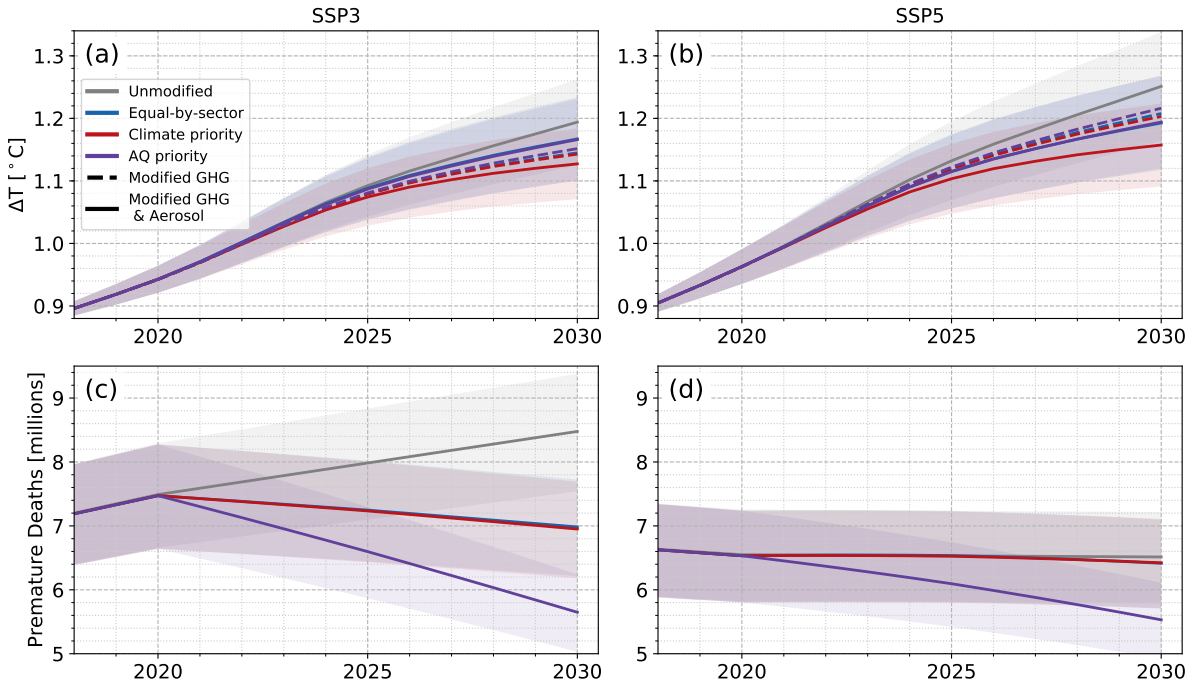

Figure 2.3. Projected global mean surface temperature change from preindustrial (a, b) and global PM2.5-caused premature deaths from anthropogenic NTCF emissions (c, d) for two SSPs (SSP3: a, c; SSP5: b, d). Dashed temperature lines have modified CO_2[e] and unmodified aerosol; solid lines have modified aerosol and modified CO_2[e] (except Unmodified). The equal-by-sector and AQ priorities nearly overlap in (a) and (b). Similarly, the climate priority and equal-by-sector priorities nearly overlap in (c) and (d). The shading for temperature change represents uncertainties in climate feedbacks, calculated as two standard deviations from a FaIR ensemble, and the shading for premature deaths represents uncertainty bounds from the 95% confidence interval of the dose-response curve from Burnett et al. (2018). The shading therefore does not represent random error, but rather a range of possible outcomes.

before aerosols are considered. Despite both being implementations of the Paris Agreement, the resulting temperature change from GHGs differs between the SSPs (Figure 2.3a vs Figure 2.3b, dashed lines), because some countries do not have reduction targets (and therefore follow the no-policy SSP) and some countries benchmark their reduction against "business as usual," which we take to be the no-policy SSP.

Especially for the global temperature time series, the uncertainty bounds overlap between all priorities. This uncertainty reflects the scientific uncertainty of the climate system response to a change in radiative forcing. These uncertainties are therefore correlated, and we would

expect differences between priorities despite the wide range of possible absolute temperature differences from preindustrial. The uncertainty range for premature mortality comes reflects only statistical uncertainty in the dose-response curves derived in epidemiological studies and therefore does not account for emissions uncertainties, model uncertainties, or parameterization errors. Therefore, the presented uncertainty range for premature mortality is also not random.

When countries optimize for their own air quality (purple, solid), global temperature is higher than it is under other priorities, though for both SSPs it is nearly identical to the outcome from the equal-by-sector priority. By definition, the climate priority has the lowest temperature in 2030 for both SSPs, and the magnitude of the difference is fairly large: -0.02°C (SSP3, red dashed vs solid) and -0.05°C (SSP5, red dashed vs solid). For comparison, the CO_2[e] reductions cause about -0.05°C (SSP3, blue dashed vs gray) and -0.04°C (SSP5, blue dashed vs gray). Therefore, the temperature change associated with the range of potential aerosol emissions under the Paris Agreement may be as large as the temperature reduction from its associated greenhouse gas reductions. [43] estimate changes to short-lived pollutants would cause -0.03°C, which is somewhat lower than our estimates. This is unsurprising considering that the bounding priorities explored here are only constrained by CO_2[e] emissions, not by other economic and political factors.

Estimated global aerosol-induced premature deaths are shown in Figure 2.3 c,d. In 2015, we calculate about 6.8 million premature deaths (SSP3 and SSP5), which is of a similar magnitude, but slightly slower than the 8.9 million calculated by [3], likely in part because our estimate does not include all sources of PM2.5. The AQ priority has the lowest mortality by definition and there are substantial differences between the three priorities. For both SSPs, the equal-by-sector priority results in more premature deaths from air pollution than either of the other priorities. The difference between equal-by-sector and AQ priority are 1.3 million (SSP3) and 0.9 million (SSP5) premature deaths in 2030. For SSP3 the equal-by-sector priority is less desirable from a global standpoint than the climate priority, since it contains neither the temperature nor the health benefits of aerosols. This result suggests that a politically expedient

approach of reducing emissions from all economic sectors equally may come at a substantial cost to health and climate outcomes.

2.4.4 Tradeoffs between air quality and cooling

To better evaluate potential tradeoffs between air-quality-optimized and climate-optimized NDC implementations, we explored regional differences in outcomes for our three policy priorities. Figure 2.4a shows the tradeoffs between premature mortality from aerosol pollution and global temperature increase (ΔT) as policy priorities shift (SSP5: Figure A2.5). (To obtain an approximate estimate of the regional contribution to global ΔT, we assume linearity and scale the global ΔT with the country-level aerosol forcing.) The tradeoffs between health and climate tend to be smaller in regions of the world with more existing pollution control like Oceania, North America, and Europe (Figure 2.4b; SSP5: Figure A2.6).

The attractiveness of the equal-by-sector priority in terms of climate and health outcomes varies considerably by region. In some regions, such as Europe, North America and Asia (excluding China), it improves upon air quality outcomes relative to the climate priority, and it improves upon temperature outcomes relative to the AQ priority. Under these circumstances, whether such an option is attractive will depend on the perceived political or other benefits of a sectorally equitable climate policy approach. However, for some regions (i.e. Africa, Middle East, China), an equal-by-sector priority results in both climate and air quality outcomes that are inferior to those in one or both of the other prioritizations (a dominated option). In these regions, avoiding a climate policy approach which simply mandates equal cuts across all sectors would have clear health and climate benefits. In other words, a lack of a deliberate consideration of aerosol consequences in climate policy would be more consequential for African, South American, and Middle Eastern countries.

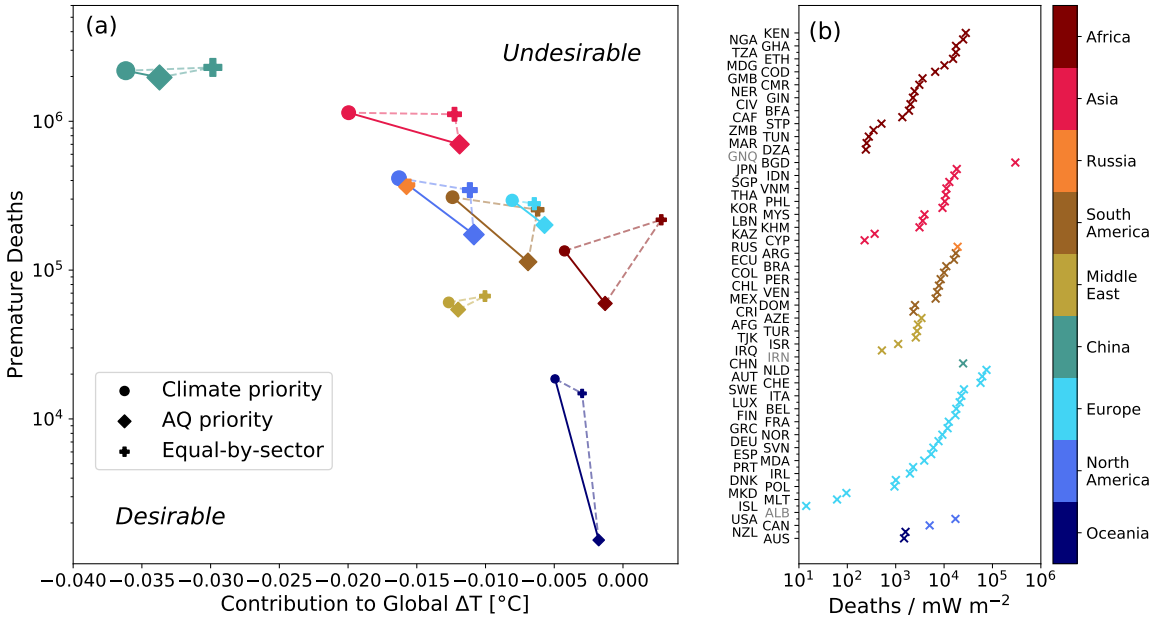

Figure 2.4. Tradeoff between air quality optimization and temperature optimization of NDCs for SSP3. (a) contains the regional sum of estimated anthropogenic PM2.5 premature deaths and contribution to global temperature change. Marker area is proportional to CO_2[e] emissions of each region. (b) shows air pollution deaths / mW $^{-2}$ of cooling moving between climate priority and AQ priority country-level slopes of the solid lines in panel (a). Panel (a) only includes the countries with explicit goals, which are the same countries as shown in panel (b). Gray country names indicate zero or undefined slopes (i.e. death or forcing difference between the two priorities are very nearly identical.

2.5 Discussion and Conclusion

Having made GHG emissions reductions commitments under the Paris Agreement, countries are now faced with numerous pathways to meet self-imposed targets. We estimate outcomes associated with three imagined policy priorities that are all consistent with the NDCs. Incorporating co-emissions into an NDC assessment framework introduces the possibility of both co-benefits and negative side effects in meeting the temperature targets specified in the Paris Agreement. On short time scales, the global temperature ambiguity from the aerosol co-emissions is of a similar magnitude to the temperature changes from GHG emissions reductions commitments. Metrics like GWP*, which uses cumulative CO_2 emissions and current emissions of short-lived pollutants to quantify temperature impacts, could be a practical way to include the temperature impact of non-GHG emissions in NDCs [25, 44], but may obscure substantial tradeoffs between additional marginal decreases in temperature and reductions in health impacts.

While previous work has highlighted opportunities for co-benefits in decarbonization [45, 46, 20], our analysis does indicate some considerable tradeoffs between temperature and health outcomes will need to be contended with in meeting near-term emissions reductions goals. For some regions, it is unclear which of the presented priorities are preferable. Finding an acceptable solution would require value judgements about the relative benefits of local avoided PM2.5 mortality, global temperature change and political expedience. However, the tradeoff varies by several orders of magnitude (Figure 2.4b), so it would be surprising if all countries had the same priorities for weighing temperature versus health when making aerosol policy decisions. A simple policy of requiring equal emissions reductions from all economic sectors is in some cases not a compromise between the two criteria, but rather could lead to an objectively less beneficial outcome than a more targeted prioritization of either health or temperature co-benefits. We believe that this is a strong case for explicitly considering aerosols when constructing climate policy.

The presented methodology requires many simplifications of the complexities of aerosols.

We use simple parameterizations of aerosol chemistry, physics, and transport, in addition to simple relationships between exposure and premature mortality. We also examine extreme policy priorities that are only constrained by the Paris Agreement NDCs and not other economic and technological factors. Importantly, our analysis does not include any cost optimization – a dominant consideration in many climate policy discussions.

We consider four NTCFs (BC, OC, SO_2, NO_x); other NTCFs like ozone were not considered in our analysis, and ozone presents its own set of complexities [47]. We also do not consider the impacts of changes to pollution transport between countries or altered dynamics that can arise from local differences in radiative forcing if countries pursue different policies [48, 49]. Assuming a continued global trend of reductions in NTCFs, the impact of aerosols would diminish in longer term projections due to air quality regulation and technology changes [50, 51]. Projections tend to agree that NTCFs will decline over time, but here are many uncertain factors that will determine their future emissions pathways, even in the absence of climate policy.

Other sources of uncertainty that are not considered as part of this analysis include, but are not limited to, uncertainty in the magnitude of aerosol forcing and uncertainty in emissions inventories. Multiple estimates of radiative forcing per emission exist (Table A2.2), and the choice of these estimates does have some impact on our analysis (Figures A2.7, A2.8). Choice of forcings alters the temperature change estimates provided here, but not the fundamental character of tradeoffs. For all the above reasons, we do not interpret the absolute magnitude of our results as a precise estimate of future aerosol impacts of the NDCs. Instead, we believe that this study better demonstrates relative impacts and the importance of policy priorities and tradeoffs for co-emissions in international climate policy.

We illustrate the range of global temperature and mortality impacts associated with anthropogenic aerosol changes that result from countries meeting their Paris Agreement greenhouse gas targets by 2030. In a world with fully implemented NDCs, ambiguity about the associated aerosol emissions contributes to uncertainty about global mean temperature in 2030 of the same magnitude as the expected temperature reductions from decreased greenhouse gas emissions. The

differences in mortality between the different pathways to meeting the NDCs are substantial and premature deaths due to PM2.5 could differ by more than a million people annually, illustrating the potential dangers of not considering aerosol-driven outcomes when setting climate policy.

2.6 Acknowledgements

The authors thank Massimo Tavoni for helpful feedback about this study. Pascal Polonik and Jennifer Burney are supported by NSF CNH-L #1715557 and the Robert Wood Johnson Foundation #76555. This chapter, in full, is a reprint of the material as it appears in AGU Earth's Future 2021. Polonik, Pascal; Ricke, Katharine; Burney, Jennifer. AGU, 2023. The dissertation author was the primary investigator and author of this paper.

2.A Appendix for Chapter 2

Gridded emissions (netCDFs) and the data used for Figure S3 and Figure S4 (csv table) are available for download here: https://dataverse.harvard.edu/dataset.xhtml?persistentId =doi%3A10.7910%2FDVN%2FFP0QTX&version=DRAFT. The rest of this document contains eight figures and two tables that supplement the main text of the manuscript. They occur here in the order that they are referenced in the main text.

Table A2.1. Mapping of CEDS sector to EDGAR name

CEDS sector number	EDGAR sector name
0	4B, 4C, 4D3
1	1A1b, 1A2, 1B1a, 2B
2	1A3a, 1A3b
3	1A3a, 1A3b
4	1A4
5	3.
6	6A, 6B, 6C
7	1A3d

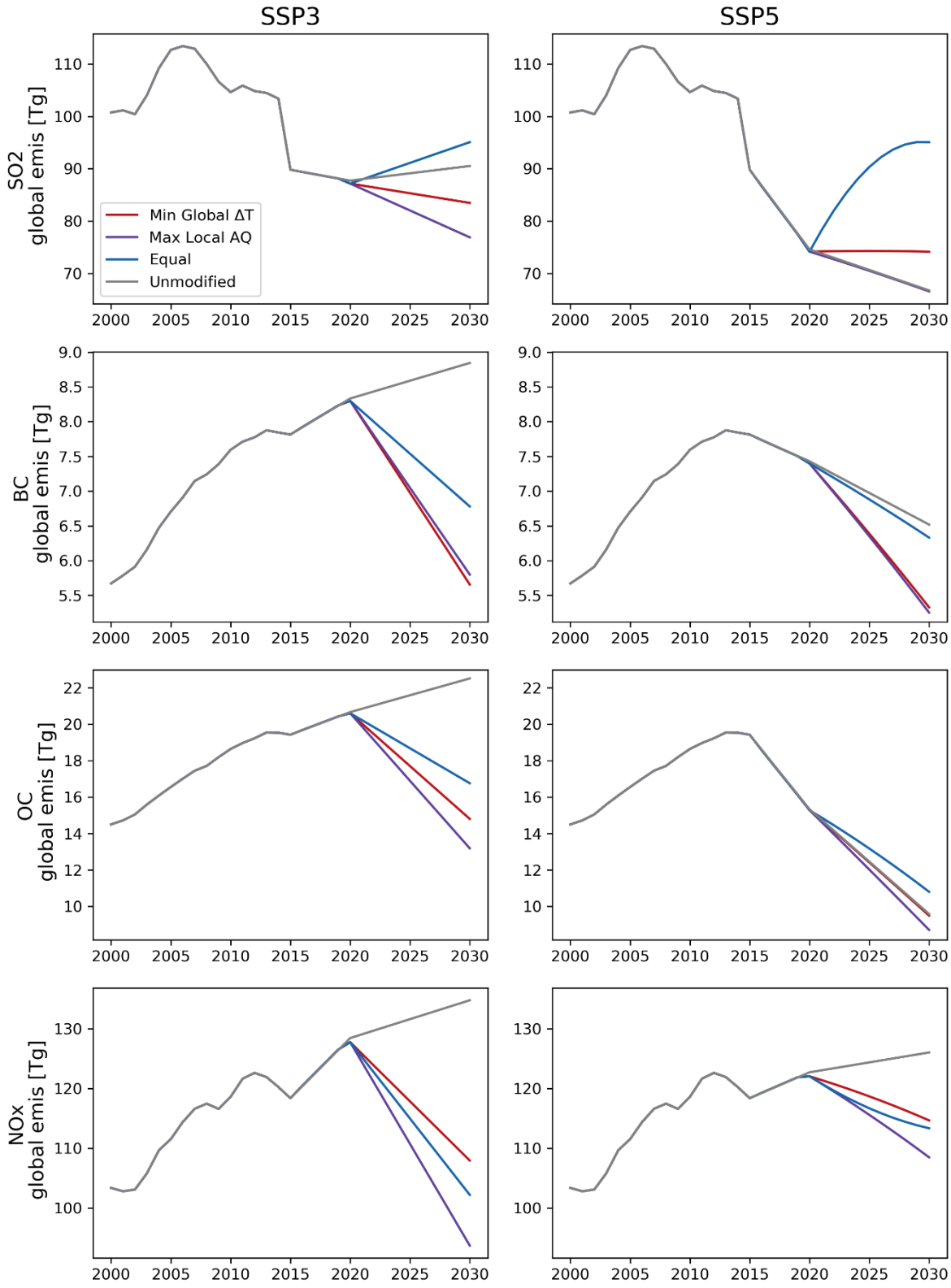

Figure A2.1. Global emissions of four NTCFs (rows) for two SSPs (columns) under the three priorities (colors) and the unmodified case.

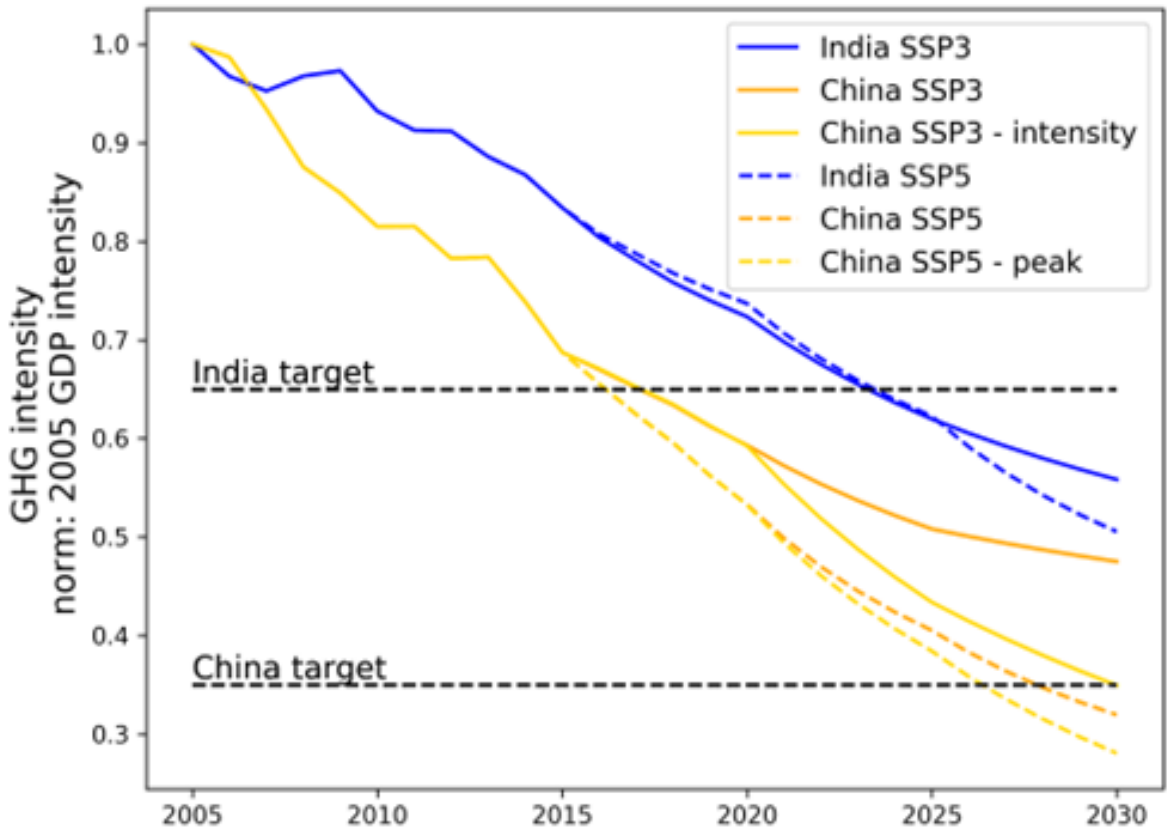

Figure A2.2. Normalized GHG intensity (India: CO2e/GDP; China: CO2/GDP) that demonstrates whether targets are met without explicit climate policy. We use the unmodified SSP for India because targets are met regardless. We use the peaking target for China SSP5 since it is more ambitious than the intensity target and the unmodified SSP. For China SSP3 we implement the intensity target.

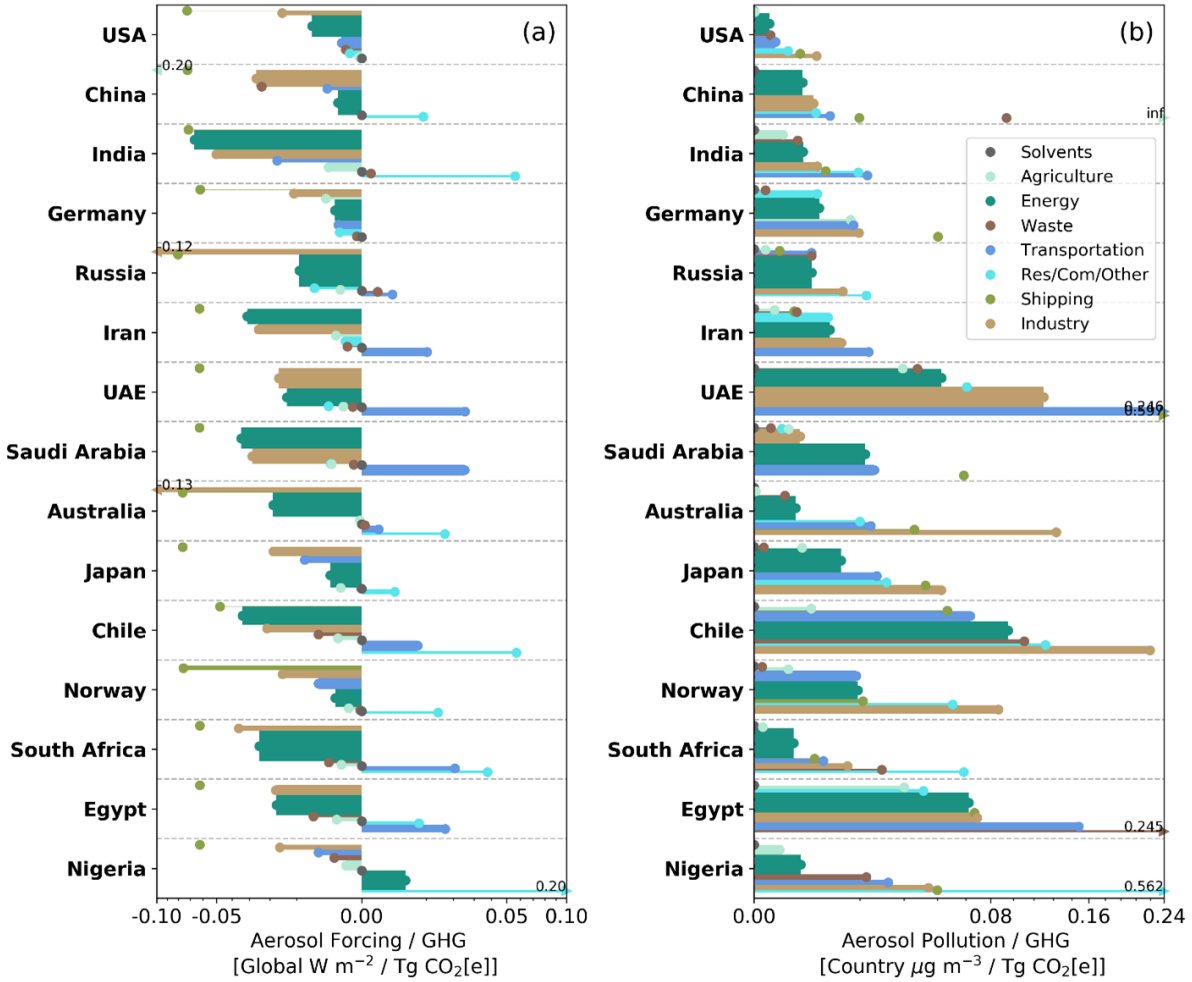

Figure A2.3. (a) Aerosol radiative forcing and (b) population-weighted additional aerosol concentration. Both are normalized by CO2[e] emissions, grouped by economic sector and only shown for select countries. Both x-axes are quadratic. Vertical bar width indicates the sector fraction of CO2[e] emissions for each country. Calculations based on unmodified SSP3 no-policy baseline emissions. Dots and bars provide identical information; dots help visualize very thin bars.

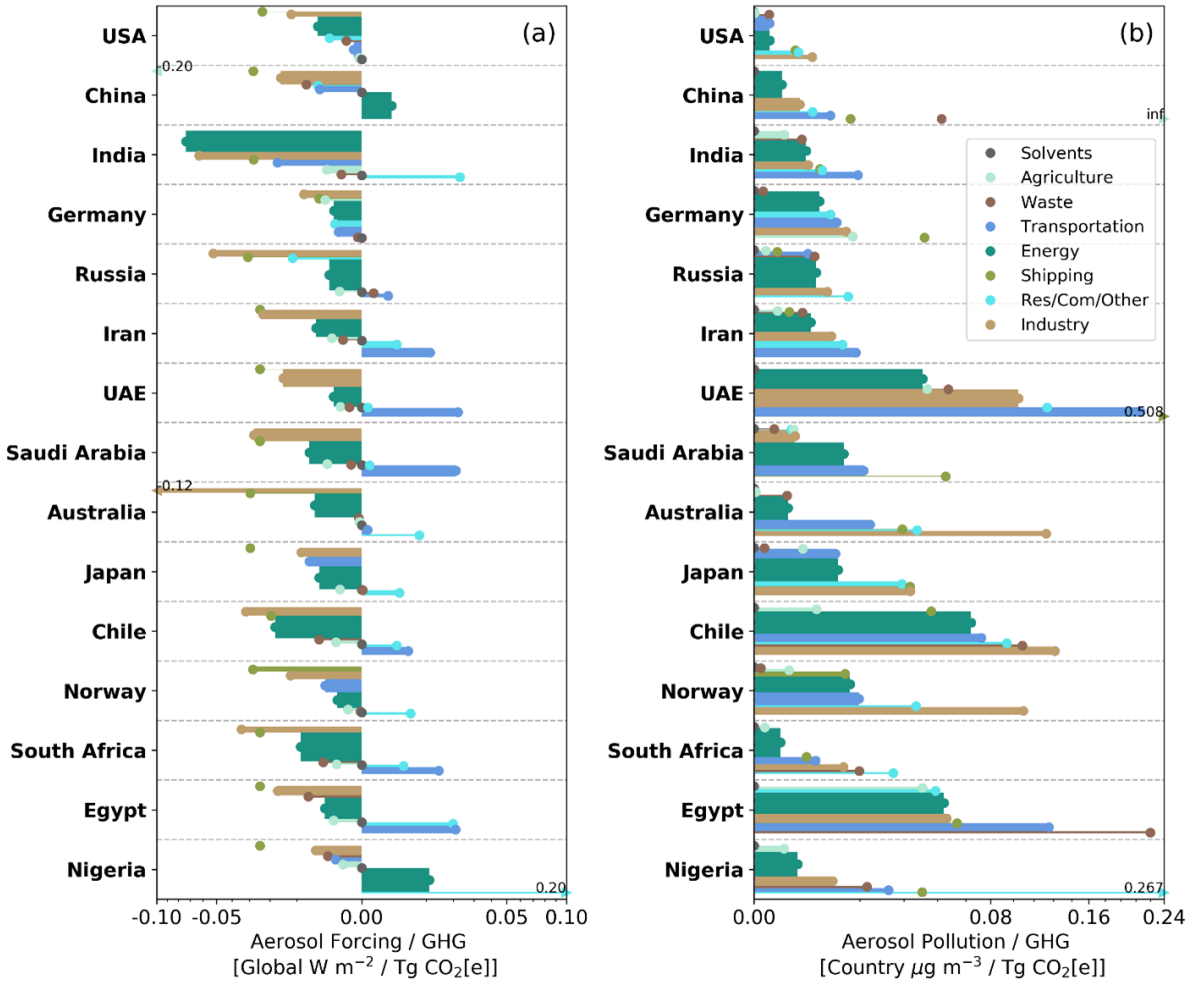

Figure A2.4. Same as Figure S3, except SSP5 instead of SSP3.

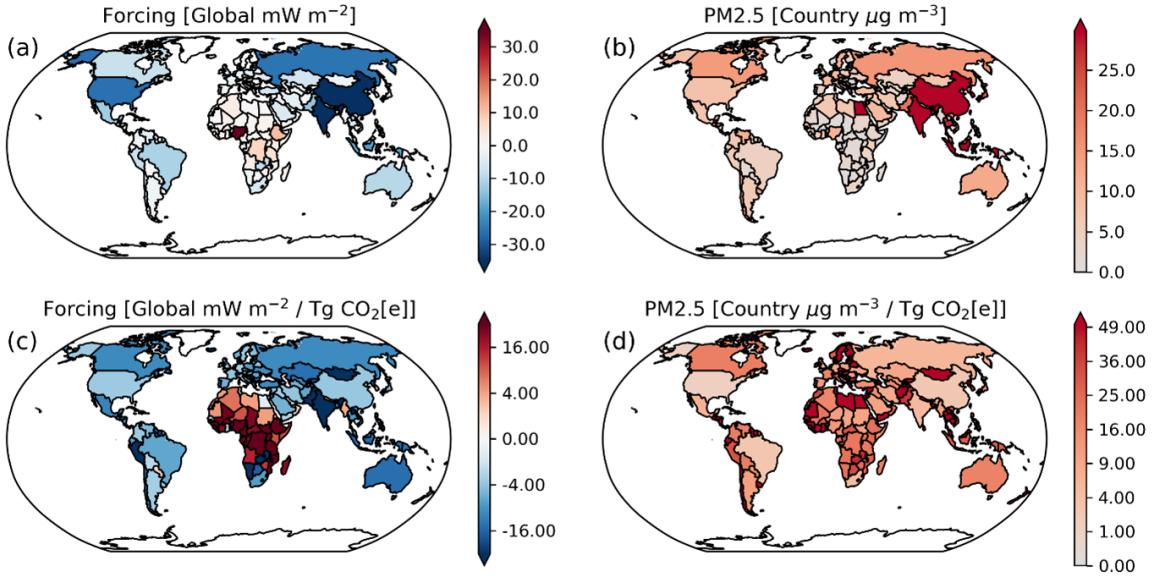

Figure A2.5. Figure S5. Same as Figure 2, except SSP5 instead of SSP3.

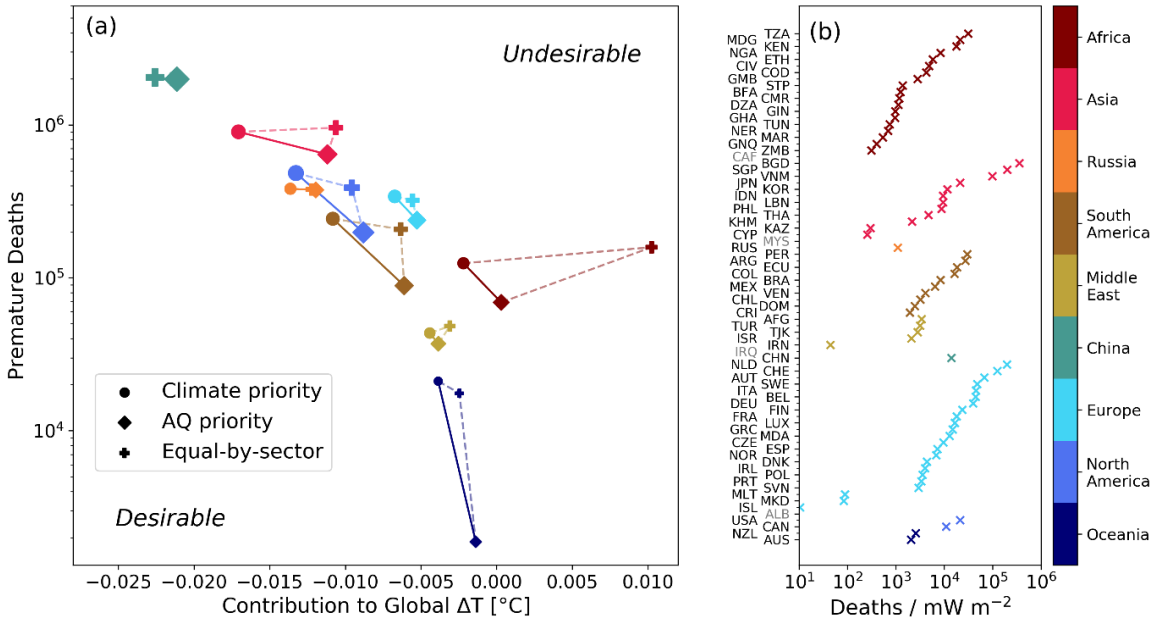

Figure A2.6. Same as Figure 4, except SSP5 instead of SSP3. Notice differences in axis limits in (a).

Table S2 compares aerosol radiative forcing as described by the FaIR climate model (version 1) and Scovronick et al. (2019). The table provides justification for the values used in the main text and highlights the forcing uncertainties associated with aerosol emissions. Here we provide a full description of how each of the values in the able was derived. FaIR: Direct forcing is given by a constant in the FaIR code. These constants are repeated in the table. Indirect forcing is calculated through a logarithmic relationship with SOx, OC, and BC emissions (constants rounded): RF_indirect_FaIR(SOx, BC, OC) = -1.95 * log(1 + 0.011*SOx + 0.014*(BC+OC)) + 0.30. Where SOx, BC, and OC are the global emissions (in Gt/yr) of each species. An option exists to scale the result to match AR5 but it is off by default, so we do not apply that option here. To calculate the marginal impact of 1 Gt of emissions on the indirect effect we remove 1 Gt of the species of interest and evaluate the difference (e.g.): RF_SOx_marginal = RF_indirect_FaIR(SOx, BC, OC) – RF_indirect_FaIR(SOx-1, BC, OC) We then sum the direct and marginal indirect forcing and multiply by the global emissions to obtain a global forcing for each species. We use global CEDS emissions from 2014 as in the main text. Scovronick et al. 2019: We use the forcing intensity (W/m2/Gt) provided in supplementary Table 3. These values provide some regional specificity, though as acknowledged in the main text, this variation is likely insufficient. These values are derived from MAGICC6 simulations in which small amounts of regional emissions are removed and the difference in global forcing is evaluated – analogous to our simple application of FaIR above. To obtain one global value for the table instead of regional values, we take the mean, weighted by the emissions in each region. To scale the forcing intensity to global forcing, we again multiply by global 2014 CEDS emissions. AR5: The global forcing values are taken from AR5 directly (p.683). Unfortunately, these are not directly comparable to the other two forcing values as they are only for the direct effect and account for preindustrial forcing. However, AR5 estimates direct and indirect forcing to be about the same (-0.45 W/m2 for both, p. 696) and preindustrial forcing is relatively small, which does allow us to roughly gauge a comparable magnitude. Implications for our study: Scovronick et al. provides the added benefit of accounting for some regional variation, which makes it preferable over an approach that

only uses FaIR. However, the NOx forcing from Scovronick et al. is several factors higher than expected based on FaIR and AR5, so we use the global value from FaIR for all regions instead. This comparison highlights that complicated nature of and scientific uncertainty around aerosol forcing, which make simple parameterizations difficult. For completeness we include replicates of Figures 3 and 4 below with the much larger NOx conversion from Scovronick et al. (2019), as Figures S7 and S8.

Table A2.2. Aerosol forcing differences between Scovronick et al. (2019) and FaIR. See full description above.

	FaIR ($W/m^2/Gt$); Direct (indirect) =total	Scovronick et al. (2019) ($W/m^2/Gt$)	Emissions (Tg=Gt, 2014 CEDS)	Scaled global FaIR (W/m^2)	Scaled global Scovronick et al. (2019) (W/m^2)	AR5 Direct only (W/m^2)
SO2	-.0062 (-0.0083) =-0.014	-0.011	112	-1.62	-1.22	-0.40
BC	+0.016 (-0.010) =0.0057	0.075	8	+0.045	+0.60	+0.40
OC	-0.0015 (-0.010) =0.012	-0.010	20	-0.23	-0.20	-0.09
NOx	-0.0012 (-0.00) =-0.0012	-0.0057	140	-0.16	-0.79	-0.11

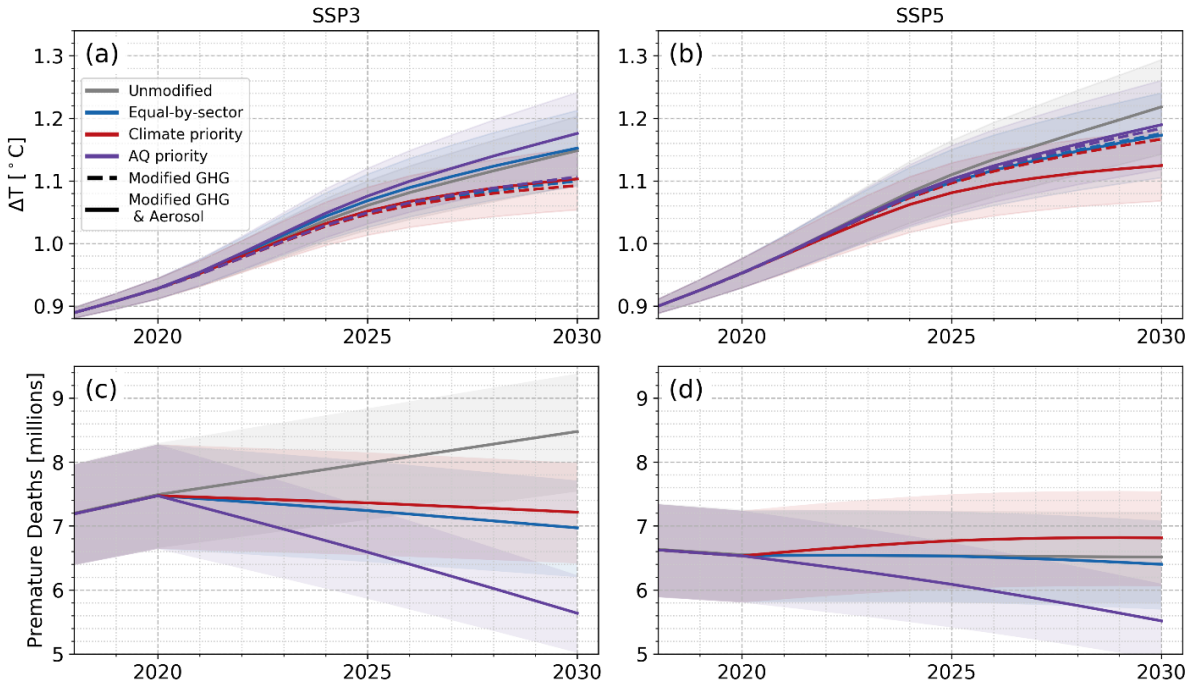

Figure A2.7. Figure S7. Same as Figure 3, but using the NOx conversion factor for Scovronick et al. (2019).

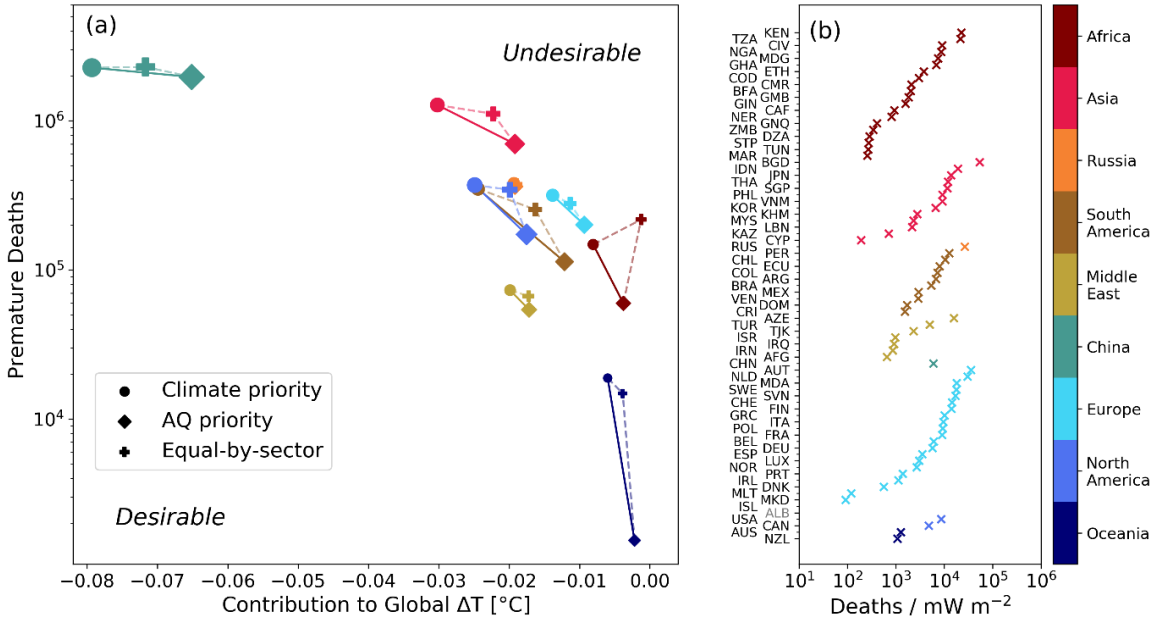

Figure A2.8. Same as Figure 4 (SSP3), but using the NOx conversion factor for Scovronick et al. (2019).

Chapter 3

Air Quality Equity in U.S. Climate Policy

3.1 Abstract

The United States government has indicated a desire to advance environmental justice through climate policy. As fossil fuel combustion produces both conventional pollutants and greenhouse gas emissions, climate mitigation strategies may provide an opportunity to address historical inequities in air pollution exposure. To test the impact of climate policy implementation choices on air quality equity, we develop a broad range of greenhouse gas reductions scenarios that are each consistent with the U.S. Paris Accord target and model the resulting air pollution changes. Using idealized decision criteria, we show that least cost and income-based emission reductions can exacerbate air pollution disparities for communities of color. With a suite of randomized experiments that facilitates exploration of a wider climate policy decision space we show that disparities largely persist despite declines in average pollution exposure, but that reducing transportation emissions has the most potential to reduce racial inequities.

3.2 Introduction

After rejoining the Paris Climate Agreement in 2021, the United States (U.S.) submitted an updated Nationally Determined Contribution (NDC), providing a vision of how the U.S. intends to cut greenhouse gas (GHG) emissions in the coming decades. The NDC set a target of 50-52% reduction of net greenhouse gas emissions by 2030 compared to 2005. Beyond its

quantitative targets, the NDC explicitly identifies climate policy as an opportunity for furthering environmental justice goals, stating, "Each policy considered for reducing emissions is also an opportunity to improve equity and support good jobs in the United States" [52]. In an effort to meet these targets, the U.S. recently passed the Inflation Reduction Act (IRA)[53], which promotes emission reduction largely through financial incentives, and aims to invest in disadvantaged communities by providing funds for financial and technical assistance for zero-emissions technologies, grants for community-led projects, and funding to reduce air pollution where pollution exceeds national standards. Many details for implementation of the IRA are unresolved, making technical strategies for satisfying its objectives particularly salient.

GHG emissions are often co-emitted with criteria pollutants, which damage human health [3, 54]. These pollutants sometimes consist of, or subsequently form, fine particulate matter (PM2.5), which causes and exacerbates a wide variety of other health conditions [55], and leads to more than 100,000 premature deaths in the U.S. annually [56]. It has been repeatedly demonstrated that the burden of air pollution is not experienced equally among demographic groups in the U.S. [57, 58, 59]. While reductions in GHG emissions would be expected to improve average air quality, bestowing a wide array of health, economic and other benefits [60, 61], reductions in air pollution disparities are not guaranteed. While previous studies agree that reductions in GHG emissions are associated with air quality co-benefits, they disagree about the impact on racial disparities - some finding substantial improvements and others finding little change [62, 63, 64]. Furthermore, these previous studies are geographically limited to California and explore equity co-benefits as a byproduct of climate policies rather than an explicit decision criterion.

Here we first contextualize the current state and recent trends of national and state-level air quality disparities using existing best-estimates of PM2.5 concentrations across the contiguous U.S. We then use a harmonized dataset of GHG and criteria air pollutant (CAP) emissions sources as a baseline from which we can model the impact of changing greenhouse gas emissions on CAP emissions. We use this dataset to generate two types of illustrative NDC-constrained emissions

pathways, each of which represents a 50% reduction in total U.S. greenhouse gas emissions with varying magnitudes and spatial distributions of co-emitted criteria air pollution. We simulate outcomes of these pathways using an air quality model InMAP [65], which provides spatially explicit maps of PM2.5 concentrations that result from specified emissions. We then aggregate these concentrations by race and ethnicity at state and national levels to assess impacts on both average exposures and exposure disparities. We also estimate costs for each pathway using a bottom-up approach for each sector independently that accounts for factors including up-front capital costs, regionally varying fuel costs, and estimates of operations and maintenance costs. More detail is available in the Methods and the Supporting Information (SI).

Our first set of pathways meet the U.S. NDC by applying highly idealized decision criteria, targeting reductions based on e.g., income, race, or economic efficiency. In these pathways, we sort national emissions by the physical or socioeconomic characteristics of their source location and then remove GHG and co-pollutant sources from the top of the sorted list until the national GHG target is met. These represent extreme cases where national policy is carried out cohesively under one specific priority by removing all emissions from: the most polluted regions (henceforth referred to as, *PM2.5 Exposure*), the neighborhoods with the highest fraction people of color (henceforth, *POC*), the lowest income communities (henceforth, *Income*); and by removing the cheapest to abate carbon emissions (henceforth, *Least cost*). For example, in the *Income* pathway, we sort emissions by county-level median income and then remove all sources from the lowest income locations until the GHG target is met. The *Equal* pathway is the exception; we reduce greenhouse gas emissions proportionally by the same fraction from all point and non-point sources by an equal percentage such that the GHG target is met, reducing co-emitted CAP emissions simultaneously. The second set of simulations meets the NDC by randomly reducing emissions from different sectors and regions to explore air quality impacts and tradeoffs of a more idiosyncratic implementation of climate policy (see Methods). As a reference, we also simulate the air quality using the unmodified 2017 National Emissions Inventory (NEI) for all available emissions except those involving fires, which we refer to as Unmodified 2017.

Raw output concentrations do not match with observations for several reasons, including poorly constrained emission inventories, imperfect model parameterizations, simplified meteorology, and notably the omission of mostly non-anthropogenic emission sources like forest fires, agricultural burning, sea salt, and desert dust (Figure A3.11). We therefore bias-correct our results using best available estimates of PM2.5 ([65], see Methods) and present results as differences between simulations. Because anthropogenic and non-anthropogenic emissions are not fungible in their policy relevance, non-bias-corrected results are presented in the SI. We present results both as exposures and as disparities; exposure is defined as the population-weighted mean PM2.5 concentration, and disparity is subsequently defined as the percent difference between a given demographic's exposure and the population average exposure; both are calculated at national or state levels. A positive disparity means that a group is disproportionately impacted, and a decrease in disparity requires that a demographic has a larger reduction in exposure than the population average.

The combination of observations and simulations of PM2.5 concentrations, aggregated into exposures and disparities, allows us to quantify past and potential future air quality and air quality equity impacts of changing emissions.

3.3 Results

For context, we first quantify historical air quality disparities in PM2.5 exposures over the contiguous U.S. Disparities are pervasive across racial and ethnic minority groups nationally and across the vast majority of U.S. states (Figure 3.1a) and although overall air quality in most of the U.S. improved over the past decade, disparities have generally increased. Intuitively, the national average exposures for each demographic group are driven by the major population centers of those groups, which differ considerably for Asian, Black, and Hispanic communities (Figure 3.1b). We find increases in disparities for people of color nationally and in 37 of 48 states. Previous work has also found increasing disparities over time using different metrics and

datasets [66]. Sensitivity analyses like removing low density census tracts yield consistent results (Figure SA3.2). In this context of deepening environmental inequities we look to understand the extent to which equity can be enhanced in parallel with GHG-mitigating climate policy.

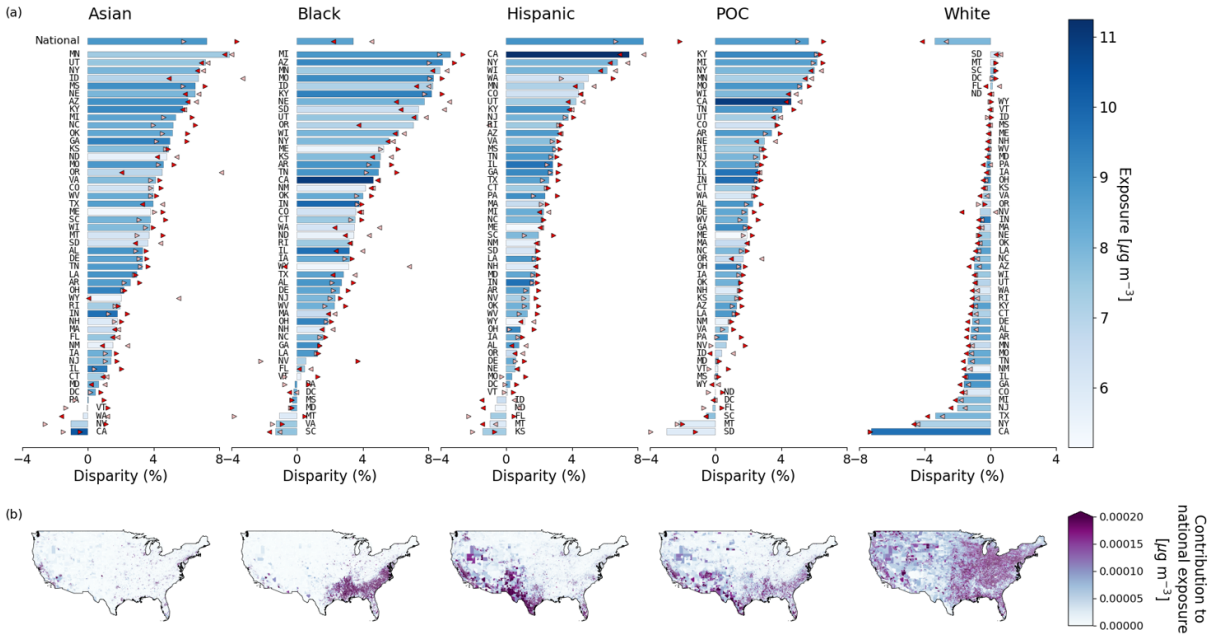

Figure 3.1. National and state-level relative disparities in air pollution exposure by race and ethnicity in the contiguous United States. (a) Bars indicate national (top) and state-level disparities for each racial/ethnic group. The bar color indicates the average absolute exposure to respirable particulate matter (PM2.5) of each group within each state in the 2010s. The red triangles show 2010 (light red) and 2019 (dark red) disparities, estimated from fitting a linear trend through annual disparities. (b) Maps of the contribution of each tract to national disparities, which is calculated as the product of tract PM2.5 concentration and the population of the specified group in each tract, divided by the total national population of that group. The sum of the national contributions values yields the population-weighted exposures for each group.

To quantify how these disparities and exposures might change under climate policy, we model several idealized pathways to meet the national GHG emission reduction target. As described above, we target counties with high historical pollution, high fraction people of color, low income, lowest cost of mitigation, and by equal fraction without any prioritization. We then simulate the air pollution distributions resulting from the new NDC-constrained emissions using InMAP. Output is aggregated to tracts, bias-corrected, and used to calculate exposures and disparities of five racial/ethnic groups (see Methods).

Every NDC-constrained pathway we constructed would reduce national PM2.5 exposure relative to the present day (Unmodified 2017), but reductions vary by 10-15% (between 0.8 and 1.2 μg m^{-3}, Figure 3.2a). Estimated annualized costs for these pathways vary substantially, between about $190 billion to $340 billion, where the *Least cost* pathway is much less expensive than the rest (Figure 3.2c; uncertainty analysis in Figure SA3.3). Despite large methodological differences, the emission reductions in our *Least cost* pathway are largely consistent with the results from integrated assessment models (IAMs), which simulate coupled energy systems [67]. As shown in those models, we also find that reducing the majority of emissions from power plants and the transportation sector is required to meet targets and is more economical than decarbonizing other sectors (Figure SA3.4).

In all pathways, White communities continue to experience lower-than-average exposures while Asian and Hispanic communities continue to experience higher-than-average exposures (Figure 3.2b), though absolute exposures decline in all cases (Figure 3.2d). This highlights that the air quality co-benefits of implementing the U.S. NDC are alone insufficient to overcome the long and pervasive history of disproportionate environmental impacts on minority communities [57, 68]. National Black disparities consistently decline in all pathways, largely because anthropogenic emissions lead to more air pollution in the Eastern U.S. (Figure SA3.1a), where Black people make up a larger portion of the population. Since these emissions must be reduced to meet the NDC, the pollution in the Eastern U.S. declines disproportionately. This finding is consistent with recent historical trends (Figure 3.1). We note however, that the magnitude of the national Black disparities depends strongly on the bias correction, which incorporates missing non-anthropogenic emission sources as well as model biases. When considering only uncorrected anthropogenic emission from the EPA inventory, Black communities are the most disproportionately impacted group by a substantial margin and the pathways have little impact on the total disparities (Figure SA3.5), highlighting the potentially consequential influence that inclusion of non-anthropogenic sources in air quality baselines could have on setting national scale air quality equity priorities.

Substantial variation in disparities (Figure 3.2a, 3.2b) and exposures (Figure 3.2c, 3.2d) exists between pathways, ranging from -2 to 0% for Black communities and 8 to 12% for Hispanic communities (Figure 3.2b). A national prioritization of emission reductions in communities of color (*POC* pathway) is the only pathway explored here that reduces disparities for all non-White groups. While in some cases climate policy can be used as a means to reduce inequity in air pollution exposure in the U.S., there is no guarantee that cutting GHG emissions will lead to that result. Indeed, relative to the baseline represented by Unmodified 2017, inequities can be amplified under certain climate policy priorities, including two pathways that represent economically and politically favorable priorities: the *Least cost* pathway, and the *Income* pathway, which prioritizes low income communities - a common proxy for racial and ethnic dimensions of environmental injustice, including in contemporary climate-related regulations [53].

For all demographics, the exposure reduction from implementing any iteration of the NDC is larger than the variation between the different idealized pathways (Figure 3.2a), emphasizing the robust air quality co-benefits of GHG emission reductions. State exposures and disparities are affected similarly to the national exposures and disparities (Figure SA3.6); exposures decline, while disparities remain roughly constant.

For comparison, we also conducted No Industry and No Agriculture simulations, which are not constrained by the NDC, and therefore have quite different GHG emissions reductions than the NDC-constrained pathways. These sectors are not comprehensively represented in our pathways due to both current technological limitations for decarbonization and practical data limitations, so to illustrate that their omission does not drive our finding of residual disparities, we demonstrate their individual impacts by modeling PM2.5 distributions without their criteria pollutant emissions. Completely removing the emissions from these sectors does not diminish disparities, though it would convey large total air quality benefits.

We next implemented a set of 300 randomized climate policy experiments, still constrained by the NDC, but no longer based on idealized decision criteria. Instead, GHG emissions and their accompanying co-emissions are randomly removed throughout the country until the

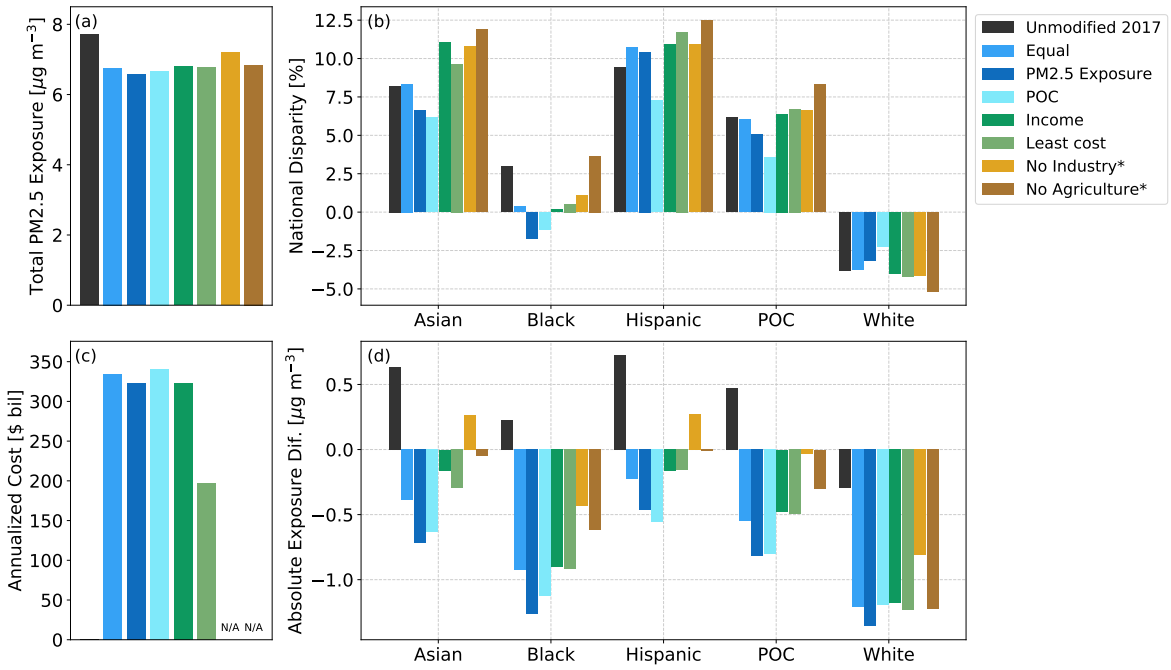

Figure 3.2. Exposures and disparities of PM2.5 after implementing idealized policy priorities to meet emission reduction targets. (a) Total average national particulate matter exposure, (b) national disparities by demographic group, (c) annualized costs of mitigation, and (d) absolute exposure difference by demographic group. Absolute exposure difference refers to the difference in exposure from the Unmodified 2017 total exposure in (a). All pathways lead to reductions in absolute PM2.5 exposures and entail annualized costs of $190-340 billion. The No Industry and No Agriculture simulations, marked with asterisks, are not NDC-constrained and do not have cost estimates.

NDC target is met (see Methods). The randomly removed emissions are by design less targeted than the idealized pathways and therefore the variation in total and demographic-specific exposures between the randomized experiments is roughly half as large as from the idealized decision pathways (Figure SA3.7). However, this spread still allows us to explore relationships (or lack thereof) between the properties of different pathways and their outcomes.

For example, there is little correlation between national POC pollution exposure and national policy cost (Figure 3.3a), implying that it may be possible to implement national GHG emission reduction while optimizing air quality equity, without substantially increasing costs. However, as shown using the minimum cost pathways above, simply ignoring the equity dimension and focusing entirely on cost can still worsen air quality disparities, so implementation would need to be sectorally and spatially targeted. We also show that residential electrification is largely responsible for higher pathway costs (Figure 3.3a), though industry also contributes to a lesser extent (Figure SA3.8d). The strong correlation between total population exposure and national POC exposure (Figure 3.3b), indicates that these two outcomes are tightly coupled across pathways. However, residual variation in POC exposure is strongly associated with the magnitude of emissions reductions from the transportation sector. The reverse pattern is true for the electricity sector (Figure SA3.8g), in part because electricity and transportation are the largest sources of greenhouse gas emissions, so NDC-constrained random pathways with high transportation emission reduction are also associated with low electricity emission reduction.

Transportation emissions drive differences in disparities between randomized pathways, as illustrated in Figure 3.4, which summarizes the national and state disparity changes and shows the impact of removing transportation emissions on exposures and disparities (Figure 3.4c,f). Since each randomization includes a different combination of sectoral reductions, we are able to demonstrate that transportation reductions reduce disparities and exposures disproportionately for people of color (changes from all sectors are shown in Figure SA3.9). Each randomization is associated with a new set of national disparities (Figure 3.4a). Black disparities decrease relative to present day, while Hispanic and Asian disparities increase, and POC and White

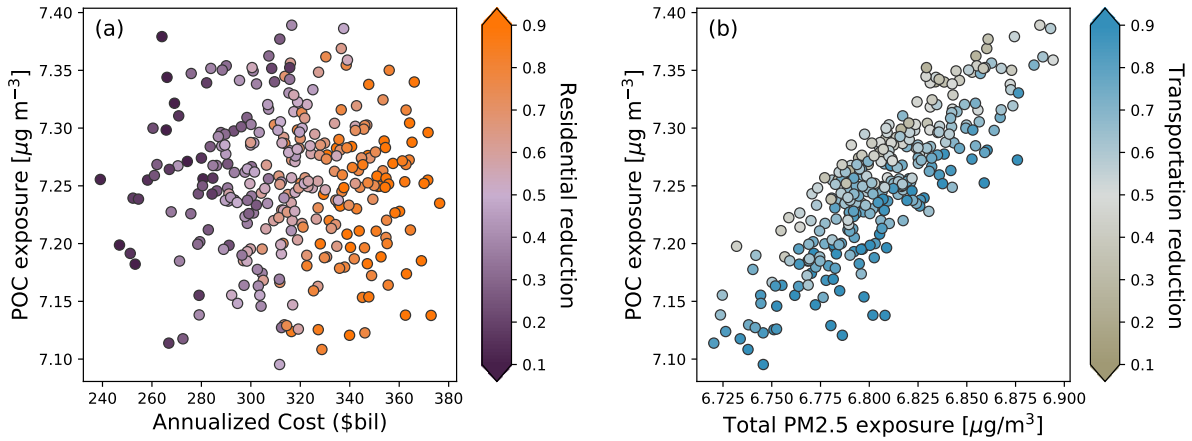

Figure 3.3. Sectoral influence in randomized experiments. National POC exposure as a function of cost, colored by reductions in residential emissions (a), and national population-average exposure colored by reductions in transportation emissions (b). There is little relationship between cost and POC exposure, but POC exposure and total exposure are strongly correlated. Costs in the randomized experiments are strongly dependent on the residential sector (a) and POC exposures tend to be lower when more transportation emissions are reduced (b).

disparities remain relatively similar, though the slight skew towards increase and decrease, respectively. The difference between the distributions is substantially smaller without bias correction (Figure SA3.10), but the relative positions are similar. The increase in Hispanic and decrease in Black disparities are consistent with recent historical trends (Figure 3.1); as are the skews for POC and White disparities. All exposures decline as a result of emission reduction (Figure 3.4d, 3.4e), which reiterates the co-benefits of climate policies. Distributions of state disparities remain largely unchanged (Figure 3.4b), but reductions in transportation emissions are associated with disproportionate exposure and disparity reductions (Figure 3.4c, 3.4f, see Methods). In most states, transportation emission reductions improve air quality for all demographics while simultaneously exhibiting large equity co-benefits compared to other sectors. Residential emissions demonstrate a similar but less pronounced pattern (Figure SA3.9).

3.4 Discussion

Our results suggest that it is indeed possible to reduce, but not eliminate, air pollution exposure disparities through targeted implementation of climate policy. We find the largest

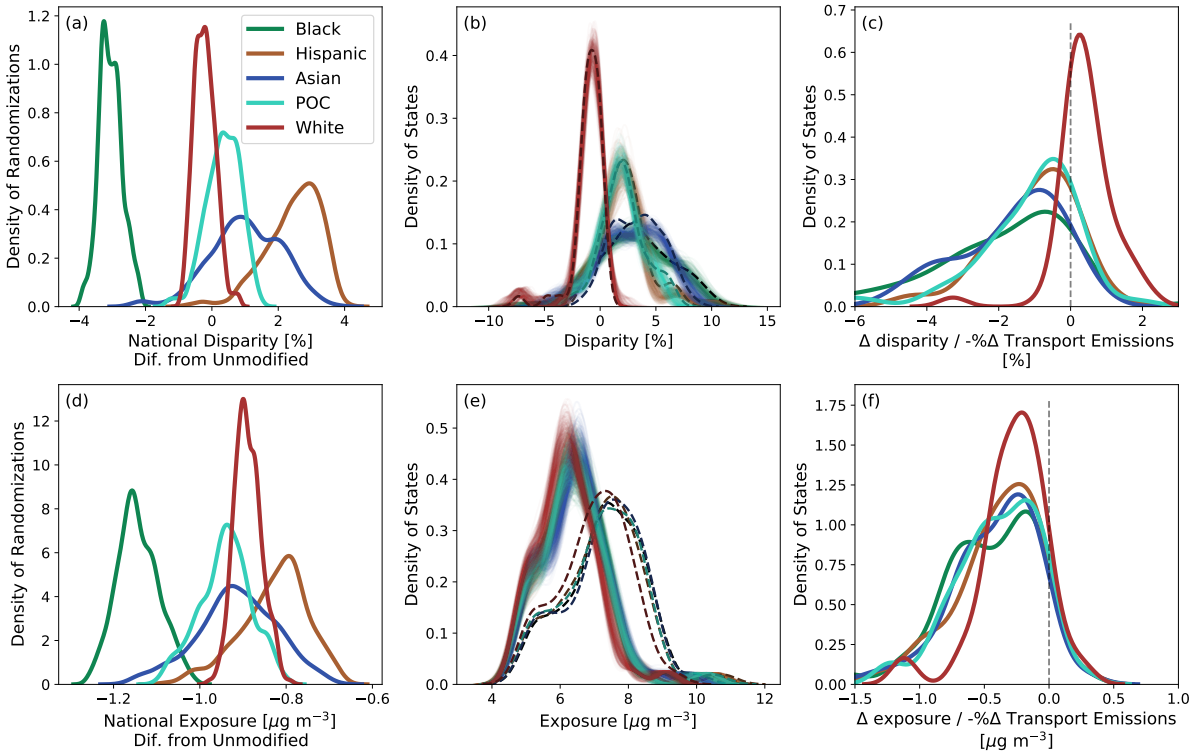

Figure 3.4. Disparity and exposure changes and transportation influence in randomized experiments. (a) Distributions of changes in national disparity relative to the Unmodified 2017 case for each randomized experiment (N=300 per distribution) (b) Distribution of state disparities (N=48 per distribution) in each randomized experiment (faint solid lines, N=300 distributions) and the Unmodified 2017 case (darker dashed lines). (d, e) Equivalent distributions as for (a) and (b), using exposure instead of disparity. (c, f) Distributions of state-level linear regression coefficients (N=48 per distribution) from modeling disparity (c) and exposure (f) using fractional change in all four sectors; only transportation coefficients are shown as they have the most disparate impact.

disparity reductions arise from directly targeting emission reductions in communities of color, but explicit consideration of race in environmental policy has thus far been explicitly avoided to limit potential legal challenges [69]. We find that strategies that avoid this political and legal sensitivity by targeting income, cost, or equal fractions across sectors and counties, are not particularly effective at reducing disparities. The use of historical pollution exposure (*PM2.5 Exposure* pathway) for targeting is moderately effective at reducing disparities (Figure 3.2b), and even more effective at reducing relative exposures (Figure 3.2d). This implies that explicitly targeting air pollution reduction in communities with historically high pollution, as is done in some contemporary U.S. climate policy, could reduce racial pollution disparities, though the continued use of income could have the opposite effect.

As with all modeling studies, our results are subject to model bias and model limitations. InMAP, the reduced complexity air quality model used here, only outputs annual average outdoor PM2.5 therefore does not capture daily or seasonal variations, indoor air quality, or the impact of air pollutants like NOx, ozone, or heavy metals. The inputs are based on one national emission inventory and one year of meteorological dataset, which are imperfect and do not capture the interannual variability of meteorology or human behavior. However, the high spatial resolution and low computational time allow us to run many simulations and calculate racial/ethnic pollution exposures and disparities.

Disparities and exposures are both useful metrics for air quality equity. Disparities are a socially and ethically relevant concept, and a stated priority of the U.S. federal government, while exposure translates directly to health impacts and observations. If changes in disparity and changes in exposures are not perfectly correlated, some amount of exposure reduction may be substituted for additional disparity reductions. Although such a pathway is possible, this tradeoff appears unlikely to occur in practice when policies are constrained by a greenhouse gas emission target (Figure 3.3b). As has been previously proposed, prohibiting unequal exposure changes from new projects that require environmental impact assessments (e.g. freeways, power plants, etc.) would decrease differences over time [70], which would inevitably also lead to decreases in

disparities.

We only address the impact of emissions that are not directly anthropogenic, like desert dust and wildfire smoke, through a bias correction. These emissions are not an input to the model and therefore are also not included in our NDC implementations. However, despite confounding factors like inherent model bias, we interpret the bias correction as an approximate incorporation of these missing emissions (Figure SA3.1c). Generally, the inclusion of these sources results in a decrease in disparities for POC. In particular, given that a larger fraction of the Black population lives in the Eastern half of the US, the national-scale Black disparity is decreased because the correction decreases the contrast between the Eastern and Western halves of the country (Figure SA3.1). Wildfires, in particular, have more annual variation in their intensity and location compared to regulated emissions sources, and have been increasing in magnitude in recent years [71]. This trend has renewed efforts to better understand the health impacts of short-term vs. long-term exposure to smoke [72] and of wildfire smoke vs. other particulate matter [73], as well as the equity of access to indoor air pollution control [74]. Whether wildfires and similar types of sources should be included directly when calculating disparities depends on the policy objective. Health impacts are largely a function of exposure, so if the primary focus of a policy is inequity in health outcomes, then "natural" sources like wildfires are clearly pertinent. However, if the primary focus of a policy is addressing the structural inequities around, for example, siting of emissions sources, wildfires are less relevant.

All emissions reductions considered here as part of our NDC implementations are associated with improved air quality. Emission sources are rarely evenly distributed across populations, which makes crafting policy to address disparities more complicated. Industrial emissions have long been a focus of environmental justice concerns because industrial facilities have often been intentionally colocated with communities of color [75, 76]. However, our No Industry simulation and randomized experiments suggest that even large-scale industrial facility removals may not substantially reduce disparities. It is worth noting, however, that we do not analyze the impact of individual facilities, some of which are likely to have large equity

co-benefits from reduced or removed emissions.

Among all the anthropogenic sectors considered here, we identify transportation as having the greatest potential for reducing pollution in communities of color via climate policy (Figures 3.4c, SA3.9). Recent empirical studies also found that transportation impacts are inequitable, though not in the context of greenhouse gas reduction [77]. We have assumed that electrified transportation will not require new fossil fuel-based electricity generation, which is not guaranteed. This result for transportation should therefore be interpreted as a first-order estimate of removing on-road emission sources as part of climate policy, not an exhaustive representation of a full energy system that couples transportation, electric power generation, and other sectors as is often done in transportation-specific studies [78]. Studies that do include this coupling have shown population-average health benefits are concentrated in the Western U.S., but present everywhere in the U.S. when grid electricity is largely from renewable sources [79].

One challenge when creating policy to address air quality equity is that such policies target pollution sources, not pollution receptors. We have assumed in the design of our simulations that proximity to impacted communities is a good proxy for reducing concentrations in those communities; in other words that the sources causing inequitable pollution are located in the communities experiencing the inequities. Although this may often be true, the transport and transformation of pollutants through variable meteorological and chemical background conditions, can complicate this relationship. In the case of transportation, the relationship between the source and the receiver of pollutants is further complicated by the sources' mobility. Infrastructural and economic inequities means that the people or organizations responsible for the pollution are often not those who experience the burden [70, 80]. Therefore, policies that promote pollution reduction may incentivize infrastructural improvements outside of the impacted communities. Although such policies may help address air quality inequities, they may have consequences in other equity dimensions like procedural justice and the economic inequality from investments, that are beyond the scope of this study, but are nonetheless important considerations in equity-focused policy design.

With these considerations in mind, a variety of policy options exist for addressing transportation emissions. Low maintenance and fuel costs have made electric vehicles (EVs) more cost-competitive, but they are still currently more expensive than their fossil fuel counterparts. Government programs that decrease the price difference between the two options would incentivize a faster transition. This could include rebates or tax breaks for EVs, increased gas tax, subsidized at-home or public charging infrastructure, or differentiation in vehicle registration costs. Financially or infrastructurally incentivizing alternative modes of individual transportation (e.g., walking, bicycling) or modes powered by renewable energy (e.g., electric rail, electric bus, e-bikes) [81], could achieve the same air quality benefits as replacing the current fleet of fossil fuel vehicles with their electric counterparts. Furthermore, these alternatives are less energy intensive than cars and trucks, and therefore require smaller increases in renewable capacity to power them with renewable energy.

Increased air quality equity is not an inevitable consequence of climate policy. However, progress towards the NDC's equity objectives is possible with explicit consideration of the distribution of pollution reduction co-benefits. Emission reductions in the transportation sector have the greatest potential to address pervasive air pollution inequities. So although climate policy alone is unlikely to eliminate all air quality disparities, investing in clean transportation and prohibiting disparate exposure changes from new capital projects can help meet the NDC goals of mitigating climate change, while also improving environmental justice at both state and federal levels.

3.5 Materials & Methods

3.5.1 Historical PM2.5 exposure

We use annual Washington University in St. Louis (WUSTL) surface PM2.5 concentrations, V5.GL.02. [82], which combines satellite data, surface measurements, and modeling results to form a best estimate of historical PM2.5 distributions and were shown to have an annual

R2 over North America of 0.57 or 0.67 when compared to only World Health Organization collocated sensors. For trends in Figure 3.1 we use the mean of annual data within two years of 2017, meaning 2015-2019. We aggregate the 0.01x0.01 degree resolution dataset to census tracts using area weighting. Tracts have been shown to be a sufficiently high resolution for estimating disparities [83]. We use ACS5 (2013-2017) population estimates for exposure and disparity calculations.

3.5.2 Emissions

We use the most recent (2017) National Emissions Inventory (NEI) from the Environmental Protection Agency (EPA) as the underlying emissions dataset. As this study is focused on potential co-benefits of climate policy, we require inventories of both criteria pollutants and greenhouse gases (GHGs). The NEI includes some, but not all GHG emissions. Most notably for this analysis, residential and oil & gas (O&G) GHG emissions are missing. Therefore, we estimate residential GHGs using EPA emission factors and estimate O&G GHGs by running the same emissions calculations as used in the NEI for the criteria pollutants (see SI for more detail). Some emission sources were aggregated and others disaggregated using proxies (see SI). GHG and CO_2e are used interchangeably, where CO_2e is the sum of CO_2, CH_4, and N_2O, weighted by their respective GWP100 (CO_2: 1, CH_4: 25, N_2O: 298). The emissions and their respective sector categorizations have been made available through the Harvard Dataverse.

3.5.3 Idealized decision pathways

The five idealized pathways (*Equal*, *PM2.5 Exposure*, *POC*, *Income*, *Least cost*) were designed to heuristically explore the implications of a wide range of decision criteria. Total GHG emission cuts in each of these pathways meet the 50% reduction target and at least 80% reduction of GHG emissions of electricity generation, in approximate accordance with the 2035 100% clean electricity target. The *Equal* pathway does not have this 80% criteria, because emissions are removed equally from all sources to meet the NDC. The other pathways use one

county-level criterion to rank all accounted emissions from the continental U.S. and remove sources sequentially until the NDC has been met (more detail in SI). The county ranking for the *PM2.5 Exposure* pathway is based on 2015-2019 average PM2.5 concentrations from the WUSTL dataset to limit the impact of interannual variability when determining the most polluted regions. The rankings for the *POC* and *Income* pathways are based on the county-level version of the 5-year (2013-2017) American Community Survey (ACS5) from the U.S. Census Bureau. For the *POC* pathway we use the non-White, non-Hispanic fraction of the population and for the income pathway we use the median income.

Both the GHGs and the criteria pollutants of the selected sources are set to zero, thereby directly coupling the GHG emission sources. Not every emission source was considered for removal - we limit the analysis to power plants, on-road transportation, residential fossil fuel use, and a subset of industrial emissions: cement plants, steel plants, pulp and paper plants, petroleum refineries, and oil & gas production; not all criteria pollutants are removed from these sources because we assume carbon capture and storage (see SI).

3.5.4 Randomized experiments

No idealized decision criteria is imposed for the randomized experiments. Instead, we randomly select a national fractional reduction of electricity, transportation, residential, and industrial emissions required to meet the NDC. This was done by initializing a fraction from a random uniform distribution for each sector. We then calculate the total resulting emission reduction from the initialization and randomly select a sector to increment slightly; we repeat this process until we have a set of fractions that meet the greenhouse gas reduction criteria. After selecting a fraction for each sector, sources are randomly eliminated from around the country until those fractional reductions are fulfilled, again completely removing all GHGs and criteria pollutants from each source. Due to their mobile nature, we also remove nearby county emissions when removing transportation emissions (see SI).

Coefficients describing the change in exposure or change in disparity as a function of

fractional reductions in each sector (Figure 3.4) are conducted using ordinary least squares:

$$disparity_{run}^{group} = c_{ele} * f_{run}^{ele} + c_{tra} * f_{run}^{tra} + c_{ind} * f_{run}^{ind} + c_{res} * f_{run}^{res} + c_0 + \varepsilon_{run} \quad (3.1)$$

Where f is the fractional reduction in each sector's GHG emissions (shown as superscript) and each simulation (run) is a point in the regression. This is repeated for each state. The resulting coefficients (e.g. ctra for Figure 3.4c) are plotted as distributions.

3.5.5 Air quality modeling

To simulate air quality, we ran InMAP version 1.8 over the continental U.S. with the default variable grid configuration [65]. InMAP is a reduced complexity model (RCM) that finds an annual equilibrium solution using user-defined input emissions. The variable grid means that locations with higher population density have smaller horizontal resolution, which is helpful for quantifying air pollution disparities. The model output resolution is variable, with very low resolution of around 50km in low population density areas and very high resolution of up to 120m in populated areas. To make results comparable, both to observations and between simulations, we aggregate the output to census tracts using area weighting.

Area emissions were allocated to appropriate sub-county regions using spatial surrogates. On-road emissions were allocated to roads using annual average daily traffic from the Department of Transportation. Heavy trucks are limited to Interstates, Freeways, and Expressways. Residential emissions were downscaled to tracts using 2017 ACS5 tract population. Ship, port, rail, and agricultural emissions were also allocated using proxies (see SI) though they are not modified in our pathways. Shapefiles of the input emissions for the idealized pathways have been made available through the Harvard Dataverse.

InMAP is a useful tool for this type of study because it is computationally inexpensive and can therefore be used to run many more simulations than would be possible with a more conventional chemical transport model. However, despite the high spatial resolution, the

temporal resolution is limited to annual, and the model only uses one set of meteorological data. Furthermore, there is no modeling of NOx, ozone, or other air pollutants, and as with any atmospheric model results depend on parameterizations and the quality of input data. These limitations are relevant to the interpretation of this and other studies based on RCMs.

3.5.6 Bias correction

We applied a tract-level bias correction using 2015-2019 mean surface PM2.5 data from the WUSTL dataset described above. We regrid both the InMAP simulation output and the gridded WUSTL dataset to the tract level using area weighting. We take the difference between the InMAP simulation that uses the unmodified inventory, and the WUSTL dataset, and use that difference as the correction for all InMAP output such that PM2.5 absolute differences between the simulations remain unchanged but baseline concentrations are better represented (Figure SA3.1). We believe this better represents the true distribution of PM2.5 and allows the model to define the differences. Many of our figures are repeated in the SI without this bias correction to demonstrate that this methodology does not fundamentally impact the interpretation of our results.

3.5.7 Costs

We estimate costs of the NDC-constrained pathways using different bottom-up approaches for each sector. All costs are estimated relative to a fossil-fuel dependent alternative. These estimates are not intended to be exact, but rather to illustrate differences between pathways in a self-consistent manner. They represent total societal costs and do not differentiate by the different actors that may bear the burden of the costs. The costs are spatially and sectorally heterogeneous, but otherwise linear (e.g., electrifying half of cars in a certain county costs half as much as electrifying all of them). All costs, after adjusting for inflation to 2020 U.S. dollars, reflect the changes required to meet the 2030 mitigation targets and are annualized using a 5% interest rate assuming that the costs continue over time (unless otherwise specified).

Electricity sector costs are estimated as the cost of replacing existing fossil fuel power plants with the cheapest available renewable energy generation in the region using the input files to the USA Global Change Analysis Model (GCAM-USA). These costs include capital cost, grid interconnection cost, operating and maintenance cost, and fuel cost. Transportation costs are estimated as the cost of electrifying the fleet, using capital and maintenance costs based on GCAM input files and using vehicle miles traveled from the Federal Highway Administration and GCAM energy intensities for fuel costs. Residential costs are calculated as the premium required to decarbonize residential sources, specifically to electrify space heating, water heating, stoves, and dryers that are powered by natural gas, propane, or fuel oil/kerosene. This relies on purchasing costs from the gray literature and the Residential Energy Consumption Survey (RECS) for fuel costs. As described above, only some industrial sources are removed in the pathways. Since refineries and O&G facilities can be completely removed in our simulations, costs are based on the Value Added (VA) estimates from the U.S. Bureau of Economic Analysis (BEA), excluding the gross operating surplus since this is not a component of societal value. For cement, steel, and pulp and paper facilities we use the cost of implementing carbon capture and storage from Leeson et al. (2017). Details of all cost calculations are available in the SI.

3.6 Acknowledgements

P.P. and, S.R., and J.B. are supported by NSF CNH-L #1715557 and the. P.P. and J.B. are also supported by the Robert Wood Johnson Foundation #76555. We also thank Alexander Andriatis for helpful methodological discussions. This chapter, in full, is a reprint of the material as has been accepted for publication at The Proceedings of the National Academies of Sciences, 2023, Polonik, Pascal; Reese, Sean; Ricke, Katharine; Burney, Jennifer. PNAS, 2023. The dissertation author was the primary investigator and author of this paper.

3.A Appendix for Chapter 3

3.A.1 Supplementary Methods

Input emission estimations

All input emissions were estimated on a sectoral basis. Below is a description of the generation process for each of the economic sectors included in our analysis.

Sectoral grouping

The National Emissions Inventory (NEI) emissions are separated into thousands of source classification codes (SCCs), each of which have associated sectors. However, despite the available detail, the SCC codes and sectors are not particularly well suited for this study. There are two challenges with the existing NEI categorization: (1) that point sources have multiple sectors per facility, which complicates modeling, and (2) the vast majority of GHGs are grouped into an "other" category, thereby making them difficult to match to their source sectors. We therefore use the SCCs and additional information in the dataset to group emissions into supersectors, subsectors, and in some cases subsubsectors for costs. The classifications are defined in Table S1, which is described below and available for download as supplemental data. Some industrial classification codes correspond in our study to electricity generation because many power plants have multiple classification codes, including those associated with industrial combustion.

Carbon Capture and Storage implementation for industrial emissions

For cement, steel, and paper, we assume an implementation of carbon capture and storage (CCS) so we do not set emissions to zero, but rather to hypothetical efficiencies.[1] Of the criteria pollutants from these industries, only SO2 is changed, and it is scaled with CO_2e. We were unable to find industry-specific estimates and therefore use this assumption as an approximation of findings from power plant CCS, where SO2 reductions are predicted, while other emissions show less consistent changes. [84]

Mobile transportation emission reductions

One difference between random and idealized emission reductions in the modification of transportation emissions. Since transportation emissions are mobile and span between counties, when a transportation source is randomly removed, the emissions from the same source are reduced from surrounding counties. We use the distance between county centroids as an exponential scaling factor. The e-folding length scale is 50 km for automobiles and light trucks and 150 km for heavy trucks. So, for example, if one county's automobile emissions are randomly removed, the neighboring county, with a centroid 50 km away, will also have about a third of its automobile emissions removed. This additional removal of nearby transportation emissions has no impact on the total reduction of GHG or criteria pollutants. 50 km was chosen because it roughly represents the median commute distance in the U.S. 150 km for trucks is our own estimate of an average permeability across county lines. Finding truck data is challenging and would vary widely by the type of trucking, which would require more sectoral granularity than is included in our study. However, since sources are being randomly removed, this distance assumption does not have a significant impact on our results.

Residential Greenhouse Gases (GHGs)

GHGs from the residential sector are not included in the NEI. We therefore use the NO_x emission factor to back out fuel use and then multiply by CO_2, CH_4, and N_2O emission factors. All emissions factors are from the same source as used for the NEI: Chapter 1 (External Combustion) of AP-42, Fifth Edition Compilation of Air Pollutant Emissions Factors, Volume 1: Stationary Point and Area Sources (all table references in this section refer to this document). We apply the same process for non-residential nonpoint emissions, but those sources were not considered as part of this study.

- Residential natural gas - for NO_x emissions we use the factor for uncontrolled residential furnaces from Table 1.4-1. The CO_2, CH_4, and N_2O emission factors are from Table 1.4-2, using the N_2O (Uncontrolled) row for N_2O.

- Residential oil - we use the Residential Furnace row of Table 1.3-1. The CO_2 emission factor is from Table 1.3-12, using the No. 2 fuel type. The N_2O emission factor is from Table 1.3-3 (residential) and the CH_4 emission factor is from Table 1.3-8 (residential)

- Residential Kerosene - The NO_x emission factor for residential oil is very slightly different from the Residential Furnace row of Table 1.3-1, and it is taken from a separate spreadsheet of emissions factors, found at the NEI supporting document page.[1] The CO_2 emission factor is from Table 1.3-12, using the No. 1 (kerosene) fuel type. The N_2O emission factor is from Table 1.3-3 (residential) and the CH_4 emission factor is from Table 1.3-8 (residential).

- Residential Liquified Petroleum Gas - the NO_x emission factors are taken from the same sheet as kerosene. The GHG emission factors are the same as for kerosene.

Residential disaggregation

Residential emissions are provided at the county level with coarse sectoral information. More specifically, residential emissions are only separated by fuel type in the NEI. However, to calculate bottom-up costs, we require further disaggregation into different technologies. Each fuel type is separated into space heating, water heating, dryers, and stoves, using the relative energy consumption of each, based on the regional residential energy consumption survey (RECS), as is done for costs (see Costs below).

Oil and Gas Production GHGs

Nonpoint GHGs from Oil and Gas Production (O&G) are not included in the NEI. Criteria pollutants from this sector are estimated by the EPA using a publicly available Microsoft Access Database. We run these calculations for the NEI without modification. Although not included in the NEI, the output includes GHG emissions. We merge these GHGs with the NEI dataset on counties and SCCs.

Transportation grouping

We group transportation emissions into subsectoral categories for the purpose of estimating mitigation costs for this sector (see Section 3.A.1 below). Those groupings are defined based on the following SCC level three categories:

- Passenger Cars: Automobiles
- Passenger Truck or Light Commercial Truck: Light Truck
- Single Unit Short-haul Truck or Single Unit Long-haul Truck or Refuse Truck or
- Motor Home: Heavy Truck
- Motorcycle: Motorcycle
- Intercity/Transit/School Bus: Bus

Spatial proxies for InMAP modeling

InMAP takes input emissions in the form of point, line, or area shapefiles. Emissions from the NEI are given as point sources with coordinates or at the county level. We spatially allocate some county-level emissions to smaller regions using spatial surrogates to better represent their true distribution. All other area emissions were assigned to county shapefiles, which InMAP then allocates to the model grid using area weighting.

Onroad emissions are allocated based on 2017 road shapefiles from the U.S. Department of Transportation.[2] Heavy truck emissions are allocated to Interstates, Freeways, and Expressways using Annual Average Daily Traffic (AADT) and spread evenly across the length of each road segment. The same process is used for other onroad emissions but they are allocated to all available roads. Residential emissions were downscaled using 2013-2017 ACS5 census tract total population.

Ship port emissions, ship underway emissions, and rail emissions were all allocated based on area or length of corresponding 2014 NEI shapefiles for ports, shipping lines, and railways.

Agricultural emissions were allocated based on cropland in the USDA cropland data layer - connected cropland was aggregated to shapefiles without specifying crop types. Locomotive emissions are allocated to rail line shapefiles associated with the NEI County oil and gas emissions were downscaled to census tracts based on the number of wells in each tract - excluding those with non-active status - according to the Homeland Infrastructure Foundation-Level Data (HIFLD), published June 21, 2019.[3]

Mitigation cost estimates

Detailed descriptions of our approach to estimating the costs associated with sectoral emissions reductions are presented below by sector.

Electricity

To estimate the costs of decarbonizing the electricity sector we use input data from a commonly used integrated assessment model, GCAM-USA,[85] which is typically used for modeling coupled energy systems. Here, we use only the input data for the energy system, which includes capital, operating and maintenance, and grid interconnection costs for four types of renewable energy technologies: onshore wind, offshore wind, solar photovoltaics, and concentrating solar power. We take the difference between the total cost of these renewable energy sources and combined-cycle natural gas (CCNG), as this is the least cost non-renewable option available in this dataset. All costs are summed after adjusting for inflation to 2020 dollars and annualized using equations 3.2-3.5. We assume zero grid interconnection cost for CCNG plants because none is provided in the dataset and major grid expansions are likely not necessary for this energy type due to relatively easy siting of compact gas plants.

$$Annualized\ Cost = (Capital\ Costs * CRF) + Operating\ and\ Maintenance\ Costs \tag{3.2}$$

$$Capital\ Recovery\ Factor\ (CRF) = \frac{DiscountRate}{1-(1+DiscountRate)^{-Lifespan}} \tag{3.3}$$

$$Capital\ Cost_{R,T} = GCAM\ Capital\ Cost_{R,T} + GCAM\ Grid\ Interconnection\ Cost_{R,T} \tag{3.4}$$

$$Operating\ \&\ Maintenance\ Cost_{R,T} = GCAM\ Operating\ \&\ Maintenance\ Cost_{R,T} \quad (3.5)$$

where T = technology (e.g. onshore wind, offshore wind, solar PV, solar CSP, and CCNG) and R = region (REeDS region for onshore wind, offshore wind, and solar CSP; balancing area for solar PV). Natural gas fuel costs are added to operating costs using the same fuel price definition as for the residential and transportation sectors.

Costs are calculated per MW of generated electricity. To estimate the amount of required renewable generation from virtually removing fossil fuel power plants, we merge the NEI emissions with the Emissions and Generation Resource Integrated Database (eGRID), which contains electricity generation data for all power plants. There is no common identifier between the datasets and the recent available years do not overlap, so we use our own algorithm to match the 2017 NEI data with the 2018 eGRID data. We algorithmically matched the two datasets and manually checked the matching of the largest emitters, and fixed the matches when necessary. Though imperfect, this matching is required to merge generation data with criteria pollutant emissions. A harmonized national dataset of criteria pollutants, greenhouse gases, and generation would allow us to avoid this manual process and improve data reliability.

Costs are a slight function of the total generation of each energy type as given in the GCAM-USA input files. We select the cost of the lowest renewable cost in each region, which is often onshore wind. We do not exceed the total capacity for each plant type in each region (equation 3.6). The cost of replacing each power plant is then the required generation multiplied by the cost per MW.

$$Maximum\ Generation_{R,T} = REEDS\ Capacity_{R,T} * REEDS\ Capacity\ Factor_{R,T} \quad (3.6)$$

Transportation

We calculate the costs of decarbonizing transportation as the additional premium required to electrify the entire fleet of fossil-fuel-based vehicles. We consider fuel costs and non-fuel

costs, which include infrastructure, maintenance, and purchase.

Fuel Costs

To derive the fuel cost, the energy required to power the full fleet in each county is multiplied by the price of the required fuel type (equations 3.7 and 3.8). This is based on the number of vehicle miles traveled (VMT) from the Federal Highway Administration 2017 Highway Statistics (VMT by Road Type,[4] Percent VMT by Vehicle Type[5]) for motorcycles, passenger cars, light trucks, buses, and heavy trucks. The VMT is multiplied by the energy intensity (energy per VMT) from GCAM,[6] the energy density of the fuel, and the cost of the fuel (equations 3.7, 3.8).

$$Fuel\ Cost_{A,C,V} = (VMT_{A,S,R} * \%VMT_{A,S,V}) * \frac{Pop_{A,C}}{Pop_S} * Intensity_V * Price_F \tag{3.7}$$

$$Fuel\ Cost_{C,V} = Urban\ Fuel\ Cost_{C,V} + Rural\ Fuel\ Cost_{C,V} \tag{3.8}$$

where A = area (i.e. urban or rural), V = vehicle type (i.e. motorcycle, bus, automobile, light truck, heavy truck), S = state, C = county, R = road type (i.e. interstate, other arterials, other), F = fuel type. The fuel types by vehicle type are: gasoline for motorcycles, automobiles, light trucks; diesel for heavy trucks; and a combination of diesel and compressed natural gas (CNG) for buses based on national fleet averages from the DOE alternative fuels data center.[7]

Fuel prices are summarized in Table S2. For electric vehicles they were initially calculated as the average of the maximum and minimum electricity price between 2014 and 2020 from the EIA state electricity profile[8] and for gasoline vehicles, they were initially calculated as the state average AAA gasoline price in 2017. Since state-level data was unavailable for diesel vehicles we use the 2017 national average from the EIA, scaled by the state gasoline price. Natural gas prices are allocated to states based on EIA state-level 2017 prices.

However, due to large variation in fuel prices, we adjust these prices to better match current prices and future projections from the EIA's Short-Term Energy Outlook. The adjustment

factors and the final prices are given in Table S2.

To harmonize the different road types, we group roads according to the FWHA's guidelines: Freeways, Expressways, and Arterials into Other Arterials and Collectors and Local Roads into Other. The product of VMT and percent VMT by road type yields the number of miles traveled by each vehicle type in each state.

To harmonize GCAM's vehicle energy intensities with the FHWA vehicle types, we regroup GCAM's vehicle types to match the FHWA's by grouping compact, mid-sized and large cars into Passenger Cars, grouping light trucks SUVs, and trucks under 4.5 tons into Light Trucks, by assigning 4.5-12 ton trucks as Single-Unit Trucks, and by assigning trucks over 12 tons as Combination Trucks. We chose this grouping so that vehicles with similar energy intensities (MJ/VMT) would be grouped together. We assign one intensity to each group by taking the average of the intensities weighted by travel demand.[85]

To downscale to the county level, we use 2010 Census Urban/Rural Population Data[9] to calculate the fraction of urban/rural population in each county for every state. Taking each county's urban fraction and multiplying it by their state's total urban MW needed gives us an approximation for the urban MW needed for each county. The same process is done with the rural data to get the total rural MW needed for each county.

Non-fuel Costs

To derive the nonfuel costs we use state-level vehicle registration data from the 2017 Highway Statistics[10] and multiply the registrations by per-vehicle infrastructure, purchase, and maintenance costs from GCAM (equations 3.9-3.10).

$$Capital\ Cost_{A,C,V} = Regs._{A,S,V} * \frac{VMT_{A,C}}{TotalVMT_S} * (Purch.\ Cost_V + Infra.\ Cost_V) \tag{3.9}$$

$$Capital\ Cost_{C,V} = Urban\ Capital\ Cost_{C,V} + Rural\ Capital\ Cost_{C,V} \tag{3.10}$$

where Regs, Purch, and Infra are short for registrations, purchasing, and infrastructure.

Again the available vehicle types in GCAM differ from those of the VMT data. Therefore we disaggregate the truck VMT data into light trucks and heavy trucks using the State Motor Fuel Use data[11] from the same 2017 Highway Statistics assuming that light trucks use gasoline and heavy trucks use diesel. We downscale Vehicle Registrations to the county level following the same process used in 3.A.1.

Costs are adjusted for inflation to 2020 dollars. Then, using the vehicle groupings from 3.A.1, we take a mean for each group's infrastructure, purchase, and maintenance costs from GCAM. These three costs are then multiplied by the number of registrations in each state (equations 3.11-3.12) and annualized using equations 3.2 and 3.3. Lifetimes for each vehicle type are found in GCAM and annualized using a 5% interest rate.

$$Maint.\,Cost_{A,C,V} = Urban\ Regs._{A,S,V} * \frac{Urban\ VMT_{A,C}}{Total\ VMT_S} * (Maint.\,Cost_V) \tag{3.11}$$

$$Maint.\,Cost_{C,V} = Urban\ Maint.\,Cost_{C,V} + Rural\ Maint.\,Cost_{C,V} \tag{3.12}$$

Residential

We calculate the costs of decarbonizing residential sources as the additional premium required to electrify space heating, water heating, stoves, and dryers that are powered by natural gas, propane, or fuel oil/kerosene. The electric replacements considered for each of these appliances are air source heat pumps (ASHP), heat pump water heaters (HPWH), electric stoves, and electric dryers respectively. We consider fuel and purchase costs for each of these technologies, as well as the cost of upgrading a home's electric panel since panels often need to be upgraded to support additional electric appliances. Fuel costs are derived by using residential propane and natural gas consumption data from the 2015 Residential Energy Consumption Survey (RECS). This consumption is converted to MWh and multiplied by the regional price of electricity. Nonfuel costs are derived by calculating the number of housing units that have a fossil fuel appliance and multiplying them by the costs of an electric version of that appliance.

Panel costs are spread across appliance types based on fuel consumption of each appliance type under the assumption that on average the energy intensity of an appliance will dictate the need for new electrical panels.

Capital Costs

To calculate capital costs we merge 2017 estimates of county housing units from the census bureau[12] with data from the 2015 Residential Energy Consumption Survey (RECS).[13] HC3.1, HC6.1, and HC8.1 of the RECS survey, provide the fraction of homes within each census region that have appliances of a specific fuel type. We multiply this fraction by the number of housing units in each county to get the number of appliances that can be electrified. We then multiply each appliance type by the purchasing price as provided in a 2019 E3 Report on Residential Building Electrification in California [86], to get the total capital cost for each county to decarbonize residential appliances (equation 3.13).

$$Capital\ Cost_{C,T} = \frac{Housing\ Units_{R,T,F}}{HousingUnits_{R,T}} * Housing\ Units_{C} * Purchase\ Cost_{T,F_{elec}} \tag{3.13}$$

Panel costs are spread across appliance types based on fuel consumption of each appliance type (as described in 3.A.1) under the assumption that on average the energy intensity of an appliance will dictate the need for new electrical panels. Total panel costs are calculated by multiplying the number of homes that have a fossil fuel appliance by the cost of an electric panel from the E3 report.

Fuel Costs

Residential propane and natural gas consumption is also provided in ce5.2 of the RECS survey for census regions. To disaggregate this to the county level, we use the fraction of housing units of a county relative to the census total. This allows us to get natural gas and propane consumption to the county level by multiplying the fraction with the census region consumption data. Disaggregating consumption in this manner means that we assume that housing units consume identical amounts of energy. Each county's BTU consumption was then converted to

MWh and multiplied by the price of electricity to get the fuel cost (equation 3.14).

$$FuelCost_{C,T} = \frac{Housing\ Units_C}{HousingUnits_R} * Energy\ Consumption_{R,T,F} * Fuel\ Cost_{T,F} \tag{3.14}$$

where C = County, R = Census Region, T = Technology (i.e. ASHP, HPWH, Stove, Dryer), F = Fuel Type (i.e. electricity, natural gas, propane, heating oil).

A similar process was conducted for fuel oil/kerosene, but instead of using RECS data to upscale regional consumption, we used NEI residential NO_x emissions as a proxy for consumption data. Specifically we use the emission factor from table 1.3-1 of an EPA report on Fuel Oil combustion[14] to convert pounds of NO_x emissions into gallons of fuel oil, which we convert to MWh. As with natural gas and propane, this is then multiplied by the state-level price of electricity to get the fuel cost. As for electricity generation and transportation, we correct fuel costs by a fuel-specific constant (Table S2).

Industry

Since refineries and O&G facilities can be completely removed in our pathways, costs are based on the Value Added (VA) estimates from the U.S. Bureau of Economic Analysis (BEA). We do not include the gross operating surplus since this is not a component of societal value. For refineries we use the VA of Petroleum and Coal Products industry and for oil and gas we use the VA of the Oil and Gas Extraction industry. We then divide by the respective CO_2e emissions to obtain a cost of carbon removal. This results in a cost of \$136/TCO_2e for petroleum and \$258/TCO_2e for O&G.

For cement, steel, and pulp and paper facilities we use the cost of implementing CCS from [87]. For cement and pulp and paper we use the given numbers of \$39.4/TCO_2 and \$57.2/TCO_2, respectively, though it is worth noting that pulp and paper is based on a single estimate rather than an average as for other industries. For steel, \$76.6/TCO_2 is given for the first 65% of CO_2 emissions and \$86.4/TCO_2e is given for an additional 27% CO_2 emissions; we use a weighted average of \$79.5/TCO_2. Industry costs are not adjusted for inflation or with an interest rate as

with all other costs.

Data and Documentation Links

1. state_comparison ERTAC SS_version7_4 spreadsheet. Last accessed: 3/4/2023.
   https://gaftp.epa.gov/air/nei/2017/doc/supporting_data/nonpoint/?C=N;O=D
2. Department of Transportation road shapefiles by state, where [[State]] is replaced by the name of each state. Last accessed 3/4/2023.
   https://www.fhwa.dot.gov/policyinformation/hpms/shapefiles/[[STATE]]2017.zip
3. Homeland Infrastructure Foundation-Level Data (HIFLD). Last accessed: 3/4/2023.
   https://hifld-geoplatform.opendata.arcgis.com/datasets/oil-and-natural-gas-wells/
4. GCAM v6 Documentation: GCAM-USA. https://jgcri.github.io/gcam-doc/gcam-usa.html
5. Table VM-2 - Highway Statistics 2017
   https://www.fhwa.dot.gov/policyinformation/statistics/2017/vm2.cfm
6. Table VM-4 - Highway Statistics 2017. Last accessed 3/5/2023.
   https://www.fhwa.dot.gov/policyinformation/statistics/2017/vm4.cfm
7. Transit Buses by Fuel Type. Last accessed 3/5/2023. https://afdc.energy.gov/data/10302
8. EIA state electricity profile 2021. Last accessed 3/5/2023
   https://www.eia.gov/electricity/state/
9. 2010 Census Urban/Rural Population Data
   https://www2.census.gov/geo/docs/reference/ua/County_Rural_Lookup.xlsx
10. State-level vehicle registrations 2017. Table MV-1. Last accessed 3/5/2023.
    https://www.fhwa.dot.gov/policyinformation/statistics/2017/mv1.cfm

11. State-level motor-fuel use 2017. Table MF-21. Last accessed 3/5/2023.
https://www.fhwa.dot.gov/policyinformation/statistics/2017/mf21.cfm

12. Total housing units. US Census. Last accessed 3/5/2023.
https://www.census.gov/data/datasets/time-series/demo/popest/
2010s-total-housing-units.html

13. Residential Energy Consumption Survey 2015. US EIA. Last accessed 3/5/2023.
https://www.eia.gov/consumption/residential/data/2015/

14. AP-42 VOL. I: 1.3: Fuel Oil Combustion. US EPA. Last accessed 3/5/2023.
https://www.epa.gov/sites/default/files/2020-09/documents/1.3_fuel_oil_combustion.pdf

3.A.2 Supplementary Tables

Table A3.1 is used to define sectors. It can be found uploaded separately as supplementary data. It contains the information we used to define the supersectors, subsectors, and subsubsectors in this study. The 'sector,' 'scc level two,' and 'scc level three/four columns,' and 'facility source type,' and 'Datasets' columns are from the national emissions inventory. The 'eGRID_sector' is from the matched eGRID dataset. The 'Modified' column indicates whether each SubSubsector is modified in the pathways. The 'Cost_Group' indicates which group each subsubsector is in for the cost calculations. The entries in the NEI and eGRID columns define what those criteria need to start with. If the entry starts with 'contains' then the following text can be anywhere in the description (of the descriptor indicated by the column name), not just at the beginning.

Table A3.1. National average fuel cost for each fuel type and the adjustment factors used to obtain those prices from historical averages.[1]

Fuel Type:	**Low Adj Price (adjustment factor)**	**Middle Adj Price (adjustment factor)**	**High Adj Price (adjustment factor)**
Electricity	$0.105 /kWh (1.2)	$0.115 /kWh (1.4)	$0.123 /kWh (1.8)
Natural Gas	$12.00 /1000 ft3 (1)	$14.40 /1000 ft3 (1.2)	$16.80 /1000 ft3 (1.4)
Gasoline	$2.40 /gallon (1)	$3.60 /gallon (1.5)	$4.80 /gallon (2)
Diesel	$2.58 /gallon (1)	$3.87 /gallon (1.5)	$5.16 /gallon (2)
Propane	$2.39 /gallon (1)	$2.87 /gallon (1.2)	$3.35 /gallon (1.4)
Fuel Oil/Kerosene	$2.70 /gallon (1)	$4.05 /gallon (1.5)	$5.40 /gallon (2)

[1]The fuel price is the average 2014-2020 national fuel price, multiplied by an adjustment factor, which was selected to reflect the projected prices in the EIA's Short-Term Energy Outlook at the time of writing to 2021-2022 prices.

3.A.3 Supplementary Figures

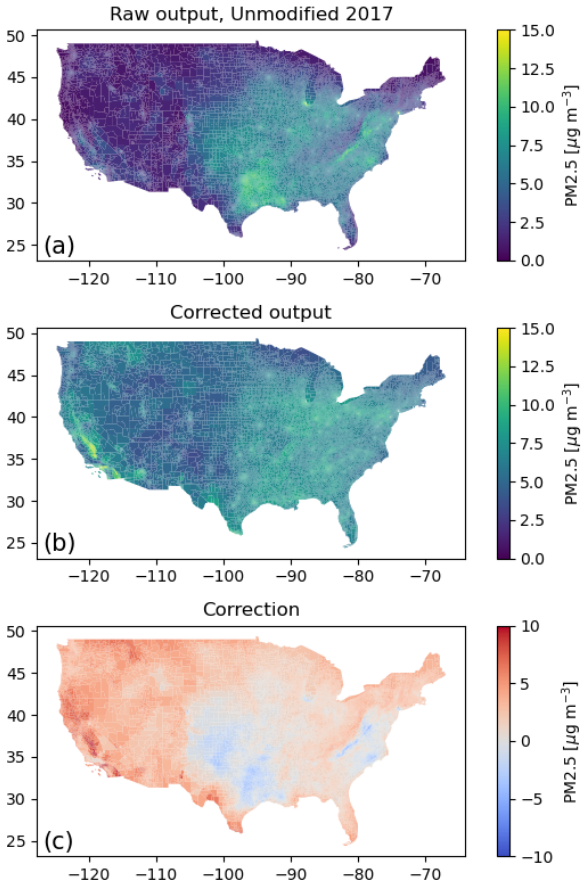

Figure A3.1. (a) Maps of raw InMAP output using Unmodified 2017 NEI emissions (not including fire emissions) and our spatial proxies. (b) Map of corrected output. For the Unmodified 2017 case, this is by definition the same as the WUSTL dataset averaged over 2010-2019. (c) The correction applied to get from (a) to (b). The same correction is applied to all InMAP output in this study, meaning that (a) and (b) are different for different simulations and (b) will not always equal the WUSLT dataset. All maps are regridded from their original resolutions to the census tract level. The correction is the result of missing and imperfect emissions inputs as well as model bias. It is applied to all simulations and therefore largely impacts absolute exposures and disparities rather than the differences between simulations.

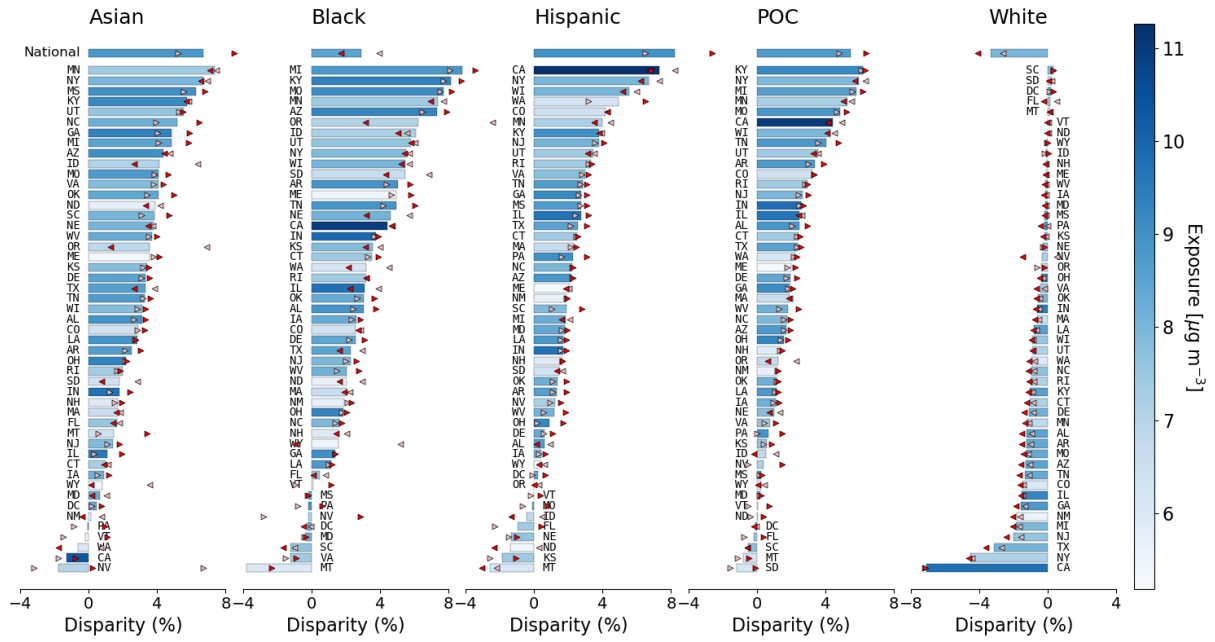

Figure A3.2. This figure is the same as the top panel of Figure 1 but with 5% lowest density tracts removed. Data are area averaged since population data are not available at the same very high resolution as the original dataset. To test the impact of large, low population tracts on the result, we remove low density tracts and show that disparities are persistent.

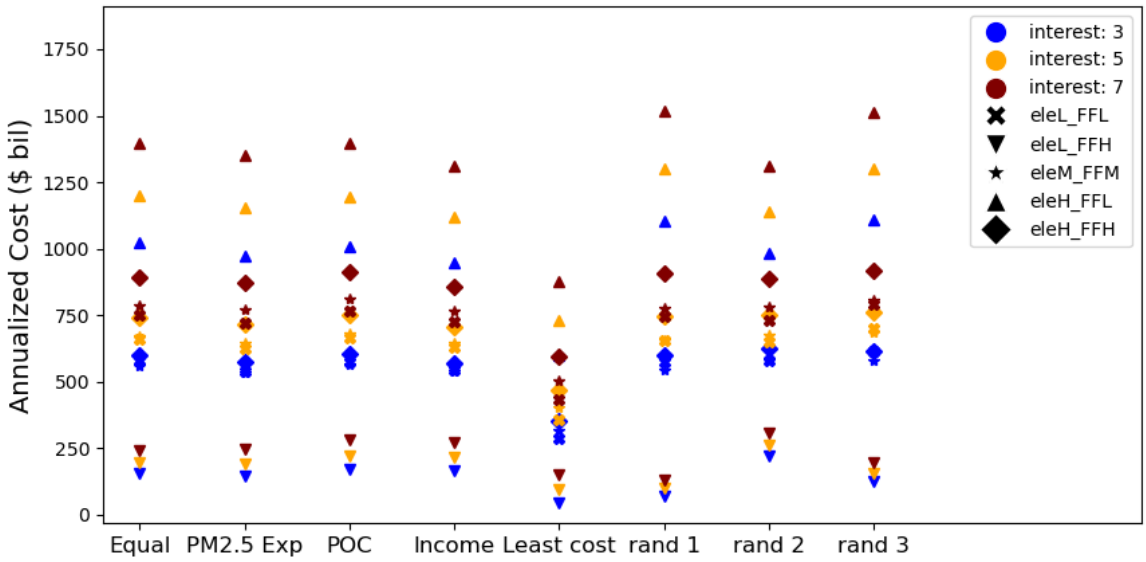

Figure A3.3. Cost ranges from different assumptions about high/medium/low electric costs (labeled as ele H/M/L) and fossil fuel costs (labeled as FF H/M/L) and different interest rate assumptions (3%, 5%, 7%). For example, eleL_FFH yields the lowest cost because decarbonization is most favorable when electrification costs are assumed to be low and fossil fuel costs are assumed to be high. The permutations of high/medium/low electricity and fossil fuel cost assumptions are shown as different symbols and interest rate assumptions are shown as different colors. Cost ranges are shown for the NDC-constrained pathways from Figure 1 and for three of the random experiments. The costs in the main text and the costs used for the Least cost pathway are based on the middle estimate (eleM_FFM, interest 5). This figure demonstrates that there are a wide range of cost estimates depending on model assumptions but that the relative magnitude of costs are consistent.

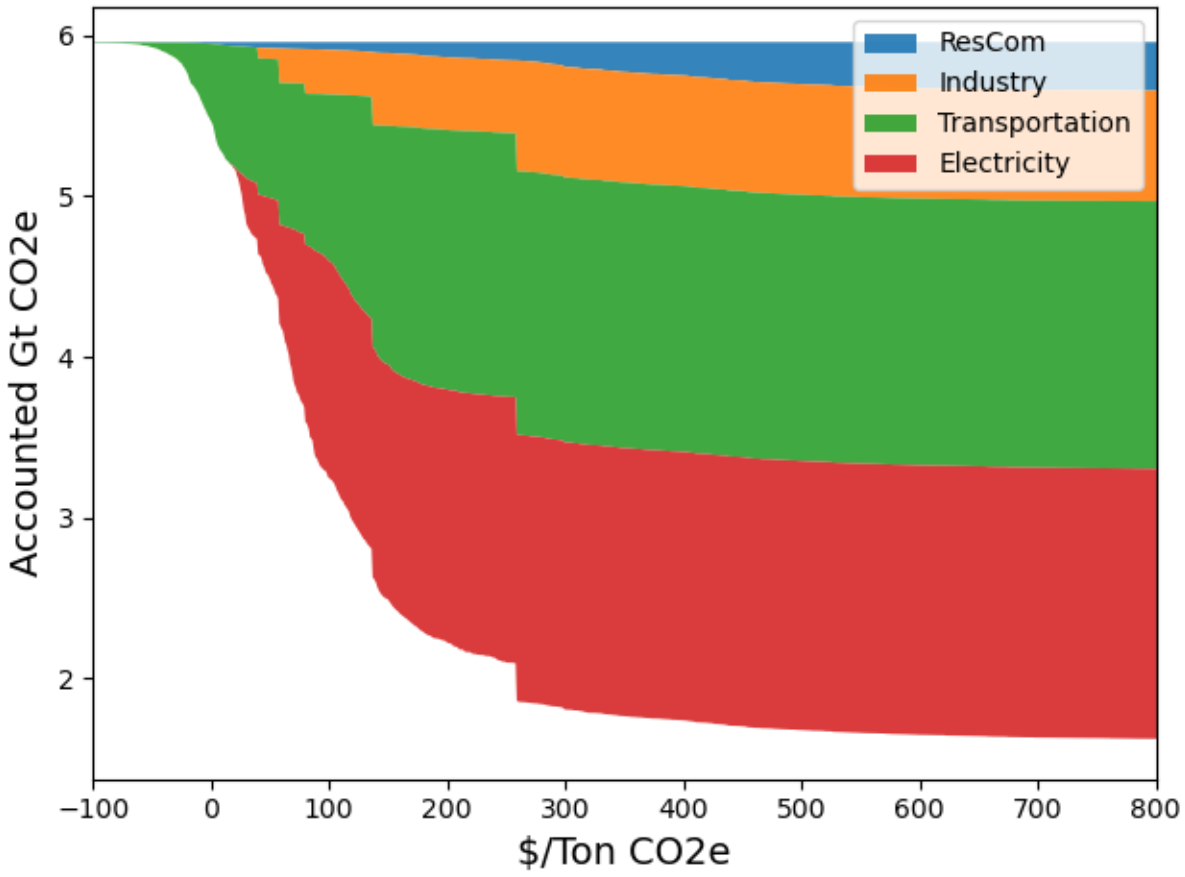

Figure A3.4. Stacked marginal abatement cost curve that results from our middle cost estimate. Curves are calculated by sorting the county-level costs for each sector and taking the cumulative sum of corresponding CO_2e emissions. Industry costs occur in discrete levels because we use one cost for each industry sub-sector (e.g. cement) from the literature. Emissions do not reach zero mostly because we do not assign costs to all greenhouse gas emissions. This figure demonstrates the cost per ton of reducing emissions - as more emissions are removed, the cost increases. Transportation and electricity emissions make up a large fraction of the total and tend to occur at lower prices.

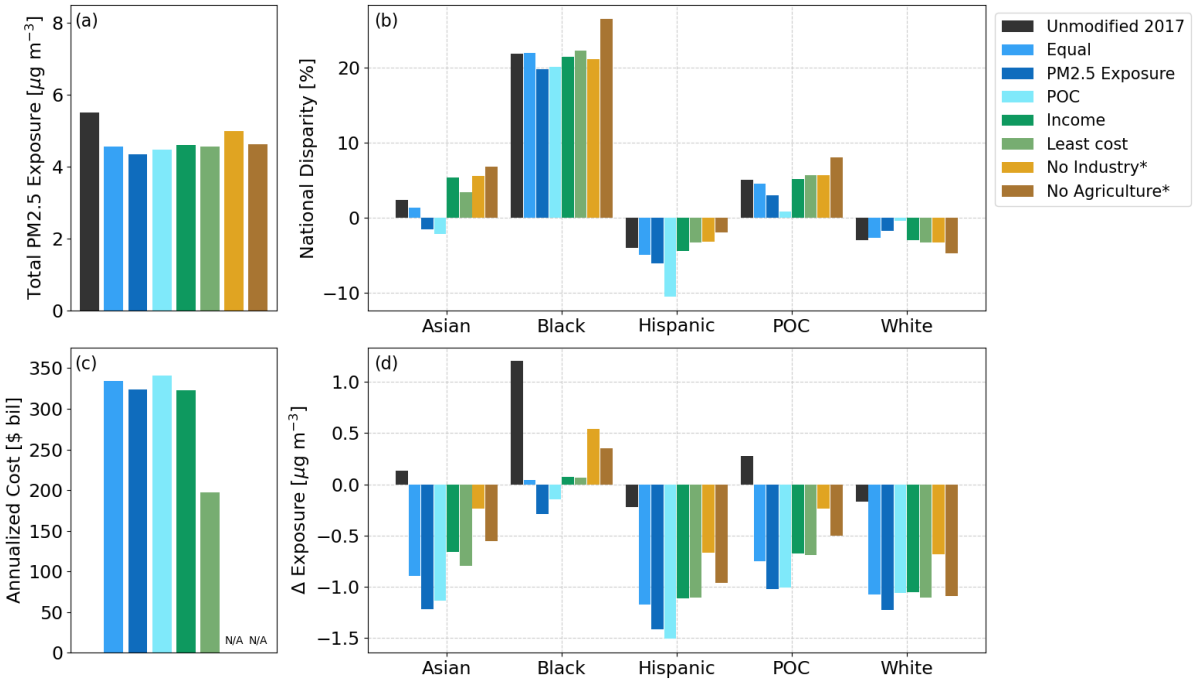

Figure A3.5. This figure is the same as Figure 2 but without bias correction. It demonstrates that the absolute magnitude of disparities and exposures are impacted by the use of the correction, though the difference in magnitudes between pathways remain consistent.

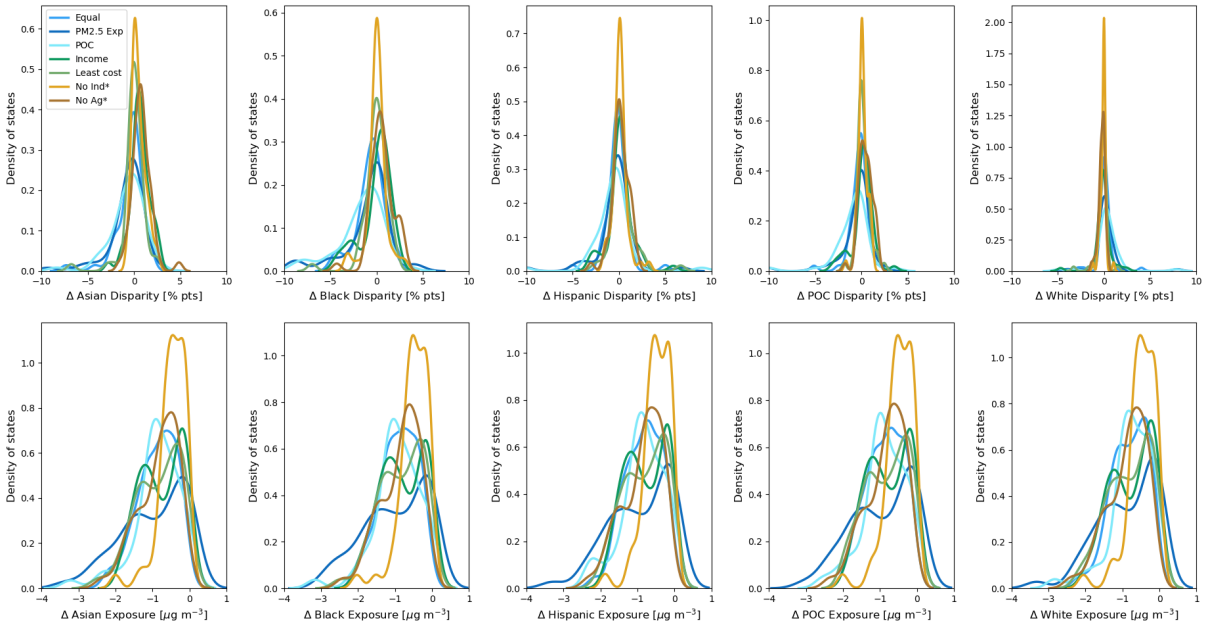

Figure A3.6. Distributions of state-level disparities for the idealized pathways shown in Figure 2. The top row shows disparities and the bottom row shows exposures. All are shown as a difference from the Unmodified 2017 case. When compared to Figure 2, this figure demonstrates that national-level changes between pathways are robust at the state level.

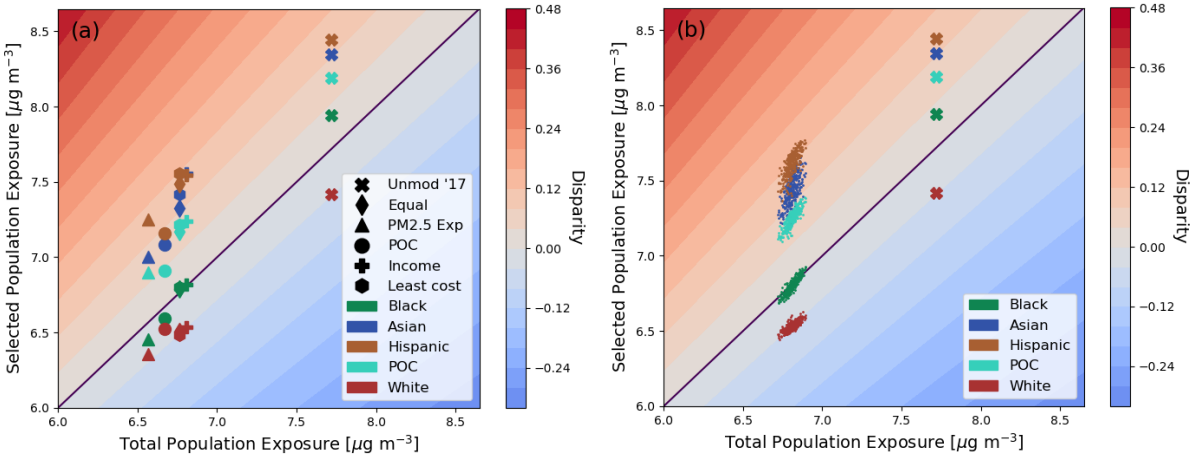

Figure A3.7. Total exposures, demographic-specific exposures, and disparities for different simulations. Disparity is a function of demographic-specific exposure and total exposure and is therefore shown in the background as contours. Exposures and disparities are shown for the idealized decision pathways (a) and randomized experiments (b) and Unmodified 2017 baseline emissions shown with an x. The colors indicate which racial/ethnic group is being used to calculate the selected population exposure and symbols are used to differentiate between experiments. This figure simultaneously shows how national exposures and disparities vary in the different simulations, by demographic.

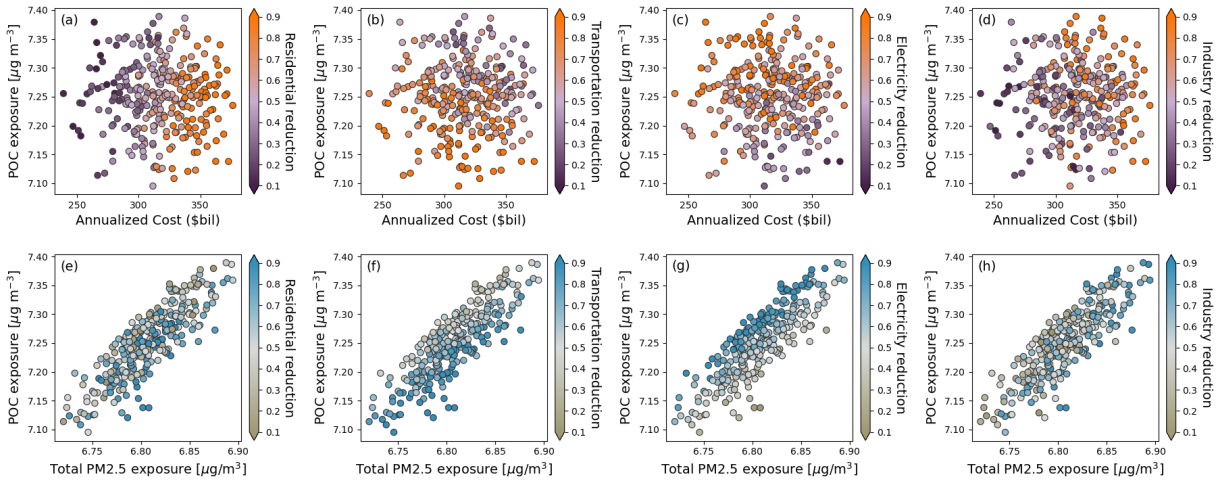

Figure A3.8. The first row (a-d) shows the relationship between POC exposure and total annualized cost of each randomized NDC-constrained simulation. The colors represent the fraction that the indicated sector has been reduced, between 0 (no reduction) and 1 (fully removed). The bottom row (e-h) shows the relationship between POC exposure and population-weighted PM2.5 exposure, with the fractional reduction indicated in color as for (a-d). (a) and (f) are identical to the panels in Figure 3. This figure contains all sectors to justify the selection of the main text panels. Panel (g) is noteworthy because it also shows a strong gradient for electricity emission reduction. However, random simulations with large reductions in electricity emissions often have relatively small reductions in transportation emissions because these two sectors account for large fractions of GHG emissions and the randomized pathways are constrained by total GHG reduction. We show in subsequent figures and text that we believe the change in transportation emissions (panel (f)) are the largest source of variation in disparities between randomized pathways (see Figure 4c, 4f).

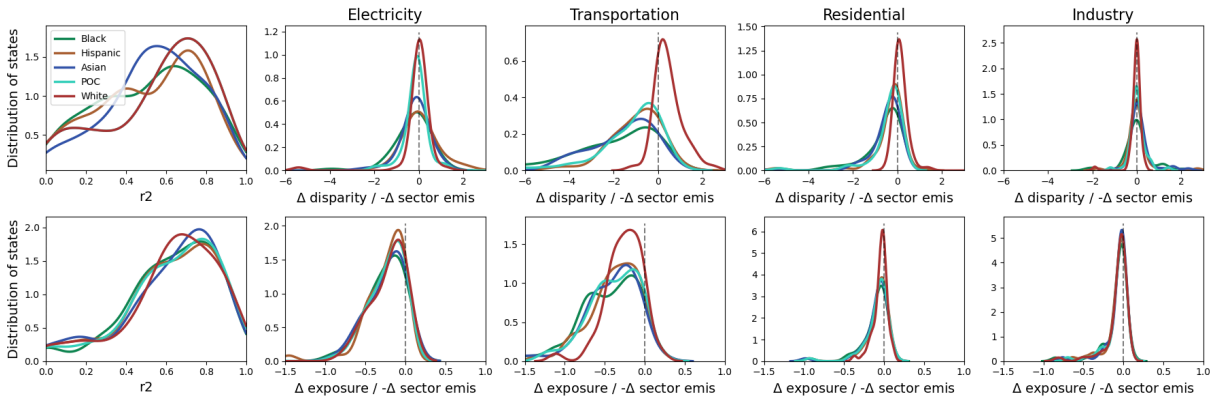

Figure A3.9. Coefficient of determination (r^2) and regression coefficients (as in Figure 4 c,f) for four sectors. The fraction is defined as the fraction of those considered in this study. For example, transportation only includes mobile on-road emissions and industry only includes the sectors described in the methods. This expanded version of Figure 4 shows that transportation stands out amongst the four sectors, which is the focus in the main text. The units for disparity change are in percentage points and the units for exposure change are μg m^{-3}. These distributions therefore show how disparity and exposures would change under a full removal of emissions from a sector. Given the setup of the randomized simulations, in practice, these can be interpreted as marginal changes (e.g. a 10% reduction would yield 10% of the unit indicated on the x axis).

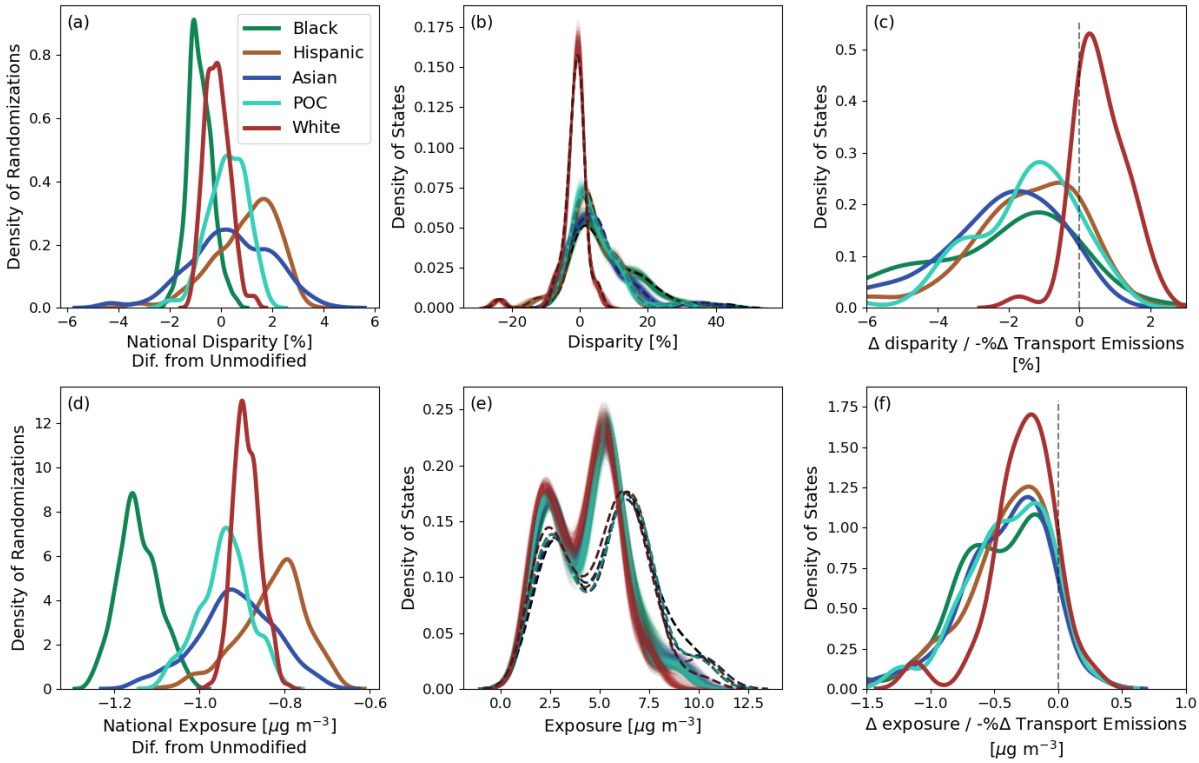

Figure A3.10. This figure is the same as Figure 4 but with no bias correction. This figure, when compared to Figure 4, demonstrates that relative differences are robust to the application of the bias correction.

Chapter 4

The spatial structure of Earth's climate and statistical estimation of climate impacts

4.1 Abstract

Many climate impacts studies rely on empirical statistical methods to isolate the impact of changing environmental factors on human outcomes of interest. However, this research has largely ignored the physical dynamics of the climate system, and how that underlying structure of climate might influence estimates from such models. Here we use a combination of real-world measurements, climate model output, and simulations to show how one basic feature of Earth's climate – the different characteristic correlation length scales of temperature and precipitation – contributes to biased historical and projected impact estimates in a standard empirical framework. Furthermore, we explore how by focusing on the impact of local fluctuations, these common empirical approaches may miss the impact of shifts in mean climate, another source of potentially significant underestimation of climate impacts.

4.2 Introduction

The quantification of climate impacts on human systems has largely relied on the statistical estimation of relationships between weather and outcome observations from the recent

past, followed by projection of those relationships under different future climate and adaptation scenarios [88, 89]. Advances and refinements to this methodological apparatus have resulted in increasingly granular impact assessments across a wide array of sectors – from health and mortality [90, 91, 92, 93], to crop yields [94, 95, 96] and total factor productivity [97, 98], to economic output [99, 100, 101, 102] – and form the basis for estimates of the Social Cost of Carbon (SCC)[103].

Although these empirical statistical models of historical impacts vary in their details, they share a common form:

$$Y_{it} = \sum_k \beta_{k,T} \cdot f(T_{it}) + \sum_k \beta_{k,P} \cdot f(P_{it}) + \mathbf{X}_{i,t} + \varepsilon_{it} \tag{4.1}$$

Here, Y is an outcome observed at locations i and times t, and $\hat{\beta}_k$ are best-fit coefficients (estimated by ordinary least squares or another regression method) that define the surface relating Y_{it} to temperature (T_{it}) and precipitation (P_{it}). $\mathbf{X}_{i,t}$ are included to control for various confounds that could vary across space, time, or both. $f(T_{it})$ and $f(P_{it})$ may take on more complicated functional forms – e.g., higher-order polynomials, splines, bins, or lagged structures – to capture potential non-linear responses.

The coefficients $\hat{\beta}_k$ can then be combined with (e.g.) bias-corrected climate model projections to estimate future impacts for all locations based on local changes in T and P (with $\mathbf{X}_{i,t}$ usually assumed to be constant into the future; i.e., in the absence of adaptation):

$$\Delta\hat{Y}_i = \left(\sum_k \hat{\beta}_{k,T} \cdot f(T_i + \Delta T_i) + \sum_k \hat{\beta}_{k,P} \cdot f(P_i + \Delta P_i) \right) - \left(\sum_k \hat{\beta}_{k,T} \cdot f(T_i) + \sum_k \hat{\beta}_{k,P} \cdot f(P_i) \right). \tag{4.2}$$

Although powerful and flexible, this framework rests on several assumptions that can be difficult to meet in the context of estimating climate impacts. Perhaps most obvious is the need for an appropriate form for the functional surface relating weather realizations to Y. Since the structure of this impact relationship is often not known ex-ante, researchers often estimate a range of specifications, and use fit metrics or cross-validation techniques to select a

preferred model. [100, 104] Less obvious but equally important are choices about the spatial and temporal scales of observation, i and t. Human and socioeconomic outcomes of interest (for example, population, income, health, agriculture) are often gathered and reported according to administrative boundaries. Environmental data may be gathered in a more spatially continuous manner, but their measurement is also often subject to capacity constraints. Measuring both outcomes and environmental drivers at appropriate scales can be challenging, and matching them for analysis adds further complication. [105, 106, 107] In contrast to current efforts towards improving the functional form and the exposure and outcome data, with few exceptions,[106] the climate impacts literature has paid little attention to the ways in which physical climate dynamics are or are not appropriately represented in empirical statistical frameworks, and the implications of the physical connections within the climate for impact estimation in such models.

Here we start from the distribution of global land-based temperature and precipitation measurements to demonstrate the fundamentally different spatial correlation length scales for these two parameters. We explore the distribution of measurement uncertainty as well as the interplay between imperfect measurement and spatiotemporal aggregation in empirical statistical estimation of impacts. By combining temperature and precipitation measurements with both real-world outcome data (Gross Domestic Product, or GDP, reported at different spatial scales [101]) and simulated outcome data, we are able to explore the interplay between physical climate features and statistical methods. We explicitly address the ways in which the correlation of climate variables and changing mean climate state pose unique problems in conjunction with standard methods for improved causal inference, and conclude with guidance for how future analyses might best account for these features, especially where credible projection of future impacts is an objective.

4.3 Results

4.3.1 Measurement of climate and spatial correlation lengths of temperature and precipitation

We begin by describing the state of available temperature and precipitation surface measurements. While gridded products are increasingly available from a spectrum of models and in situ and remotely sensed observations, these products rest on ground-truthing to surface observations. We therefore explore the global distribution of these measurements and their characteristics (Figure 4.1).

Unsurprisingly, measurements are concentrated in more economically-developed regions like the United States and Western Europe (Figure 4.1 (a-c)). The number of global observations is also not constant in time, with availability broadly declining over recent decades, especially in South America and Africa. This means that climate is especially poorly measured – in both space and time – in these tropical regions. Although understood though everyday experience and physical principles, these data nevertheless clearly show how T and P vary on different spatial scales. Figure 4.1 (d-i) reveals that the length scale of the correlation between neighboring measurements is about an order of magnitude smaller for P than for T, across a variety of environments. The shorter length scales for P are not due to imperfections in the measurements but are rather a physical property of the climate: temperatures are principally governed by insolation and planetary waves, while precipitation is driven largely by fronts and convective cells.

4.3.2 Measurement error and the spatial scale of analysis

One immediate consequence of these different correlation length scales is that data products that include any type of interpolation between station measurements (e.g., the University of Delaware global gridded T and P product) inevitably induce more error in P than in T at between-station locations. Moreover, some regions are much more subject to interpolation (and thus measurement error) than others. Though every measurement contains some fundamental

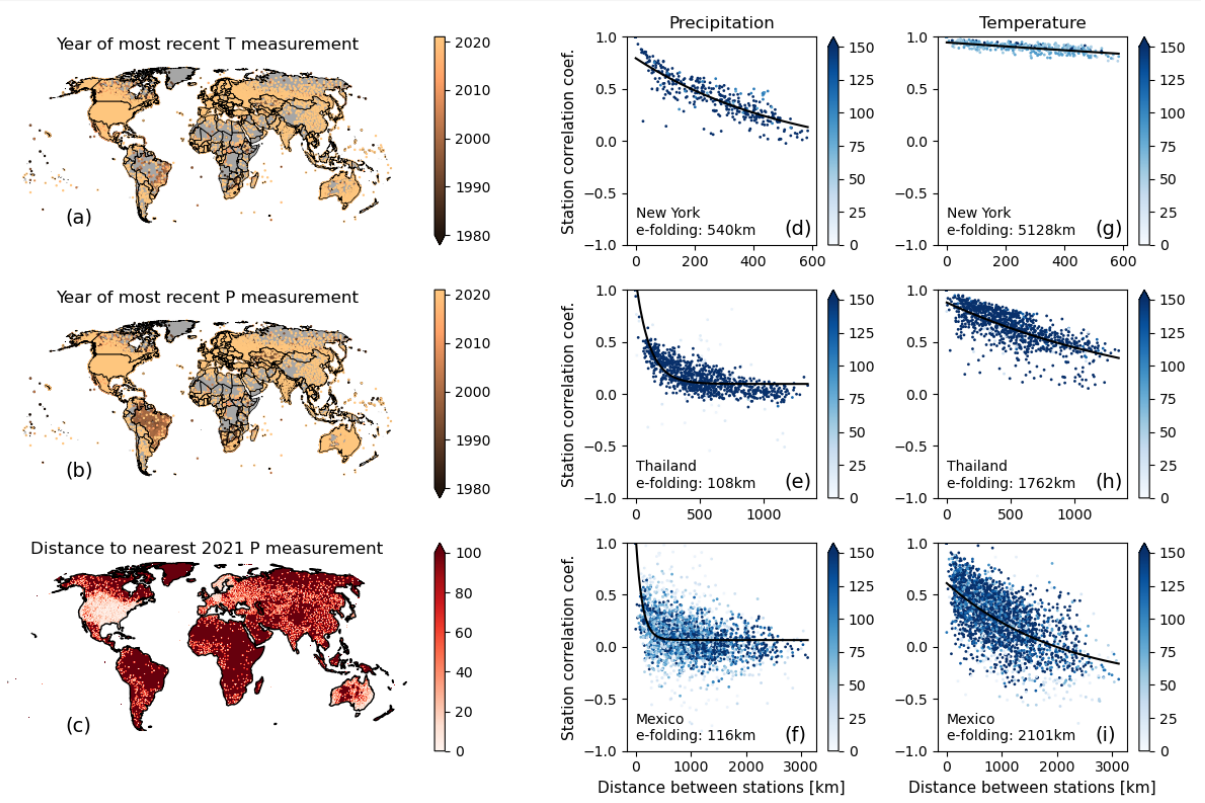

Figure 4.1. Measurements of temperature and precipitation reveal their characteristic spatial correlation length scales. **(a)** Measurement station locations for temperature in the Global Historical Climatology Network (GHCN) database and their most recent year of reported data in color. **(b)** Same as (a) but for precipitation. **(c)** The distance in kilometers from every location on Earth to the nearest 2021 precipitation measurement in the GHCN (note that distances that exceed 100km have been grouped together for presentation) **(d-i)** The correlations between monthly precipitation anomalies (d-f) and temperature anomalies (g-i) measured at stations in three regions (New York state, Thailand, and Mexico). In each panel, the correlations between station anomalies are plotted along with an exponential fit; this curve provides an estimate of the e-folding distance, or the characteristic spatial correlation scale for each parameter in that region. Note that the horizontal axes have different limits for the three different regions (top, middle, and bottom rows).

uncertainty due to equipment limitations and sampling, the additional induced measurement error from interpolation between stations of parameters with distinct spatial correlation lengths means that measurement error varies heterogeneously across T_{it} and P_{it} in Eqn. 4.1. We use the ensemble spread of the NOAA/CIRES/DOE Twentieth Century Reanalysis Project to show that measurement uncertainty is indeed higher in the same regions that lack dense observations

(Figure 4.2).

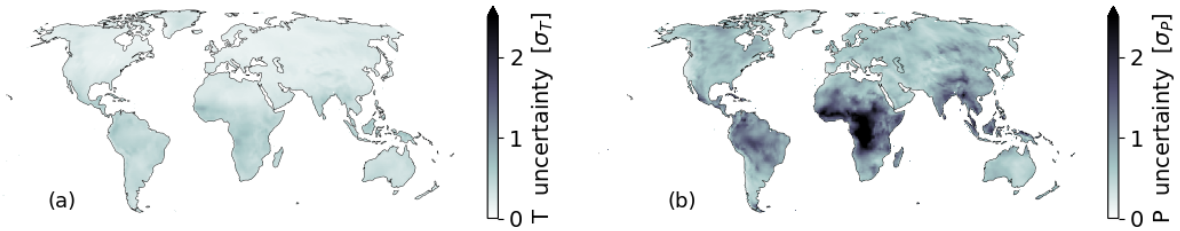

Figure 4.2. An estimate of uncertainty in T (a) and P (b) in units of interannual standard deviation, using NOAA/CIRES/DOE reanalysis data. Both panels show the relationship between variability in T and P in historical Earth system model runs (1980-2015) compared to the variability in mean T and P, as an estimate of how much measurement uncertainty likely exists in locations with few surface stations (see Methods for details).

This measurement error in global gridded (or interpolated) products is important not just for an appropriate local understanding of exposures to environmental factors, but also because it directly interacts with statistical estimation methodologies. In particular, regression analysis typically assumes no error in predictor variables, and finds the set of best-fit coefficients that minimize the distance between observed outcomes and predicted outcomes in Y-space alone. In this framework, measurement error in predictor variables (e.g., T_{it}, P_{it}, $X_{i,t}$ in Eqn. 4.1) leads to attenuation bias, or a suppression of the magnitude of fit coefficients.[108] Because P_{it} is both more variable and measured less well than T_{it}, statistical impact models are likely to suffer from disproportionate attenuation bias in the $\hat{\beta}_P$ coefficients relative to the $\hat{\beta}_T$ coefficients.

We demonstrate this by using an idealized modeling framework that allows us to specify the relationships between T_{it}, P_{it}, Y_{it}, and then adjust the relative strengths of impacts and simulate different types of measurement error. Specifying the 'true' outcome with real climate data allows us to explore how different features of the system contribute to biases in estimated coefficients and/or predicted outcomes. In our idealized model, we generate an outcome variable Y_{it} with a known quadratic relationship with T and P at the grid cell level. We then add different types of measurement errors to T and P (in part derived from the analysis in Figure 4.2), and then estimate the fit parameters and predicted outcomes with the imperfect simulated measurements (See

Methods). Figure 4.3 (left panel, labeled 'Pixel') shows the results of this analysis, presented in terms of marginal impacts (so the impact on $\hat{Y}$ of a unit change in T or P_{it}). The 'true' relationship (black lines in each panel) is a concave quadratic, where Y is maximized at an optimum value of T and P. Addition of realistic measurement error, of the magnitude shown in Figure 4.2, results in the estimated fits shown in solid red (T) and blue (P). This error leads to attenuation bias for both parameters, but it is much more pronounced for P, as expected. We also reverse (dashed lines) and randomize (dotted lines) the location of the measurement error to demonstrate the impact of different error distributions (see Figure A4.1 for explicit representations of these distributions). Again, the measurement error of any sort causes clear attenuation bias in all cases, and disproportionately for P; this is expected since the uncertainty in P is larger than for T, even relative to interannual variability. However, the magnitude of the effect depends strongly on the location of the measurement error, demonstrating that while imperfect observations are a well known source of attenuation bias, the magnitude of errors in environmental measurements are not randomly distributed in space but rather systematically larger in certain climate zones like the tropics. The heterogeneity in both climate and our measurement of it has helped condition the magnitude of attenuation bias likely embedded in current damage function estimates.

This same idealized modeling framework allows us to explore the interplay measurement error and the spatial scale of analysis. The empirical statistical framework (Eqn. 4.1) requires that outcome data and environmental observations must be aggregated or disaggregated to the same spatial and temporal resolution even though the natural length and time scales of analysis are generally different for social and natural systems (and different between temperature and precipitation). [101] As a result, researchers face a choice about how to match predictor and outcome data for analysis. While it is true that disaggregation of data (i.e., moving to higher resolution) leads to a higher number of observations (n) and thus improved statistical power, if those higher-resolution data are in fact estimates that include measurement error as described above, analysis at higher spatial resolution can have the pernicious effect of producing higher statistical confidence in more biased measurements (as in Figure 4.3, left panels).

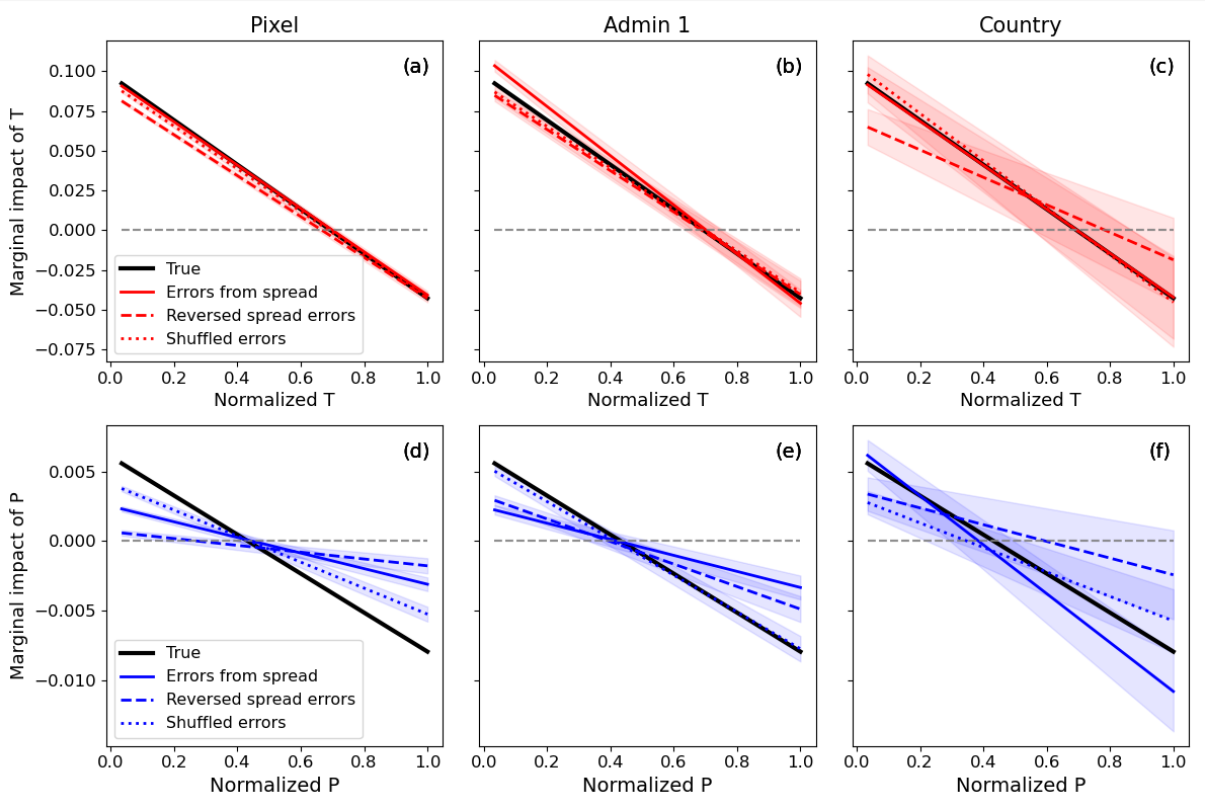

Figure 4.3. Marginal impact functions under measurement uncertainty. Each figure shows the derivative of an idealized outcome variables with a known quadratic relationship (black) and the estimated impact after adding error to the independent variables (color). Errors from spread are defined using Figure 4.2. Swapped errors are the same except the location of high and low errors have been reversed. Shuffled errors have randomized locations of the same errors. Marginal change for the temperature relationship are shown in the top row and marginal changes in precipitation are shown in the bottom row. The columns contain the same information for three levels of spatial aggregation.

Perhaps counterintuitively, spatial aggregation tends to decrease measurement error because multiple measurements are combined into the unit of analysis (Figure 4.4). However, this comes at the cost of decreasing the number of observations and thereby increasing the standard errors of predicted coefficients and outcomes. This is evident as the analysis in Figure 4.3) moves from 0.5° pixel to Administrative level 1 (e.g., state, province) and finally to Country level (right panel). Country-scale analysis has less bias in *P* than pixel-scale analysis, but much wider confidence bands on those estimates. At all levels of aggregation, there is an asymmetry in the relative bias of the T and P coefficients (Figure 4.4). This is largely caused

by the higher variability in P, which means that an uncertainty of one standard deviation causes more uncertainty in the outcome than a standard deviation of uncertainty in T. We show this by re-estimating model coefficients across a wide range of added T and P errors. Figure 4.4 shows only the relative bias in T and P, while Figure A4.3 also shows the T and P components of the outcome individually.

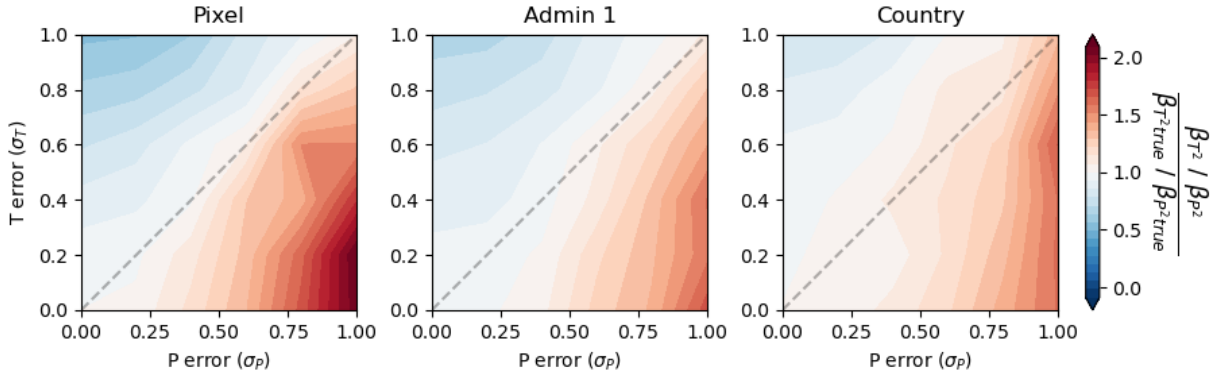

Figure 4.4. Relative bias in the strength of estimated temperature versus precipitation impacts on an outcome Y in an idealized modeling framework. Contours show the estimated ratio of the quadratic components of T and P, under uniform added error in T and P, to the true ratio of those components (specified ex-ante). Red shading indicates that T is overvalued relative to P. Error is added as a function of unit-level interannual standard deviation of T (vertical axis) and P (horizontal axis). Regressions are population-weighted at the pixel level, while T and P are aggregated using population weighting for the administrative 1 and country-level regressions.

4.3.3 Correlation between temperature and precipitation

Hard physical links exist between temperature and precipitation. On interannual time scales, these have been negatively correlated in a majority of areas over land, particularly for populated areas (Figure 4.5). In other words, over the recent past (the time period over which empirical statistical impacts studies have been conducted), hotter temperatures have usually occurred in conjunction with drier conditions, and cooler temperatures in conjunction with wetter conditions. This poses problems in the context of empirical statistical frameworks, because they treat $T_{i,t}$ and P_{it} as inherently separable and statistically identifying estimates for $\beta_{k,T}$ and $\beta_{k,P}$ from their *independent* variation. High levels of correlation between predictor variables leads to

uncertainty, because (e.g.) there is no way to tell whether the correlated impacts in hot and dry years should be attributed to the temperature or the precipitation component of the climate. This leads directly to inflated standard errors and potential instability in coefficient estimates.

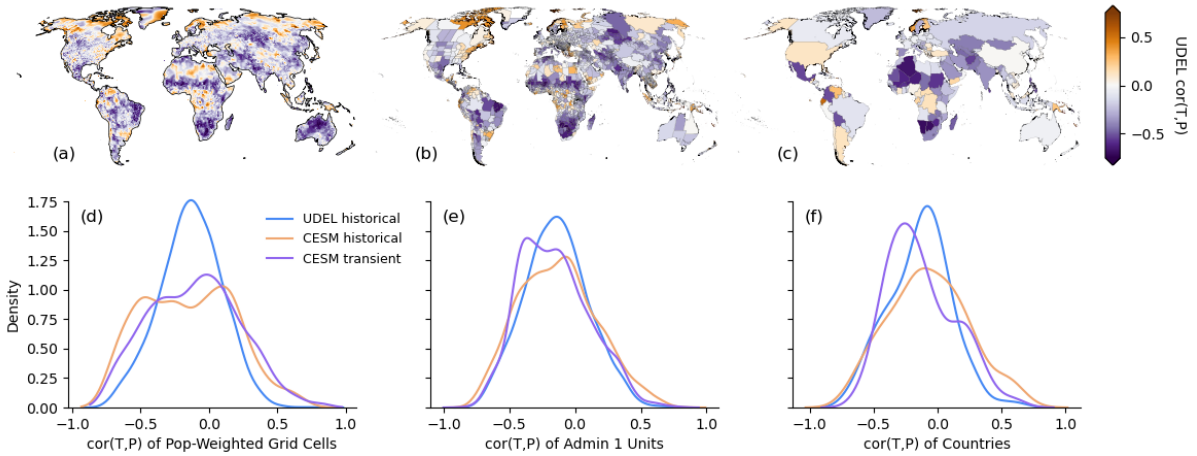

Figure 4.5. The correlation between annual average temperature and total annual precipitation at different spatial scales of aggregation. (a-c) show maps of UDEL historical $cor(T,P)$ from 1960 to 1990 using population-weighting for aggregation to administrative 1 and country levels. (d-f) show histograms of the same maps as well as the equivalents for a CESM2 historical simulation and a transient warming scenario (SSP2) from 2040 to 2070.

Empirical statistical analysis frameworks tend to assume that collinearity (correlation among predictor variables) is fundamentally a missing data problem, where more data would provide independent variation between the correlated variables, and thus enable statistical isolation of their independent effects. [109] However, in the case of climate impacts, the physical coupling can limit their separability, even with more data or higher spatial or temporal resolutions. In other words, separability might not even be meaningful in a climate impacts context because climate as a whole will evolve in different locations, and the aim of impact assessment is to quantify the collective impact of environmental changes on human outcomes.

While these limitations are well documented in the statistics and econometrics literature, a less-considered consequence of this physical correlation is that it can lead to bias in the presence of measurement error. To illustrate this, we set up an idealized simulation of two

sets of correlated, random normal data that are meant to represent T and P. For simplicity we assume that the error in T is zero and we then adjust the error in P; we do this both for a simulated outcome that is linearly dependent on T and P as well as for a quadratic dependence. For this illustrative example we assume that T and P are of approximately equal importance in determining the outcome Y. We find that the magnitude of the biases changes as a function of *both* measurement error and $cor(T,P)$. Most important, we show that the measurement error in P is in a sense propagated via correlation into the coefficient estimates for T, even though T is measured without error. That is, in addition to the expected attenuation bias in the P coefficient(s) from measurement error, the estimated coefficient(s) for (perfectly-measured) T is also affected (Figure 4.6). This interplay likely contributes the asymmetry shown in Figure 4.4. In that simulation, the idealized outcome is created using UDEL T and P, meaning there is an underlying correlational structure between T and P that is largely negative (Figure 4.5).

4.3.4 The role of mean climate state

A final interaction between the spatiotemporal structure of climate and empirical statistical analysis of human-natural systems comes in the fact that most analyses occur in 'anomaly space' – that is, they focus on the relationships between climate and outcomes of interest *within* observations over time at each location. This is attractive from a causal inference perspective, because it is well known that the variation observed in many socioeconomic outcomes between different entities, for example countries, has not been primarily driven by climate but by other differences between locations, such as economic and political institutions. Researchers understandably want to account for this type of cross-sectional variation in outcomes across units of observation to more clearly isolate the climate component.[110] Practically, this is accomplished in an empirical statistical framework through inclusion of location-specific intercepts in Equation 4.1, X_i; these simultaneously de-mean outcomes and predictor terms, such that the analysis now describes how Y_{it} changes from its mean value when a location is (e.g.) hotter or wetter *than its average*. These X_i are known in the literature as fixed effects, because they

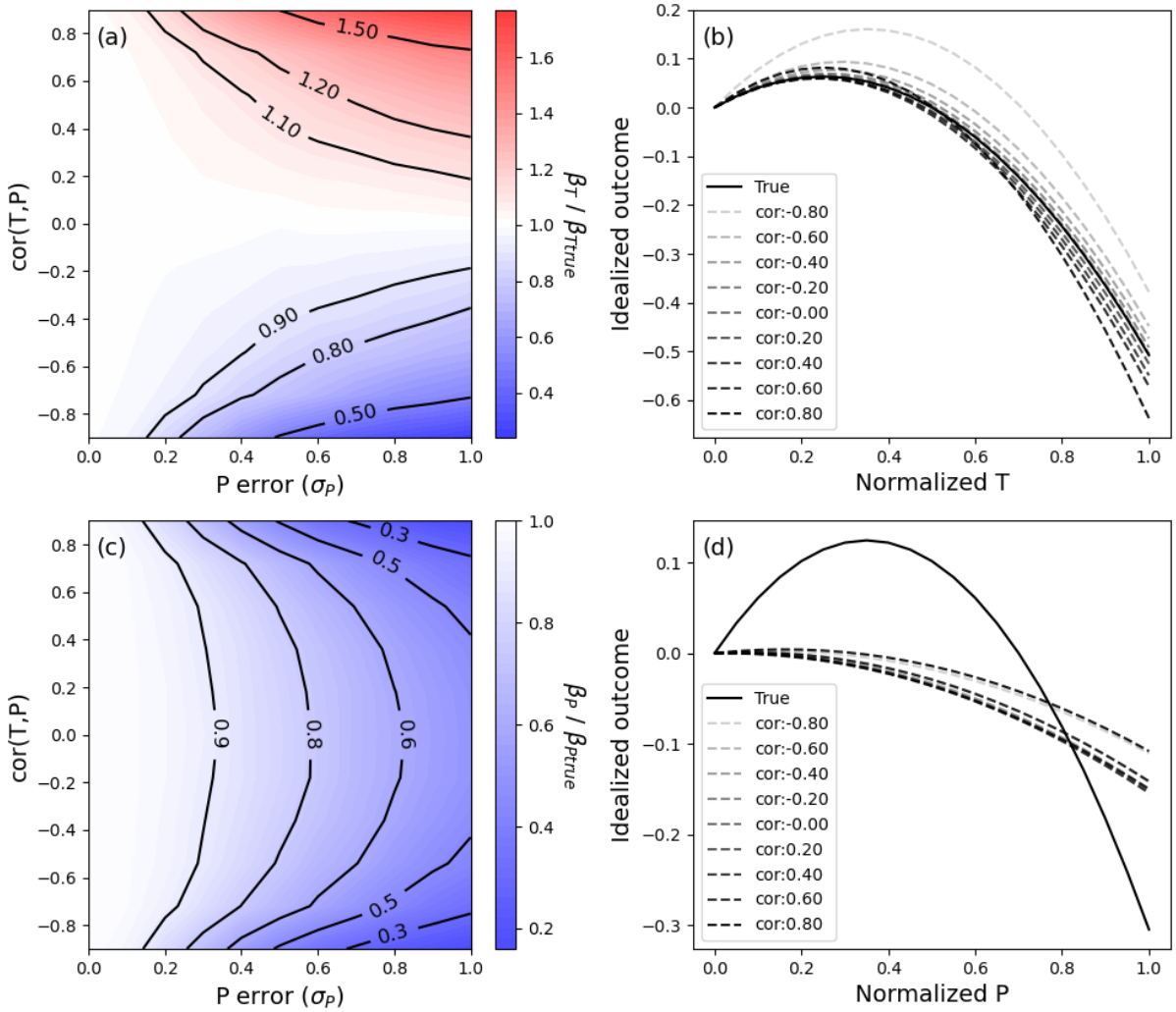

Figure 4.6. Bias in coefficients and predicted outcomes estimated with linear and quadratic regression models in the presence of measurement error in P and correlation between T and P. Bias relative to T is shown in (a,b), and relative to P in (c,d). Linear results as a function of P error are shown in a) and c), quadratic results with P error set to one standard deviation are shown in b) and d). Temperature and precipitation are given approximately equal weight in contributing to the simulated outcome. Each simulation was conducted with 50 observations per unit (i), and 30 cross-sectional units. Each model was estimated 10 times; plots show the average coefficient or outcome estimates across those 10 simulations.

are time-invariant but location-specific. However, while these fixed effects control for mean differences in outcomes across units, they also by construct include a lot of information about the mean climate state. Under climate change, this climatically rooted component of the "fixed effect" maybe become unfixed.

To demonstrate the potential importance of the mean climate state, and potential shifts in mean climate under future climate change, we utilize the GDP data described above. Using the same prediction framework as with the idealized model, except now with population-weighting, we estimate the response of per capita GDP to temperature and precipitation:

$$log(GDP_{pc})_{it} = \beta_T T_{it} + \beta_{T^2} T_{it}^2 + \beta_P P_{it} + \beta_{P^2} P_{it}^2 + \mu_i + \nu_t + \varepsilon_{it} \tag{4.3}$$

Here μ_i and ν_t are unit and time-specific intercepts (i.e. fixed effects; the ν_t analogously control for time-specific but location-*invariant* phenomena across the system of study, such as a global recession). As before, the T and P terms of this model are meant to capture the climate drivers of variation in economic output, while μ_i and ν_t account for other unobserved factors. In practice this means that the both the dependent and independent variables are demeaned, converting the regression to unit-level anomalies and removing the cross-sectional variation that accounts for much of the total variability. Although this is desirable to isolate the impacts of T and P on economic output, these "fixed effects" contain information about the mean climate of each spatial unit, which, when projecting to new climate futures, are no longer fixed. To demonstrate this temperature dependence, we fit another regression to μ_i+ν_t (here called FE, for fixed effects) with a similar quadratic form:

$$FE_{it} = \beta_0 + \beta_{T,FE} \bar{T}_{it} + \beta_{T^2,FE} \bar{T}_{it}^2 + \beta_{P,FE} \bar{P}_{it} + \beta_{P^2,FE} \bar{P}_{it}^2 + \varepsilon_{it} \tag{4.4}$$

where β_0 is an unconstrained intercept. The resulting surfaces from Eqn.4.3 and Eqn.4.4 are shown in Figure 4.7, estimated for different scales of spatial aggregation. The top row represents the estimated impacts of high frequency (annual) within-unit variability in T and P, whereas the bottom row shows the longer term association between mean climate state and GDP. This analysis underscores that a unit change in mean state temperature or precipitation is considerably larger than the interannual variability component. Moreover, the total adjusted R^2 of Eqn. 4.3

estimated with these data is above 95% for all three spatial scales of analysis, but almost all of that explanatory power comes from the fixed effects (the within-R^2 is less than 1% in all cases). When fitting Eqn. 4.4 with the fixed effects extracted from those regressions, we find that the T and P terms jointly explain about a quarter of the variation (adjusted R^2 of 0.22-0.25, depending on the spatial scale). Practically, this means that fixed-effects models like Eqn. 4.3 are discarding a lot of climate-related variation in the name of causal identification.

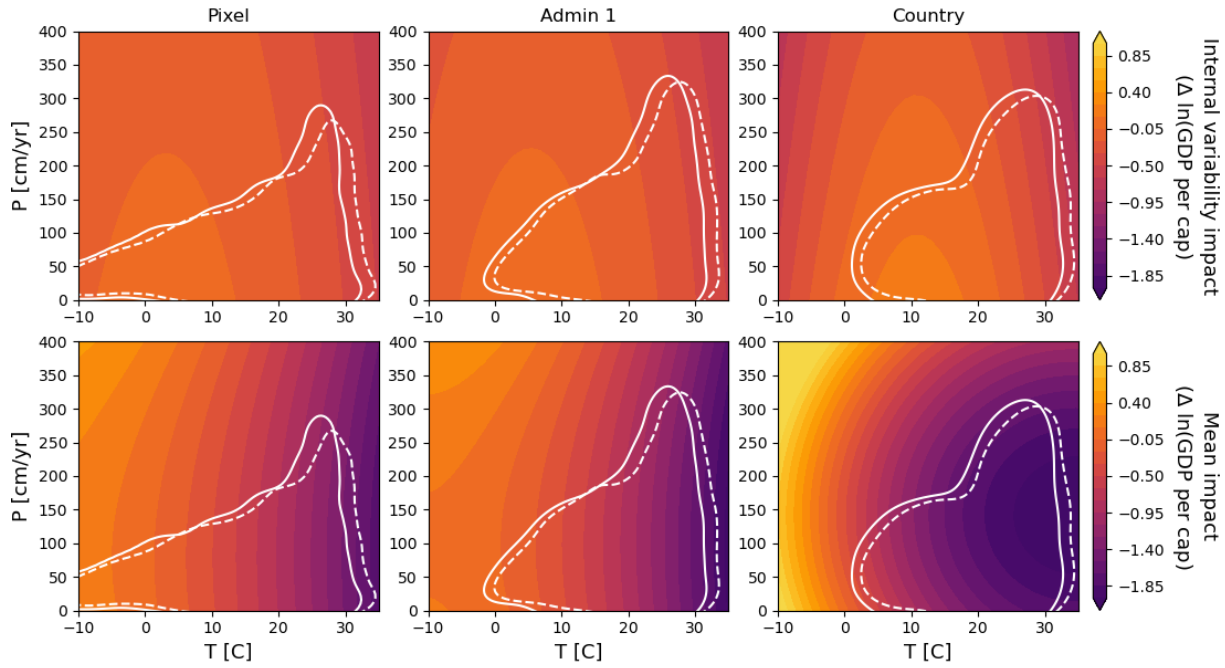

Figure 4.7. Surfaces resulting from Eqn. 4.3 (top row) and Eqn.4.4 (bottom row). The top row represents the relationship using only the internal variability of each country and the bottom row shows the remaining cross-sectional relationship. The solid contour indicates the distribution of 90% of 1990 data data, and the dashed contour shows the same for 2050.

This tradeoff between information and causal identification may be desirable in terms of most accurately determining the response surface of (e.g.) GDP for the recent past, but it presents significant issues when considering projections of future impacts. Numerous studies and reviews have discussed the conditions and assumptions under which Eqn.4.2 may be used, but in all cases it is important to note that its direct application conflates changes in mean climate state with interannual variability in the future. [111]

Here we separate these two time scales and allow for the response to a mean climate shift to differ from the response to interannual variability. This two-part projection (from Eqn.4.3 and Eqn.4.4) is shown for predicted climate-driven GDP impacts in 2050 in Figure 4.8. A key difference in our methodology is that we only project forward the portion of fixed effects from from Eqn.4.3 that are truly climate invariant (i.e., the residuals from Eqn.4.4). We then allow the mean state relationship to evolve independently (according to Eqn.4.4) from the impact of interannual variability (from Eqn.4.3) out to 2050. We find that, except for select locations in the tropics where large changes in precipitation are predicted, temperature effects dominate GDP damages. Consistent with previous studies, when considering interannual variability (Eqn.4.3) some cold regions at high latitudes are projected to benefit from climate change, whereas lower latitude regions are projected to see significant harms (4.8). After adding projections from shifts in the mean climate state, damages are nearly universal, though tropical locations are still projected to experience worse outcomes than mid- or high- latitude locations (Figure 4.8).

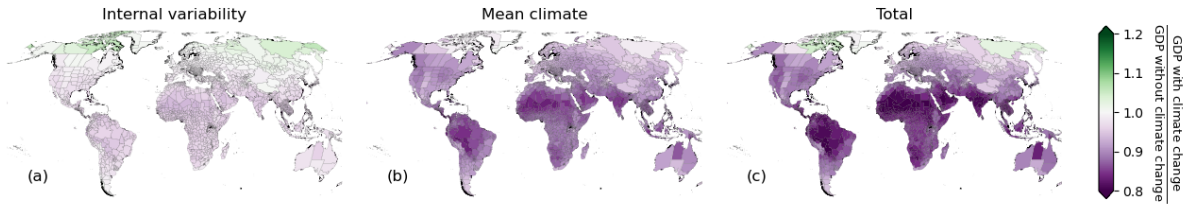

Figure 4.8. Maps showing the ratio of predicted GDP with and without climate change by 2050 using CESM SSP2 climate projections. (a) includes only the results from a traditional panel model that uses internal variability. (b) includes only the impact of a shift in the mean climate (assuming that future cross-sectional relationships look like past cross-sectional relationships). (c) is the total of both the internal variability and mean change components.

4.3.5 Combining idealized and real-world models for more accurate impact estimates

Lastly, we combine the various methodological corrections described above, from Figures 4.2 and 4.3, with our GDP model (as in Figure 4.8). We tune the idealized model to match the GDP data, and then iterate to back out the ”true” regression coefficients that yield the same estimated parameters as the GDP regression, assuming the error distribution from Figure

4.2. The resulting estimated GDP impacts are shown in Figure 4.9b, and compared to an uncorrected projection in Figure 4.9c. The correction demonstrates that even for the traditional panel regression (i.e., without separating the cross-sectional mean component from above), GDP impacts may be substantially underestimated, often accounting for an additional 1-2 percentage points of GDP damage.

As shown in Figure 4.3, the bias is substantially larger for P than for T 4.9d. It is therefore unsurprising that after applying the correction, P accounts for a larger fraction of the predicted GDP impacts (Figure 4.9d). In this case the GDP panel regressions indicate that T accounts for a much larger fraction of GDP impact than P, and the changes in (c) are still largely dominated by changes in T. However, this correction serves as evidence that attenuation contributes to the undervaluation of P[101] and suggests that other analyses focused on impacts or regions where P plays a larger role (e.g., agricultural productivity studies) are subject to significant underestimates if no correction for measurement error is applied.

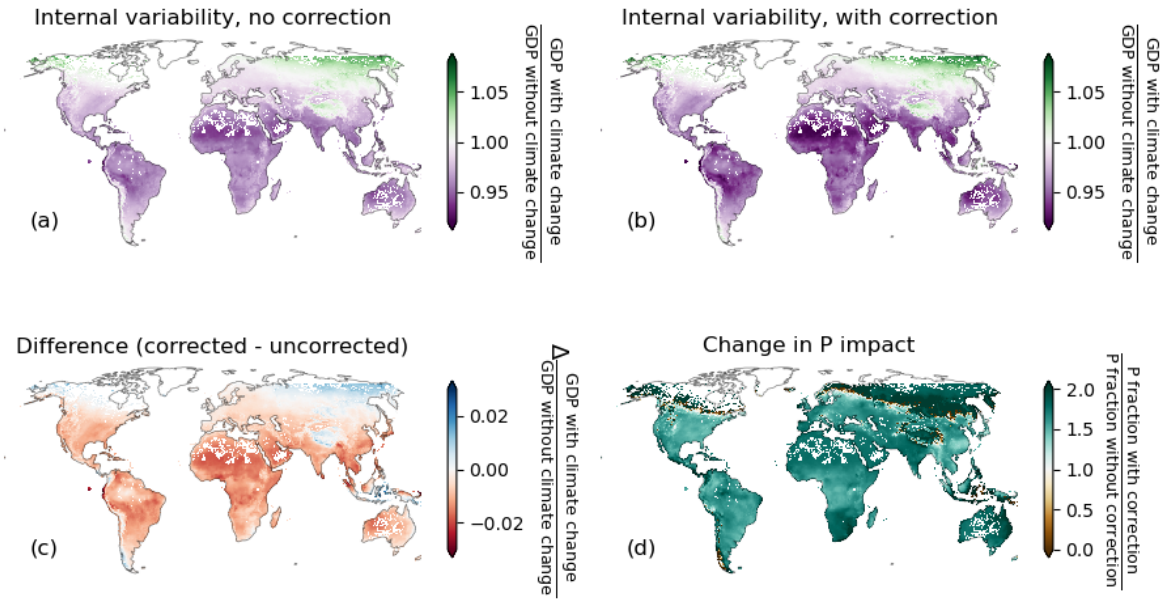

Figure 4.9. Pixel-level maps showing the ratio of predicted GDP with and without climate change by 2050 using CESM SSP2 climate projections. (a) includes only the results from a traditional panel model that uses internal variability. (b) contains the same information as (a) but includes a correction for measurement uncertainty, and (c) is the difference between (a) and (b). (d) shows the increase in the fraction of P impacts.

4.4 Discussion

Our analysis demonstrates that the spatio-temporal structure of Earth's temperature and precipitation in the recent past has contributed to biased historical and projected impact estimates in standard empirical frameworks. This bias is exacerbated by both measurement constraints and the statistical approaches used for causal identification. Specifically, our analysis reveals that climate impact estimates have likely underestimated the impact of precipitation changes on key outcomes, and this is worse in empirical models that utilize location-specific intercepts designed to account for outcome differences that are non-climate related (i.e., location fixed effects). Despite the impact being significantly larger for precipitation, other studies have also shown this bias for temperature in different contexts [112]. We also show that, perhaps counterintuitively, impacts may be better identified at moderate spatial aggregation, because attenuation bias can be quite large at high spatial resolutions. However, there is a trade-off between reducing measurement error on one side and losing granular detail and maintaining statistical power on the other side.

We highlight that correlation between temperature and precipitation can lead to biased estimates in the presence of measurement error, especially when measurement error is not uniform across multiple independent variables. Although this is not necessarily a surprising finding, it is not well documented in the climate impact literature and is particularly pertinent when considering environmental variables with fundamentally different physical properties. Since there is more variation in $cor(T,P)$ across larger spatial scales, this source of bias is likely more important for regional- or smaller-scale studies where $cor(T,P)$ may be more homogeneous across the study area.

One pervasive result in studies applying statistical climate impact models has been that the magnitude of damages driven by changes in temperature often dominate those driven by changes in precipitation - sometimes the effect of precipitation is even statistically insignificant.[88, 99] In the case of agriculture, it has been shown that soil moisture is a better predictor of crop

yields than using T and P individually,[109] highlighting that the coupled nature of T and P can drive outcomes, as T and P jointly determine soil moisture. In at least one case the relative unimportance of P is explained as an adaptation to larger natural variability[113]. In other cases it is simply treated as a confounding variable when trying to identify the impact of T, despite the fact the treatment of T and P is functionally identical and the reverse interpretation would be equally valid (e.g. Cai et al., (2016), often citing Auffhammer et al. (2012)). [114, 106] If effects of T and P are misattributed, projections will be inaccurate because historical correlations between T and P are will not necessarily remain consistent with the past in a changing or changed climate. This situation is especially relevant to impact projections for solar geoengineering scenarios, which often demonstrate that temperature changes can be largely halted by reflecting sunlight, but only with large residual regional precipitation changes that do not factor strongly into GDP impact estimates.[115, 116]

Lastly, we illustrate the potential importance of more explicitly considering the mean climate state as part of climate projections. Though we appreciate the aims of causal analysis, we also note that its fundamental signal-to-noise tradeoffs limit its applicability for future projections. Quadratic fixed effect models allow for different responses at different T and P[117, 110] but the use of unit-specific intercepts removes information about the mean climate, which will not stay fixed as the climate changes. (This is also true for $cor(T,P)$, which we show introduces its own complications into impacts estimation, and is projected to change heterogeneously as shown in Figure A4.2) Using a cross-sectional approach to model how fixed effects are climate-dependent (as we do here) implies some level of environmental determinism or possibilism, the implications of which are part of a long-running discussion among environmental geographers [118]. We recognize that the methodology used here is unconventional; we intend for it to demonstrate the strong climate dependence of the fixed effects commonly assumed to be stationary and encourage climate impact researchers to consider new ways that the mean climate state could be more explicitly modeled in future analyses, with the explicit goal of more credible impacts projection.

There have been a number of efforts to address some of the issues outlined above.

Some studies split analyses into a set of more local ones to test whether models are robust to location.[119] Satellite measurements are improving ground-truthing and using machine learning models to increase fidelity of remotely-sensed weather data and disaggregating socioeconomic outcome data.[120] As mentioned earlier, some studies are using more integrated measures like soil moisture to improve 'exposure' estimates,[121] or building heuristic models with functional forms that have a basis in physical models. Other numerical techniques like error-in-variables methods acknowledge measurement error in predictors and outcomes and minimize (e.g.) a Euclidian distance to the response surface, though these techniques are also imperfect.[122] Spatial first differences techniques use gradients in cross-sectional data to estimate impacts, avoiding use of fixed effects entirely. However, such a method would need to more explicitly account for the correlation between T and P to facilitate credible projections.

The considerations laid out in this analysis are not simple to address individually, and become even more complicated when considered in combination. However, recognizing potential pitfalls and drawing on the physical sciences literature about measurement quality, environmental coupling, and biophysical interactions can help improve empirical estimates of the impacts of climate change. A first natural takeaway from our analysis is that improved measurement networks that increase coverage in underserved regions will be especially powerful. However, in the meantime, as data are made available at increasing granularity, it is ever more important to understand the underlying fundamental spatial scales of both the physical system and its measurements, and making informed choices about the optimal scale of analysis based on the goals at hand. If modeling future impacts is an objective, our analysis highlights that new techniques may be helpful in allowing researchers to separately model the responses of human systems to larger, slower-moving mean-state shifts versus local anomalies. The physical sciences can also contribute to solutions by improving measurement networks and providing easily accessible error estimates when publishing datasets. Improving climate impact assessments will require further communication between these two communities.

4.5 Methods

4.5.1 Data

For surface air temperature and monthly precipitation, we used the monthly University of Delaware (UDEL) datasets, which have a 0.5° resolution. We take the annual mean for T and the annual sum for P. For our uncertainty estimate in gridded T and P, we used data from the NOAA/CIRES/DOE Twentieth Century Reanalysis (V3). Support for the Twentieth Century Reanalysis Project version 3 dataset is provided by the U.S. Department of Energy, Office of Science Biological and Environmental Research (BER), by the National Oceanic and Atmospheric Administration Climate Program Office, and by the NOAA Earth System Research Laboratory Physical Sciences Laboratory. These data were provided by the NOAA PSL website. Reanalysis data was interpolated to 0.5° resolution to match the other datasets. To quantify uncertainty, we use the model ensemble spread since model standard deviations are not provided directly. We approximate the standard deviation by dividing the spread by 4, assuming that the spread is approximately equal to $\pm 2\sigma$. Annual data are not available, so we combine monthly spread into an annual spread by taking the square root of the mean squared monthly standard deviation. We then divide by the annual grid cell standard deviation of the mean over time to to obtain the uncertainty metric. We use data from 1980 to 2015 as this is a common time-frame for empirical climate impact studies. This metric is then applied to the UDEL data my multiplying the metric by UDEL grid cell standard deviation. The UDEL standard deviation and the spread metric are both shown in Figure A4.1 Climate data for projections to 2050 were taken from CESM2 SSP245. We take the mean from 2045 to 2055 as the average 2050 condition to smooth internal variability.

We use the purchasing power parity adjusted gross domestic product (GDP PPP) data from Kummu et al. [123], which is allocated to 5 arc minute grid cells from administrative 1 and country data, depending on data availability. For our pixel-level analysis we aggregate to 0.5° by summing grid 6x6 grid cells to the UDEL grid. As is done for other variables in the same dataset,

we then normalize by population using the HYDE 3.2 dataset[124], which was aggregated to the pixel level in the same way as the GDP dataset. All data (including T and P) were aggregated to the administrative 1 and country levels using a rasterized map created from shapefiles from the Global Administrative Areas dataset (GADM 3.6) using the Python package geocube. When spatially aggregating we applied population weighting.

4.5.2 Idealized Model Framework

We implement several slightly different versions of the idealized regression model but in all cases we create the outcome variable as an exact function of T and P and then add error to one or both T and P, estimate the coefficients, and compare them to the known relationships:

$$y_{i,t} = \beta_T T_{i,t} + \beta_{T^2} T_{i,t}^2 + \beta_P P_{i,t} + \beta_{P^2} P_{i,t}^2 \tag{4.5}$$

$$\hat{y}_{i,t} = \hat{\beta}_T (T_{i,t} + \delta_{T,i,t}) + \hat{\beta}_{T^2} (T_{i,t} + \delta_{T,i,t})^2 + \hat{\beta}_P (P_{i,t} + \delta_{P,i,t}) + \hat{\beta}_{P_{i,t}}^2 (P_{i,t} + \delta_{P,i,t})^2 + \varepsilon_{i,t} \tag{4.6}$$

δ is applied as a function of the standard deviation of the annual mean for T and annual sum for P. This means that if, for example, a standard deviation of error applied to a grid cell, for each year in the dataset we draw randomly from a standard normal distribution and multiply the result by the grid-cell level standard deviation. The linear case in Figure 4.6 does not include the quadratic terms in Eqn. 4.5 or Eqn. 4.6 but is otherwise the same. In some cases we select T and P from a random normal distribution and vary $cor(T,P)$. In the cases where we use the UDEL dataset as the underlying T and P, the correlational structure of that dataset is retained.

4.6 Acknowledgements

This chapter, in full, is currently being prepared for submission for publication of the material. Polonik, Pascal; Ricke, Katharine; Burney, Jennifer. The dissertation author was the primary investigator and author of this paper.

4.A Appendix for Chapter 4

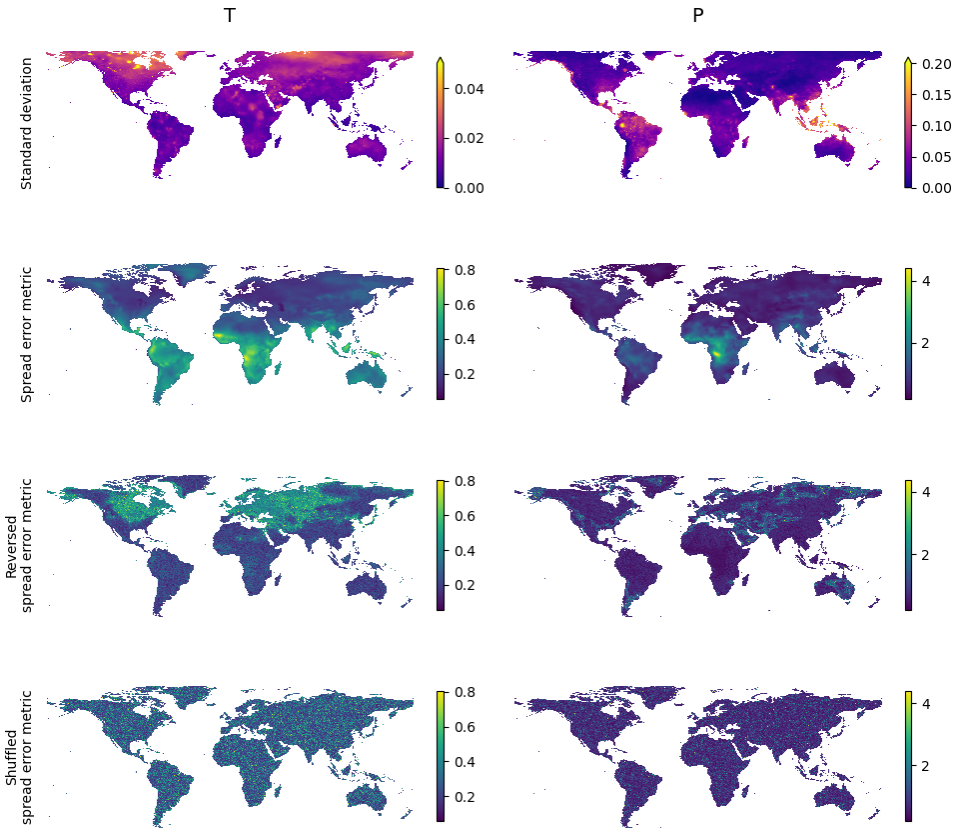

Figure A4.1. Maps of the standard deviations of T and P from the UDEL dataset and of spread metrics from the NOAA-CIRES-DOE Twentieth Century Reanalysis Project. The spread metric was calculated as the reanalysis spread (i.e. range), divided by four to get an approximate standard deviation of the uncertainty, divided by the model interannual standard deviation. This represents the uncertainty relative to local interannual variability. The reversed spread metric swaps the location of the highest and lowest uncertainties and the shuffled spread metric randomizes the spatial distribution globally. These metrics are multiplied by the standard UDEL grid cell interannual standard deviation (top row) to add regional uncertainties to the idealized model simulation. The Spread error metric (second row) contains the same information as Figure 4.2

.

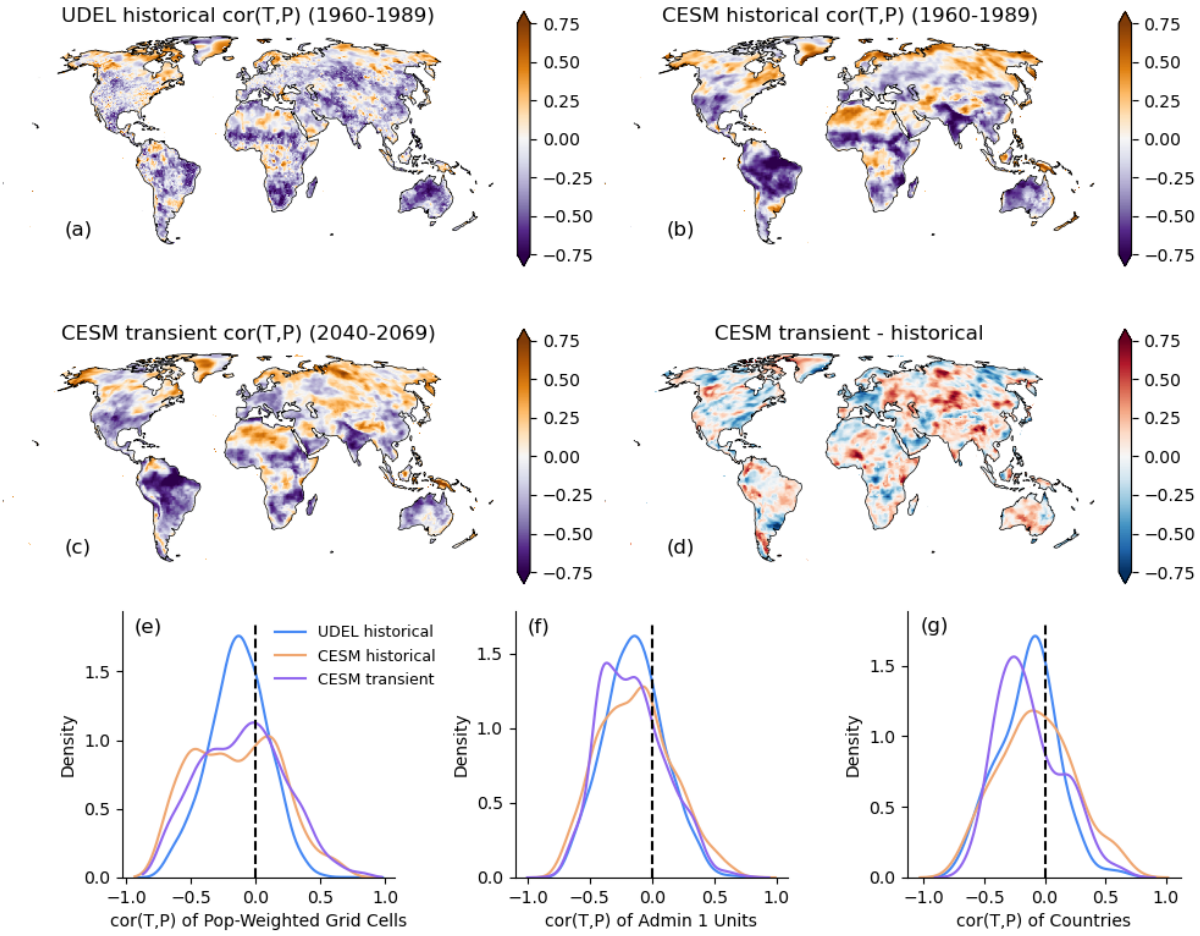

Figure A4.2. Annual correlation between T and P. **(a)** Historical cor(T,P) in the University of Delaware gridded dataset. **(b)** Historical cor(T,P) from the CESM2-WACCM historical simulation. **(c)** Future cor(T,P) as predicted by the CESM2-WACCM middle-of-the-road climate change simulation (SSP245). **(d)** the difference between panels c and b. **(e-g)** Distribution of cor(T,P) in panels (a-c) at different levels of aggregation: **(e)** grid cell, **(f)** administrative 1 units (e.g. US states), and **(g)** countries).

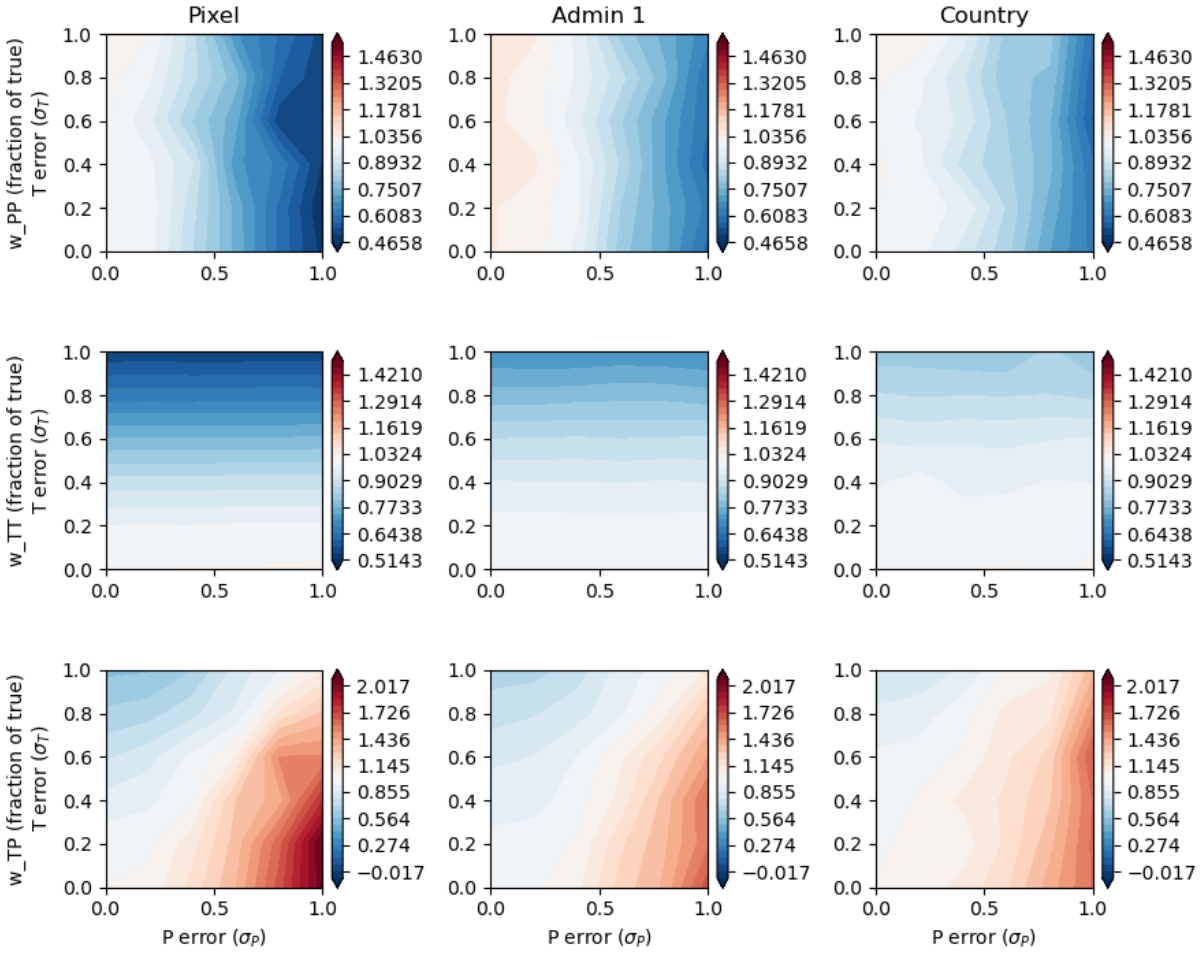

Figure A4.3. Same as Figure 4.4, except including separate T (top row) and P (middle row) components.

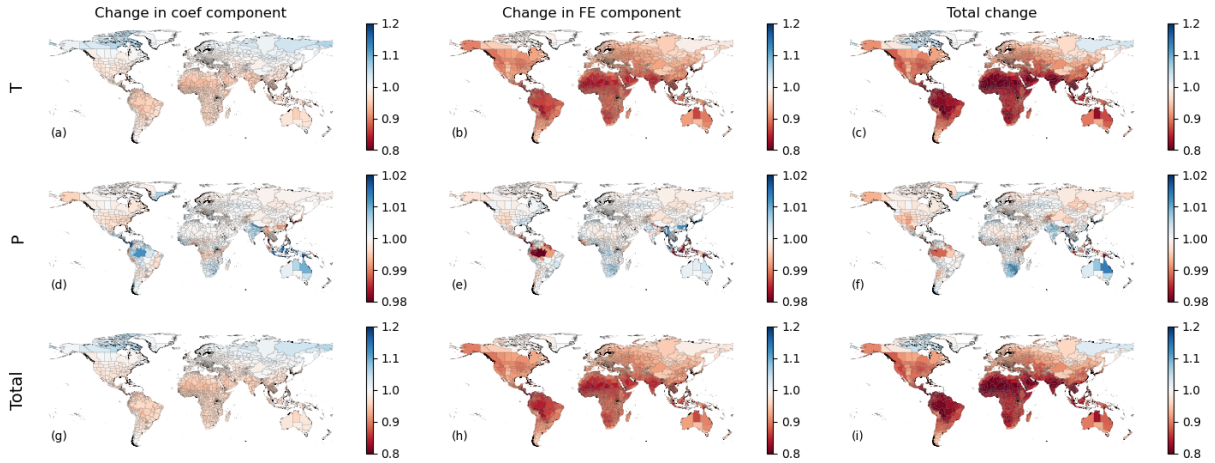

Figure A4.4. GDP projections from internal variability and mean components, broken down by (a-c) T, (d-f) P, and the total (g-i). Note the color bar is an order of magnitude smaller for P than for the other two rows.

Chapter 5

Conclusion

In this thesis, I use idealized modeling to constrain how human decisions may influence the outcomes of environmental policies. In Chapter 2, I show that the dual impact of aerosols on both climate and human creates interesting tradeoffs, but that considering them explicitly as part of international policies can have clear co-benefits for both climate and health individually. In Chapter 3, I show that reducing greenhouse gas emissions will not inevitably be accompanied by improvements to racial equity in the air quality distribution in the United States. However, I do show that some targeted prioritization and cuts to emissions in the transportation sector, can have equity co-benefits. Lastly, in chapter 4, I show how climate impact models are influenced by physical properties of the climate system and conclude that there are multiple ways in which climate impacts may be underestimated. Although there is no way to predict outcomes of human decisions with certainty, these studies draw on Earth science and make use of idealized modeling to help us move towards more informed environmental decision-making.

Bibliography

[1] V. Masson-Delmotte, P. Zhai, S. Pirani, C. Connors, S. Péan, N. Berger, Y. Caud, L. Chen, M. Goldfarb, and P. M. Scheel Monteiro, "Ipcc, 2021: Summary for policymakers. in: Climate change 2021: The physical science basis. contribution of working group i to the sixth assessment report of the intergovernmental panel on climate change," 2021.

[2] J. J. West, S. J. Smith, R. A. Silva, V. Naik, Y. Zhang, Z. Adelman, M. M. Fry, S. Anenberg, L. W. Horowitz, and J.-F. Lamarque, "Co-benefits of mitigating global greenhouse gas emissions for future air quality and human health," *Nature Climate Change*, vol. 3, pp. 885–889, Oct. 2013. Number: 10 Publisher: Nature Publishing Group.

[3] R. Burnett, H. Chen, M. Szyszkowicz, N. Fann, B. Hubbell, C. A. Pope, J. S. Apte, M. Brauer, A. Cohen, S. Weichenthal, J. Coggins, Q. Di, B. Brunekreef, J. Frostad, S. S. Lim, H. Kan, K. D. Walker, G. D. Thurston, R. B. Hayes, C. C. Lim, M. C. Turner, M. Jerrett, D. Krewski, S. M. Gapstur, W. R. Diver, B. Ostro, D. Goldberg, D. L. Crouse, R. V. Martin, P. Peters, L. Pinault, M. Tjepkema, A. v. Donkelaar, P. J. Villeneuve, A. B. Miller, P. Yin, M. Zhou, L. Wang, N. A. H. Janssen, M. Marra, R. W. Atkinson, H. Tsang, T. Q. Thach, J. B. Cannon, R. T. Allen, J. E. Hart, F. Laden, G. Cesaroni, F. Forastiere, G. Weinmayr, A. Jaensch, G. Nagel, H. Concin, and J. V. Spadaro, "Global estimates of mortality associated with long-term exposure to outdoor fine particulate matter," *Proceedings of the National Academy of Sciences*, vol. 115, pp. 9592–9597, Sept. 2018. ISBN: 9781803222110 Publisher: National Academy of Sciences Section: Biological Sciences.

[4] S. Denison, P. M. Forster, and C. J. Smith, "Guidance on emissions metrics for nationally determined contributions under the Paris Agreement," *Environmental Research Letters*, vol. 14, p. 124002, Nov. 2019. Publisher: IOP Publishing.

[5] S. I. Seneviratne, J. Rogelj, R. Séférian, R. Wartenburger, M. R. Allen, M. Cain, R. J. Millar, K. L. Ebi, N. Ellis, O. Hoegh-Guldberg, A. J. Payne, C.-F. Schleussner, P. Tschakert, and R. F. Warren, "The many possible climates from the Paris Agreement's aim of 1.5 °C warming," *Nature*, vol. 558, pp. 41–49, June 2018. Number: 7708 Publisher: Nature Publishing Group.

[6] S. Rao, S. Pachauri, F. Dentener, P. Kinney, Z. Klimont, K. Riahi, and W. Schoepp, "Better air for better health: Forging synergies in policies for energy access, climate change and air pollution," *Global Environmental Change*, vol. 23, pp. 1122–1130, Oct. 2013.

[7] N. Unger, T. C. Bond, J. S. Wang, D. M. Koch, S. Menon, D. T. Shindell, and S. Bauer, "Attribution of climate forcing to economic sectors," *Proceedings of the National Academy of Sciences*, vol. 107, pp. 3382–3387, Feb. 2010. Publisher: National Academy of Sciences Section: Physical Sciences.

[8] A. M. Fiore, V. Naik, and E. M. Leibensperger, "Air Quality and Climate Connections," *Journal of the Air & Waste Management Association*, vol. 65, pp. 645–685, June 2015. Publisher: Taylor & Francis _eprint: https://doi.org/10.1080/10962247.2015.1040526.

[9] R. J. Allen, S. Turnock, P. Nabat, D. Neubauer, U. Lohmann, D. Olivie, N. Oshima, M. Michou, T. Wu, J. Zhang, T. Takemura, M. Schulz, K. Tsigaridis, S. E. Bauer, L. Emmons, L. Horowitz, V. Naik, T. v. Noije, T. Bergman, J.-F. Lamarque, P. Zanis, I. Tegen, D. M. Westervelt, P. L. Sager, P. Good, S. Shim, F. O'Connor, D. Akritidis, A. K. Georgoulias, M. Deushi, L. T. Sentman, S. Fujimori, and W. J. Collins, "Climate and air quality impacts due to mitigation of non-methane near-term climate forcers," *Atmospheric Chemistry and Physics Discussions*, pp. 1–30, Feb. 2020. Publisher: Copernicus GmbH.

[10] G. Myhre, B. H. Samset, M. Schulz, Y. Balkanski, S. Bauer, T. K. Berntsen, H. Bian, N. Bellouin, M. Chin, T. Diehl, R. C. Easter, J. Feichter, S. J. Ghan, D. Hauglustaine, T. Iversen, S. Kinne, A. Kirkevåg, J.-F. Lamarque, G. Lin, X. Liu, M. T. Lund, G. Luo, X. Ma, T. van Noije, J. E. Penner, P. J. Rasch, A. Ruiz, O. Seland, R. B. Skeie, P. Stier, T. Takemura, K. Tsigaridis, P. Wang, Z. Wang, L. Xu, H. Yu, F. Yu, J.-H. Yoon, K. Zhang, H. Zhang, and C. Zhou, "Radiative forcing of the direct aerosol effect from AeroCom Phase II simulations," *Atmospheric Chemistry and Physics*, vol. 13, pp. 1853–1877, Feb. 2013. Publisher: Copernicus GmbH.

[11] A. M. Fiore, V. Naik, D. V. Spracklen, A. Steiner, N. Unger, M. Prather, D. Bergmann, P. J. Cameron-Smith, I. Cionni, W. J. Collins, S. Dalsøren, V. Eyring, G. A. Folberth, P. Ginoux, L. W. Horowitz, B. Josse, J.-F. Lamarque, I. A. MacKenzie, T. Nagashima, F. M. O'Connor, M. Righi, S. T. Rumbold, D. T. Shindell, R. B. Skeie, K. Sudo, S. Szopa, T. Takemura, and G. Zeng, "Global air quality and climate," *Chemical Society Reviews*, vol. 41, pp. 6663–6683, Sept. 2012. Publisher: The Royal Society of Chemistry.

[12] B. H. Samset, M. Sand, C. J. Smith, S. E. Bauer, P. M. Forster, J. S. Fuglestvedt, S. Osprey, and C.-F. Schleussner, "Climate Impacts From a Removal of Anthropogenic Aerosol Emissions," *Geophysical Research Letters*, vol. 45, no. 2, pp. 1020–1029, 2018. _eprint: https://agupubs.onlinelibrary.wiley.com/doi/pdf/10.1002/2017GL076079.

[13] N. Bellouin, J. Quaas, E. Gryspeerdt, S. Kinne, P. Stier, D. Watson-Parris, O. Boucher, K. S. Carslaw, M. Christensen, A.-L. Daniau, J.-L. Dufresne, G. Feingold, S. Fiedler, P. Forster, A. Gettelman, J. M. Haywood, U. Lohmann, F. Malavelle, T. Mauritsen, D. T. McCoy, G. Myhre, J. Mülmenstädt, D. Neubauer, A. Possner, M. Rugenstein, Y. Sato, M. Schulz, S. E. Schwartz, O. Sourdeval, T. Storelvmo, V. Toll, D. Winker, and B. Stevens, "Bounding Global Aerosol Radiative Forcing of Climate Change," *Reviews of Geophysics*, vol. 58, no. 1, p. e2019RG000660, 2020. _eprint: https://agupubs.onlinelibrary.wiley.com/doi/pdf/10.1029/2019RG000660.

[14] O. Boucher, D. Randall, P. Artaxo, C. Bretherton, G. Feingold, P. Forster, V. M. Kerminen, Y. Kondo, H. Liao, and U. Lohmann, "Clouds and aerosols. Climate change 2013: The physical science basis. Contribution of working group I to the fifth assessment report of the intergovernmental panel on climate change," *K., Tignor, M., Allen, SK, Boschung, J., Nauels, A., Xia, Y., Bex, V., and Midgley, PM, cambridge University Press, Cambridge, UK and New York, NY, USA, https://www. ipcc. ch/report/ar5/(last access: 5 October 2017)*, 2013.

[15] C. W. Stjern, B. H. Samset, G. Myhre, H. Bian, M. Chin, Y. Davila, F. Dentener, L. Emmons, J. Flemming, A. S. Haslerud, D. Henze, J. E. Jonson, T. Kucsera, M. T. Lund, M. Schulz, K. Sudo, T. Takemura, and S. Tilmes, "Global and regional radiative forcing from 20 % reductions in BC, OC and SO_4 – an HTAP2 multi-model study," *Atmospheric Chemistry and Physics*, vol. 16, pp. 13579–13599, Nov. 2016. Publisher: Copernicus GmbH.

[16] Y. Zheng, S. J. Davis, G. G. Persad, and K. Caldeira, "Climate effects of aerosols reduce economic inequality," *Nature Climate Change*, vol. 10, pp. 220–224, Mar. 2020. Number: 3 Publisher: Nature Publishing Group.

[17] Q. Di, L. Dai, Y. Wang, A. Zanobetti, C. Choirat, J. D. Schwartz, and F. Dominici, "Association of short-term exposure to air pollution with mortality in older adults," *Jama*, vol. 318, no. 24, pp. 2446–2456, 2017. ISBN: 0098-7484 Publisher: American Medical Association.

[18] S. Heft-Neal, J. Burney, E. Bendavid, and M. Burke, "Robust relationship between air quality and infant mortality in Africa," *Nature*, vol. 559, pp. 254–258, July 2018.

[19] J. Bollen, B. Guay, S. Jamet, and J. Corfee-Morlot, "Co-Benefits of Climate Change Mitigation Policies: Literature Review and New Results," Apr. 2009. Publisher: OECD.

[20] N. Scovronick, M. Budolfson, F. Dennig, F. Errickson, M. Fleurbaey, W. Peng, R. H. Socolow, D. Spears, and F. Wagner, "The impact of human health co-benefits on evaluations of global climate policy," *Nature communications*, vol. 10, no. 1, pp. 1–12, 2019. ISBN: 2041-1723 Publisher: Nature Publishing Group.

[21] N. Chalmers, E. J. Highwood, E. Hawkins, R. Sutton, and L. J. Wilcox, "Aerosol contribution to the rapid warming of near-term climate under RCP 2.6," *Geophysical Research Letters*, vol. 39, no. 18, 2012. _eprint: https://agupubs.onlinelibrary.wiley.com/doi/pdf/10.1029/2012GL052848.

[22] M. O. Andreae and V. Ramanathan, "Climate's dark forcings," *Science*, vol. 340, no. 6130, pp. 280–281, 2013. ISBN: 0036-8075 Publisher: American Association for the Advancement of Science.

[23] J. Lelieveld, K. Klingmüller, A. Pozzer, R. T. Burnett, A. Haines, and V. Ramanathan, "Effects of fossil fuel and total anthropogenic emission removal on public health and

climate," *Proceedings of the National Academy of Sciences*, vol. 116, pp. 7192–7197, Apr. 2019. Publisher: National Academy of Sciences Section: Physical Sciences.

[24] Y. Wang, J. H. Jiang, and H. Su, "Atmospheric responses to the redistribution of anthropogenic aerosols," *Journal of Geophysical Research: Atmospheres*, vol. 120, no. 18, pp. 9625–9641, 2015. _eprint: https://agupubs.onlinelibrary.wiley.com/doi/pdf/10.1002/2015JD023665.

[25] M. R. Allen, K. P. Shine, J. S. Fuglestvedt, R. J. Millar, M. Cain, D. J. Frame, and A. H. Macey, "A solution to the misrepresentations of CO 2 -equivalent emissions of short-lived climate pollutants under ambitious mitigation," *npj Climate and Atmospheric Science*, vol. 1, pp. 1–8, June 2018.

[26] N. Grant, A. Hawkes, T. Napp, and A. Gambhir, "The appropriate use of reference scenarios in mitigation analysis," *Nature Climate Change*, pp. 1–6, June 2020. Publisher: Nature Publishing Group.

[27] K. Riahi, D. P. van Vuuren, E. Kriegler, J. Edmonds, B. C. O'Neill, S. Fujimori, N. Bauer, K. Calvin, R. Dellink, O. Fricko, W. Lutz, A. Popp, J. C. Cuaresma, S. Kc, M. Leimbach, L. Jiang, T. Kram, S. Rao, J. Emmerling, K. Ebi, T. Hasegawa, P. Havlik, F. Humpenöder, L. A. Da Silva, S. Smith, E. Stehfest, V. Bosetti, J. Eom, D. Gernaat, T. Masui, J. Rogelj, J. Strefler, L. Drouet, V. Krey, G. Luderer, M. Harmsen, K. Takahashi, L. Baumstark, J. C. Doelman, M. Kainuma, Z. Klimont, G. Marangoni, H. Lotze-Campen, M. Obersteiner, A. Tabeau, and M. Tavoni, "The Shared Socioeconomic Pathways and their energy, land use, and greenhouse gas emissions implications: An overview," *Global Environmental Change*, vol. 42, pp. 153–168, Jan. 2017.

[28] S. Fujimori, T. Hasegawa, T. Masui, K. Takahashi, D. S. Herran, H. Dai, Y. Hijioka, and M. Kainuma, "SSP3: AIM implementation of Shared Socioeconomic Pathways," *Global Environmental Change*, vol. 42, pp. 268–283, Jan. 2017.

[29] E. Kriegler, N. Bauer, A. Popp, F. Humpenöder, M. Leimbach, J. Strefler, L. Baumstark, B. L. Bodirsky, J. Hilaire, D. Klein, I. Mouratiadou, I. Weindl, C. Bertram, J.-P. Dietrich, G. Luderer, M. Pehl, R. Pietzcker, F. Piontek, H. Lotze-Campen, A. Biewald, M. Bonsch, A. Giannousakis, U. Kreidenweis, C. Müller, S. Rolinski, A. Schultes, J. Schwanitz, M. Stevanovic, K. Calvin, J. Emmerling, S. Fujimori, and O. Edenhofer, "Fossil-fueled development (SSP5): An energy and resource intensive scenario for the 21st century," *Global Environmental Change*, vol. 42, pp. 297–315, Jan. 2017.

[30] G. Myhre, D. Shindell, and J. Pongratz, "Anthropogenic and natural radiative forcing," 2014. ISBN: 1107415322 Publisher: Cambridge University Press.

[31] T. Vandyck, K. Keramidas, B. Saveyn, A. Kitous, and Z. Vrontisi, "A global stocktake of the Paris pledges: Implications for energy systems and economy," *Global Environmental Change*, vol. 41, pp. 46–63, Nov. 2016.

[32] World Bank, "GDP, PPP (constant 2011 international $) | Data."

[33] World Bank, "Inflation, GDP deflator (annual %)."

[34] R. M. Hoesly, S. J. Smith, L. Feng, Z. Klimont, G. Janssens-Maenhout, T. Pitkanen, J. J. Seibert, L. Vu, R. J. Andres, R. M. Bolt, T. C. Bond, L. Dawidowski, N. Kholod, J.-i. Kurokawa, M. Li, L. Liu, Z. Lu, M. C. P. Moura, P. R. O'Rourke, and Q. Zhang, "Historical (1750–2014) anthropogenic emissions of reactive gases and aerosols from the Community Emissions Data System (CEDS)," *Geoscientific Model Development*, vol. 11, pp. 369–408, Jan. 2018. Publisher: Copernicus GmbH.

[35] G. Janssens-Maenhout, F. Dentener, J. Van Aardenne, S. Monni, V. Pagliari, L. Orlandini, Z. Klimont, J.-i. Kurokawa, H. Akimoto, and T. Ohara, "EDGAR-HTAP: a harmonized gridded air pollution emission dataset based on national inventories," *European Commission Publications Office, Ispra (Italy). JRC68434, EUR report No EUR*, vol. 25, pp. 299–2012, 2012.

[36] L. Feng, S. J. Smith, C. Braun, M. Crippa, M. J. Gidden, R. Hoesly, Z. Klimont, M. v. Marle, M. v. d. Berg, and G. R. v. d. Werf, "The generation of gridded emissions data for CMIP6," *Geoscientific Model Development*, vol. 13, pp. 461–482, Feb. 2020. Publisher: Copernicus GmbH.

[37] M. J. Gidden, K. Riahi, S. J. Smith, S. Fujimori, G. Luderer, E. Kriegler, D. P. v. Vuuren, M. v. d. Berg, L. Feng, D. Klein, K. Calvin, J. C. Doelman, S. Frank, O. Fricko, M. Harmsen, T. Hasegawa, P. Havlik, J. Hilaire, R. Hoesly, J. Horing, A. Popp, E. Stehfest, and K. Takahashi, "Global emissions pathways under different socioeconomic scenarios for use in CMIP6: a dataset of harmonized emissions trajectories through the end of the century," *Geoscientific Model Development*, vol. 12, pp. 1443–1475, Apr. 2019.

[38] G. G. Persad and K. Caldeira, "Divergent global-scale temperature effects from identical aerosols emitted in different regions," *Nature Communications*, vol. 9, p. 3289, Aug. 2018. Number: 1 Publisher: Nature Publishing Group.

[39] R. J. Millar, Z. R. Nicholls, P. Friedlingstein, and M. R. Allen, "A modified impulse-response representation of the global near-surface air temperature and atmospheric concentration response to carbon dioxide emissions," *Atmospheric Chemistry and Physics*, vol. 17, pp. 7213–7228, June 2017. Publisher: Copernicus GmbH.

[40] C. J. Smith, P. M. Forster, M. Allen, N. Leach, R. J. Millar, G. A. Passerello, and L. A. Regayre, "FAIR v1.3: a simple emissions-based impulse response and carbon cycle model," *Geoscientific Model Development*, vol. 11, pp. 2273–2297, June 2018.

[41] M. Kelley, G. A. Schmidt, L. S. Nazarenko, S. E. Bauer, R. Ruedy, G. L. Russell, A. S. Ackerman, I. Aleinov, M. Bauer, R. Bleck, V. Canuto, G. Cesana, Y. Cheng, T. L. Clune, B. I. Cook, C. A. Cruz, A. D. D. Genio, G. S. Elsaesser, G. Faluvegi, N. Y. Kiang, D. Kim, A. A. Lacis, A. Leboissetier, A. N. LeGrande, K. K. Lo, J. Marshall, E. E. Matthews, S. McDermid, K. Mezuman, R. L. Miller, L. T. Murray, V. Oinas, C. Orbe, C. P. García-Pando, J. P. Perlwitz, M. J. Puma, D. Rind, A. Romanou, D. T. Shindell, S. Sun, N. Tausnev, K. Tsigaridis, G. Tselioudis, E. Weng,

J. Wu, and M.-S. Yao, "GISS-E2.1: Configurations and Climatology," *Journal of Advances in Modeling Earth Systems*, vol. 12, no. 8, p. e2019MS002025, 2020. _eprint: https://agupubs.onlinelibrary.wiley.com/doi/pdf/10.1029/2019MS002025.

[42] R. L. Miller, G. A. Schmidt, L. Nazarenko, S. E. Bauer, M. Kelley, R. Ruedy, G. L. Russell, A. Ackerman, I. Aleinov, M. Bauer, R. Bleck, V. Canuto, G. Cesana, Y. Cheng, T. L. Clune, B. Cook, C. A. Cruz, A. D. Del Genio, G. S. Elsaesser, G. Faluvegi, N. Y. Kiang, D. Kim, A. A. Lacis, A. Leboissetier, A. N. LeGrande, K. K. Lo, J. Marshall, E. E. Matthews, S. McDermid, K. Mezuman, L. T. Murray, V. Oinas, C. Orbe, C. Pérez García-Pando, J. P. Perlwitz, M. J. Puma, D. Rind, A. Romanou, D. T. Shindell, S. Sun, N. Tausnev, K. Tsigaridis, G. Tselioudis, E. Weng, J. Wu, and M.-S. Yao, "Cmip6 historical simulations (1850-2014) with giss-e2.1," *J. Adv. Model. Earth Syst.*, vol. 13, no. 1, p. e2019MS002034, 2021.

[43] M. T. Lund, B. Aamaas, C. W. Stjern, Z. Klimont, T. K. Berntsen, and B. H. Samset, "A continued role of Short-Lived Climate Forcers under the Shared Socioeconomic Pathways," *Earth System Dynamics Discussions*, pp. 1–23, Mar. 2020. Publisher: Copernicus GmbH.

[44] M. R. Allen, J. S. Fuglestvedt, K. P. Shine, A. Reisinger, R. T. Pierrehumbert, and P. M. Forster, "New use of global warming potentials to compare cumulative and short-lived climate pollutants," *Nature Climate Change*, vol. 6, pp. 773–776, Aug. 2016.

[45] M. J. H. M. Harmsen, P. van Dorst, D. P. van Vuuren, M. van den Berg, R. Van Dingenen, and Z. Klimont, "Co-benefits of black carbon mitigation for climate and air quality," *Climatic Change*, vol. 163, pp. 1519–1538, Dec. 2020.

[46] M. Li, D. Zhang, C.-T. Li, K. M. Mulvaney, N. E. Selin, and V. J. Karplus, "Air quality co-benefits of carbon pricing in China," *Nature Climate Change*, vol. 8, pp. 398–403, May 2018. Number: 5 Publisher: Nature Publishing Group.

[47] N. Unger, Y. Zheng, X. Yue, and K. L. Harper, "Mitigation of ozone damage to the world's land ecosystems by source sector," *Nature Climate Change*, vol. 10, pp. 134–137, Feb. 2020. Number: 2 Publisher: Nature Publishing Group.

[48] Y. Liu, W. Cai, C. Sun, H. Song, K. M. Cobb, J. Li, S. W. Leavitt, L. Wu, Q. Cai, R. Liu, B. Ng, P. Cherubini, U. Büntgen, Y. Song, G. Wang, Y. Lei, L. Yan, Q. Li, Y. Ma, C. Fang, J. Sun, X. Li, D. Chen, and H. W. Linderholm, "Anthropogenic Aerosols Cause Recent Pronounced Weakening of Asian Summer Monsoon Relative to Last Four Centuries," *Geophysical Research Letters*, vol. 46, no. 10, pp. 5469–5479, 2019. _eprint: https://agupubs.onlinelibrary.wiley.com/doi/pdf/10.1029/2019GL082497.

[49] F. Luo, L. Wilcox, B. Dong, Q. Su, W. Chen, N. Dunstone, S. Li, and Y. Gao, "Projected near-term changes of temperature extremes in Europe and China under different aerosol emissions," *Environmental Research Letters*, vol. 15, p. 034013, Feb. 2020. Publisher: IOP Publishing.

[50] M. Harmsen, O. Fricko, J. Hilaire, D. P. van Vuuren, L. Drouet, O. Durand-Lasserve, S. Fujimori, K. Keramidas, Z. Klimont, G. Luderer, L. Aleluia Reis, K. Riahi, F. Sano, and S. J. Smith, "Taking some heat off the NDCs? The limited potential of additional short-lived climate forcers' mitigation," *Climatic Change*, June 2019.

[51] A. Hienola, A.-I. Partanen, J.-P. Pietikäinen, D. O'Donnell, H. Korhonen, H. D. Matthews, and A. Laaksonen, "The impact of aerosol emissions on the 1.5\hspace0.167em°C pathways," *Environmental Research Letters*, vol. 13, p. 044011, Mar. 2018. Publisher: IOP Publishing.

[52] United States of America, "Nationally Determined Contribution. Reducing Greenhouse Gases in the United States: A 2030 Emissions Target," Apr. 2021.

[53] J. A. Yarmuth, "Text - H.R.5376 - 117th Congress (2021-2022): Inflation Reduction Act of 2022," Aug. 2022. Archive Location: 2021/2022.

[54] D. Shindell and C. J. Smith, "Climate and air-quality benefits of a realistic phase-out of fossil fuels," *Nature*, vol. 573, pp. 408–411, Sept. 2019. Number: 7774 Publisher: Nature Publishing Group.

[55] B. Bowe, Y. Xie, Y. Yan, and Z. Al-Aly, "Burden of Cause-Specific Mortality Associated With PM2.5 Air Pollution in the United States," *JAMA Network Open*, vol. 2, p. e1915834, Nov. 2019.

[56] A. L. Goodkind, C. W. Tessum, J. S. Coggins, J. D. Hill, and J. D. Marshall, "Fine-scale damage estimates of particulate matter air pollution reveal opportunities for location-specific mitigation of emissions," *Proceedings of the National Academy of Sciences*, vol. 116, pp. 8775–8780, Apr. 2019. Publisher: National Academy of Sciences Section: Physical Sciences.

[57] C. W. Tessum, D. A. Paolella, S. E. Chambliss, J. S. Apte, J. D. Hill, and J. D. Marshall, "PM2.5 polluters disproportionately and systemically affect people of color in the United States," *Science Advances*, vol. 7, p. eabf4491, Apr. 2021. Publisher: American Association for the Advancement of Science Section: Research Article.

[58] T. W. Collins, S. E. Grineski, Y. Shaker, and C. J. Mullen, "Communities of color are disproportionately exposed to long-term and short-term PM2.5 in metropolitan America," *Environmental Research*, p. 114038, Aug. 2022.

[59] H. M. Lane, R. Morello-Frosch, J. D. Marshall, and J. S. Apte, "Historical Redlining Is Associated with Present-Day Air Pollution Disparities in U.S. Cities," *Environmental Science & Technology Letters*, vol. 9, pp. 345–350, Apr. 2022. Publisher: American Chemical Society.

[60] D. Shindell, M. Ru, Y. Zhang, K. Seltzer, G. Faluvegi, L. Nazarenko, G. A. Schmidt, L. Parsons, A. Challapalli, L. Yang, and A. Glick, "Temporal and spatial distribution of health, labor, and crop benefits of climate change mitigation in the United States,"

Proceedings of the National Academy of Sciences, vol. 118, Nov. 2021. Publisher: National Academy of Sciences Section: Physical Sciences.

[61] B. J. Sergi, P. J. Adams, N. Z. Muller, A. L. Robinson, S. J. Davis, J. D. Marshall, and I. L. Azevedo, "Optimizing Emissions Reductions from the U.S. Power Sector for Climate and Health Benefits," *Environmental Science & Technology*, vol. 54, pp. 7513–7523, June 2020. Publisher: American Chemical Society.

[62] Y. Li, A. Kumar, Y. Li, and M. J. Kleeman, "Adoption of low-carbon fuels reduces race/ethnicity disparities in air pollution exposure in California," *Science of The Total Environment*, p. 155230, Apr. 2022.

[63] T. Wang, Z. Jiang, B. Zhao, Y. Gu, K.-N. Liou, N. Kalandiyur, D. Zhang, and Y. Zhu, "Health co-benefits of achieving sustainable net-zero greenhouse gas emissions in California," *Nature Sustainability*, vol. 3, pp. 597–605, Aug. 2020. Number: 8 Publisher: Nature Publishing Group.

[64] C. M. Anderson, K. A. Kissel, C. B. Field, and K. J. Mach, "Climate Change Mitigation, Air Pollution, and Environmental Justice in California," *Environmental Science & Technology*, vol. 52, pp. 10829–10838, Sept. 2018. Publisher: American Chemical Society.

[65] C. W. Tessum, J. D. Hill, and J. D. Marshall, "InMAP: A model for air pollution interventions," *PLOS ONE*, vol. 12, p. e0176131, Apr. 2017. Publisher: Public Library of Science.

[66] A. Jbaily, X. Zhou, J. Liu, T.-H. Lee, L. Kamareddine, S. Verguet, and F. Dominici, "Air pollution exposure disparities across US population and income groups," *Nature*, vol. 601, pp. 228–233, Jan. 2022. Number: 7892 Publisher: Nature Publishing Group.

[67] J. Bistline, N. Abhyankar, G. Blanford, L. Clarke, R. Fakhry, H. McJeon, J. Reilly, C. Roney, T. Wilson, M. Yuan, and A. Zhao, "Actions for reducing US emissions at least 50% by 2030," *Science*, vol. 376, pp. 922–924, May 2022. Publisher: American Association for the Advancement of Science.

[68] A. Nardone, J. A. Casey, R. Morello-Frosch, M. Mujahid, J. R. Balmes, and N. Thakur, "Associations between historical residential redlining and current age-adjusted rates of emergency department visits due to asthma across eight cities in California: an ecological study," *The Lancet Planetary Health*, vol. 4, pp. e24–e31, Jan. 2020.

[69] L. Friedman, "White House Takes Aim at Environmental Racism, but Won't Mention Race," *The New York Times*, Feb. 2022.

[70] R. Bluhm, P. Polonik, K. S. Hemes, L. C. Sanford, S. A. Benz, M. C. Levy, K. L. Ricke, and J. A. Burney, "Disparate air pollution reductions during California's COVID-19 economic shutdown," *Nature Sustainability*, pp. 1–9, Apr. 2022. Publisher: Nature Publishing Group.

[71] M. Burke, A. Driscoll, S. Heft-Neal, J. Xue, J. Burney, and M. Wara, "The changing risk and burden of wildfire in the United States," *Proceedings of the National Academy of Sciences*, vol. 118, p. e2011048118, Jan. 2021. Publisher: Proceedings of the National Academy of Sciences.

[72] A. Karanasiou, A. Alastuey, F. Amato, M. Renzi, M. Stafoggia, A. Tobias, C. Reche, F. Forastiere, S. Gumy, P. Mudu, and X. Querol, "Short-term health effects from outdoor exposure to biomass burning emissions: A review," *Science of The Total Environment*, vol. 781, p. 146739, Aug. 2021.

[73] G. Chen, Y. Guo, X. Yue, S. Tong, A. Gasparrini, M. L. Bell, B. Armstrong, J. Schwartz, J. J. K. Jaakkola, A. Zanobetti, E. Lavigne, P. H. Nascimento Saldiva, H. Kan, D. Royé, A. Milojevic, A. Overcenco, A. Urban, A. Schneider, A. Entezari, A. M. Vicedo-Cabrera, A. Zeka, A. Tobias, B. Nunes, B. Alahmad, B. Forsberg, S.-C. Pan, C. Íñiguez, C. Ameling, C. De la Cruz Valencia, C. Åström, D. Houthuijs, D. Van Dung, E. Samoli, F. Mayvaneh, F. Sera, G. Carrasco-Escobar, Y. Lei, H. Orru, H. Kim, I.-H. Holobaca, J. Kyselý, J. P. Teixeira, J. Madureira, K. Katsouyanni, M. Hurtado-Díaz, M. Maasikmets, M. S. Ragettli, M. Hashizume, M. Stafoggia, M. Pascal, M. Scortichini, M. de Sousa Zanotti Stagliorio Coêlho, N. Valdés Ortega, N. R. I. Ryti, N. Scovronick, P. Matus, P. Goodman, R. M. Garland, R. Abrutzky, S. O. Garcia, S. Rao, S. Fratianni, T. N. Dang, V. Colistro, V. Huber, W. Lee, X. Seposo, Y. Honda, Y. L. Guo, T. Ye, W. Yu, M. J. Abramson, J. M. Samet, and S. Li, "Mortality risk attributable to wildfire-related PM2·5 pollution: a global time series study in 749 locations," *The Lancet Planetary Health*, vol. 5, pp. e579–e587, Sept. 2021.

[74] M. Burke, S. Heft-Neal, J. Li, A. Driscoll, P. Baylis, M. Stigler, J. A. Weill, J. A. Burney, J. Wen, M. L. Childs, and C. F. Gould, "Exposures and behavioural responses to wildfire smoke," *Nature Human Behaviour*, pp. 1–11, July 2022. Publisher: Nature Publishing Group.

[75] S. A. Perlin, D. Wong, and K. Sexton, "Residential Proximity to Industrial Sources of Air Pollution: Interrelationships among Race, Poverty, and Age," *Journal of the Air & Waste Management Association*, vol. 51, pp. 406–421, Mar. 2001. Publisher: Taylor & Francis _eprint: https://doi.org/10.1080/10473289.2001.10464271.

[76] R. Rothstein, *The color of law: A forgotten history of how our government segregated America*. Liveright Publishing, 2017.

[77] G. H. Kerr, D. L. Goldberg, and S. C. Anenberg, "COVID-19 pandemic reveals persistent disparities in nitrogen dioxide pollution," *Proceedings of the National Academy of Sciences*, vol. 118, p. e2022409118, July 2021. Publisher: Proceedings of the National Academy of Sciences.

[78] F. Tong and I. M. L. Azevedo, "What are the best combinations of fuel-vehicle technologies to mitigate climate change and air pollution effects across the United States?," *Environmental Research Letters*, vol. 15, p. 074046, July 2020. Publisher: IOP Publishing.

[79] D. Tong, G. Geng, Q. Zhang, J. Cheng, X. Qin, C. Hong, K. He, and S. J. Davis, "Health co-benefits of climate change mitigation depend on strategic power plant retirements and pollution controls," *Nature Climate Change*, pp. 1–7, Nov. 2021. Bandiera_abtest: a Cg_type: Nature Research Journals Primary_atype: Research Publisher: Nature Publishing Group Subject_term: Climate-change impacts;Climate-change mitigation;Environmental impact;Sustainability Subject_term_id: climate-change-impacts;climate-change-mitigation;environmental-impact;sustainability.

[80] C. W. Tessum, J. S. Apte, A. L. Goodkind, N. Z. Muller, K. A. Mullins, D. A. Paolella, S. Polasky, N. P. Springer, S. K. Thakrar, J. D. Marshall, and J. D. Hill, "Inequity in consumption of goods and services adds to racial–ethnic disparities in air pollution exposure," *Proceedings of the National Academy of Sciences*, vol. 116, pp. 6001–6006, Mar. 2019. Publisher: Proceedings of the National Academy of Sciences.

[81] P. Kuss and K. A. Nicholas, "A dozen effective interventions to reduce car use in European cities: Lessons learned from a meta-analysis and transition management," *Case Studies on Transport Policy*, Feb. 2022.

[82] A. van Donkelaar, M. S. Hammer, L. Bindle, M. Brauer, J. R. Brook, M. J. Garay, N. C. Hsu, O. V. Kalashnikova, R. A. Kahn, C. Lee, R. C. Levy, A. Lyapustin, A. M. Sayer, and R. V. Martin, "Monthly Global Estimates of Fine Particulate Matter and Their Uncertainty," *Environmental Science & Technology*, vol. 55, pp. 15287–15300, Nov. 2021. Publisher: American Chemical Society.

[83] L. P. Clark, M. H. Harris, J. S. Apte, and J. D. Marshall, "National and Intraurban Air Pollution Exposure Disparity Estimates in the United States: Impact of Data-Aggregation Spatial Scale," *Environmental Science & Technology Letters*, Aug. 2022. Publisher: American Chemical Society.

[84] J. Koornneef, A. Ramirez, T. van Harmelen, A. van Horssen, W. Turkenburg, and A. Faaij, "The impact of CO2 capture in the power and heat sector on the emission of SO2, NOx, particulate matter, volatile organic compounds and NH3 in the European Union," *Atmospheric Environment*, vol. 44, pp. 1369–1385, Apr. 2010.

[85] G. S. Mishra, P. Kyle, J. Teter, G. M. Morrison, S. Kim, and S. Yeh, "Transportation module of global change assessment model (GCAM): model documentation," *Institute of Transportation Studies, University of California: Davis, CA, USA*, 2013.

[86] A. Mahone, C. Li, Subin, Zach, Sontag Michael, Mantegna, Gabe, Karolides, Alexis, German, Alea, and Morris, Peter, "Consumer economics, greenhouse gases and grid impacts," *Energy & Environmental Economics*, Apr. 2019.

[87] D. Leeson, N. Mac Dowell, N. Shah, C. Petit, and P. S. Fennell, "A Techno-economic analysis and systematic review of carbon capture and storage (CCS) applied to the iron and steel, cement, oil refining and pulp and paper industries, as well as other high purity sources," *International Journal of Greenhouse Gas Control*, vol. 61, pp. 71–84, June 2017.

[88] T. A. Carleton and S. M. Hsiang, "Social and economic impacts of climate," *Science*, vol. 353, Sept. 2016. Publisher: American Association for the Advancement of Science Section: Review.

[89] M. Burke, J. Dykema, D. B. Lobell, E. Miguel, and S. Satyanath, "Incorporating Climate Uncertainty into Estimates of Climate Change Impacts," *The Review of Economics and Statistics*, vol. 97, pp. 461–471, 05 2015.

[90] C. Huang, A. G. Barnett, X. Wang, P. Vaneckova, G. FitzGerald, and S. Tong, "Projecting Future Heat-Related Mortality under Climate Change Scenarios: A Systematic Review," *Environmental Health Perspectives*, vol. 119, pp. 1681–1690, Dec. 2011. Publisher: Environmental Health Perspectives.

[91] R. D. Peng, J. F. Bobb, C. Tebaldi, L. McDaniel, M. L. Bell, and F. Dominici, "Toward a Quantitative Estimate of Future Heat Wave Mortality under Global Climate Change," *Environmental Health Perspectives*, vol. 119, pp. 701–706, May 2011. Publisher: Environmental Health Perspectives.

[92] A. Gasparrini, Y. Guo, F. Sera, A. M. Vicedo-Cabrera, V. Huber, S. Tong, M. de Sousa Zanotti Stagliorio Coelho, P. H. Nascimento Saldiva, E. Lavigne, P. Matus Correa, N. Valdes Ortega, H. Kan, S. Osorio, J. Kyselý, A. Urban, J. J. K. Jaakkola, N. R. I. Ryti, M. Pascal, P. G. Goodman, A. Zeka, P. Michelozzi, M. Scortichini, M. Hashizume, Y. Honda, M. Hurtado-Diaz, J. Cesar Cruz, X. Seposo, H. Kim, A. Tobias, C. Iñiguez, B. Forsberg, D. O. Åström, M. S. Ragettli, Y. L. Guo, C.-f. Wu, A. Zanobetti, J. Schwartz, M. L. Bell, T. N. Dang, D. D. Van, C. Heaviside, S. Vardoulakis, S. Hajat, A. Haines, and B. Armstrong, "Projections of temperature-related excess mortality under climate change scenarios," *The Lancet Planetary Health*, vol. 1, pp. e360–e367, Dec. 2017.

[93] A. Marsha, S. R. Sain, M. J. Heaton, A. J. Monaghan, and O. Wilhelmi, "Influences of climatic and population changes on heat-related mortality in Houston, Texas, USA," *Climatic Change*, vol. 146, pp. 471–485, Feb. 2018.

[94] D. B. Lobell and M. B. Burke, "On the use of statistical models to predict crop yield responses to climate change," *Agricultural and Forest Meteorology*, vol. 150, pp. 1443–1452, Oct. 2010.

[95] P. Zhu, J. Burney, J. Chang, Z. Jin, N. D. Mueller, Q. Xin, J. Xu, L. Yu, D. Makowski, and P. Ciais, "Warming reduces global agricultural production by decreasing cropping frequency and yields," *Nature Climate Change*, vol. 12, pp. 1016–1023, Nov. 2022. Number: 11 Publisher: Nature Publishing Group.

[96] K. Wiebe, H. Lotze-Campen, R. Sands, A. Tabeau, D. v. d. Mensbrugghe, A. Biewald, B. Bodirsky, S. Islam, A. Kavallari, D. Mason-D'Croz, C. Müller, A. Popp, R. Robertson, S. Robinson, H. v. Meijl, and D. Willenbockel, "Climate change impacts on agriculture in 2050 under a range of plausible socioeconomic and emissions scenarios," *Environmental Research Letters*, vol. 10, p. 085010, Aug. 2015. Publisher: IOP Publishing.

[97] M. Letta and R. S. J. Tol, "Weather, Climate and Total Factor Productivity," *Environmental and Resource Economics*, vol. 73, pp. 283–305, May 2019.

[98] Y. Song, B. Zhang, J. Wang, and K. Kwek, "The impact of climate change on China's agricultural green total factor productivity," *Technological Forecasting and Social Change*, vol. 185, p. 122054, Dec. 2022.

[99] M. Burke, S. M. Hsiang, and E. Miguel, "Global non-linear effect of temperature on economic production," *Nature*, vol. 527, pp. 235–239, Nov. 2015. Number: 7577 Publisher: Nature Publishing Group.

[100] R. G. Newell, B. C. Prest, and S. E. Sexton, "The GDP-Temperature relationship: Implications for climate change damages," *Journal of Environmental Economics and Management*, vol. 108, p. 102445, July 2021.

[101] R. Damania, S. Desbureaux, and E. Zaveri, "Does rainfall matter for economic growth? Evidence from global sub-national data (1990–2014)," *Journal of Environmental Economics and Management*, vol. 102, p. 102335, July 2020.

[102] M. Dell, B. F. Jones, and B. A. Olken, "Temperature Shocks and Economic Growth: Evidence from the Last Half Century," *American Economic Journal: Macroeconomics*, vol. 4, pp. 66–95, July 2012.

[103] K. Ricke, L. Drouet, K. Caldeira, and M. Tavoni, "Country-level social cost of carbon," *Nature Climate Change*, vol. 8, no. 10, pp. 895–900, 2018.

[104] M. Kalkuhl and L. Wenz, "The impact of climate conditions on economic production. Evidence from a global panel of regions," *Journal of Environmental Economics and Management*, vol. 103, p. 102360, Sept. 2020.

[105] E. Blanc and J. Reilly, "Approaches to assessing climate change impacts on agriculture: an overview of the debate," *Review of Environmental Economics and Policy*, 2017.

[106] M. Auffhammer, V. Ramanathan, and J. R. Vincent, "Climate change, the monsoon, and rice yield in India," *Climatic Change*, vol. 111, pp. 411–424, Mar. 2012.

[107] A. C. Fisher, W. M. Hanemann, M. J. Roberts, and W. Schlenker, "The economic impacts of climate change: evidence from agricultural output and random fluctuations in weather: comment," *American Economic Review*, vol. 102, no. 7, pp. 3749–3760, 2012.

[108] C. Frost and S. G. Thompson, "Correcting for regression dilution bias: comparison of methods for a single predictor variable," *Journal of the Royal Statistical Society: Series A (Statistics in Society)*, vol. 163, no. 2, pp. 173–189, 2000.

[109] J. Proctor, A. Rigden, D. Chan, and P. Huybers, "More accurate specification of water supply shows its importance for global crop production," *Nature Food*, vol. 3, no. 9, pp. 753–763, 2022.

[110] C. D. Kolstad and F. C. Moore, "Estimating the economic impacts of climate change using weather observations," *Review of Environmental Economics and Policy*, 2020.

[111] S. Hsiang, "Climate Econometrics," *Annual Review of Resource Economics*, vol. 8, no. 1, pp. 43–75, 2016.

[112] M. N. Mistry, R. Schneider, P. Masselot, D. Royé, B. Armstrong, J. Kyselý, H. Orru, F. Sera, S. Tong, E. Lavigne, A. Urban, J. Madureira, D. García-León, D. Ibarreta, J.-C. Ciscar, L. Feyen, E. de Schrijver, M. de Sousa Zanotti Stagliorio Coelho, M. Pascal, A. Tobias, Y. Guo, A. M. Vicedo-Cabrera, and A. Gasparrini, "Comparison of weather station and climate reanalysis data for modelling temperature-related mortality," *Scientific Reports*, vol. 12, p. 5178, Mar. 2022. Number: 1 Publisher: Nature Publishing Group.

[113] D. B. Lobell and M. B. Burke, "Why are agricultural impacts of climate change so uncertain? The importance of temperature relative to precipitation," *Environmental Research Letters*, vol. 3, p. 034007, July 2008. Publisher: IOP Publishing.

[114] R. Cai, S. Feng, M. Oppenheimer, and M. Pytlikova, "Climate variability and international migration: The importance of the agricultural linkage," *Journal of Environmental Economics and Management*, vol. 79, pp. 135–151, 2016.

[115] K. Ricke, J. S. Wan, M. Saenger, and N. J. Lutsko, "Hydrological consequences of solar geoengineering," *Annual Review of Earth and Planetary Sciences*, vol. 51, 2023.

[116] A. R. Harding, K. Ricke, D. Heyen, D. G. MacMartin, and J. Moreno-Cruz, "Climate econometric models indicate solar geoengineering would reduce inter-country income inequality," *Nature Communications*, vol. 11, p. 227, Jan. 2020. Number: 1 Publisher: Nature Publishing Group.

[117] C. T. McIntosh and W. Schlenker, "Identifying non-linearities in fixed effects models," *UC-San Diego Working Paper*, 2006.

[118] L. G. Hrebiniak and W. F. Joyce, "Organizational adaptation: Strategic choice and environmental determinism," *Administrative science quarterly*, pp. 336–349, 1985.

[119] T. Carleton, A. Jina, M. Delgado, M. Greenstone, T. Houser, S. Hsiang, A. Hultgren, R. E. Kopp, K. E. McCusker, I. Nath, J. Rising, A. Rode, H. K. Seo, A. Viaene, J. Yuan, and A. T. Zhang, "Valuing the Global Mortality Consequences of Climate Change Accounting for Adaptation Costs and Benefits*," *The Quarterly Journal of Economics*, vol. 137, pp. 2037–2105, Apr. 2022.

[120] M. Burke, A. Driscoll, D. B. Lobell, and S. Ermon, "Using satellite imagery to understand and promote sustainable development," *Science*, vol. 371, no. 6535, p. eabe8628, 2021.

[121] J. Proctor, S. Hsiang, J. Burney, M. Burke, and W. Schlenker, "Estimating global agricultural effects of geoengineering using volcanic eruptions," *Nature*, p. 1, 2018.

[122] R. McKitrick, "On the choice of tls versus ols in climate signal detection regression," *Climate Dynamics*, vol. 60, no. 1-2, pp. 359–374, 2023.

[123] M. Kummu, M. Taka, and J. H. A. Guillaume, "Gridded global datasets for Gross Domestic Product and Human Development Index over 1990–2015," *Scientific Data*, vol. 5, p. 180004, Feb. 2018. Number: 1 Publisher: Nature Publishing Group.

[124] K. Klein Goldewijk, A. Beusen, J. Doelman, and E. Stehfest, "Anthropogenic land use estimates for the holocene–hyde 3.2," *Earth System Science Data*, vol. 9, no. 2, pp. 927–953, 2017.